Dissertation
submitted to the
Combined Faculty of Natural Sciences and Mathematics
of Heidelberg University, Germany
for the degree of
Doctor of Natural Sciences

Put forward by

Halil Cakir

born in Mannheim, Germany

Oral examination: July 1st, 2020

Quantum Electrodynamic Theory of Few-Electron Highly Charged Ions

Referees: PD Dr. Zoltán Harman
Prof. Dr. Maurits W. Haverkort

Zusammenfassung

In dieser Arbeit werden quantenelektrodynamische (QED) Effekte in hochgeladenen Ionen mit wenigen Elektronen untersucht. Die Wechselwirkung des Elektrons mit dem Kern wird auf eine nichtstörungstheoretische Art berücksichtigt. Es wird ein vielseitiger Ansatz zur Berechnung der Selbstenergie-Korrektur vorgestellt, bei dem endliche Basissätze mit analytischen Methoden kombiniert werden. Der Ansatz ist auf Vielelektronen-Ionen unter Verwendung der Abschirmungspotential-Näherung anwendbar. Die Methode wird angewendet um Selbstenergie-Korrekturen des Energieniveaus des Elektrons im $4d_{3/2}$ Zustand von $^{131}\mathrm{Xe}^{17+}$ und der Energie der Elektronenanregung $4d \to 4f$ in $^{187}\mathrm{Re}^{29+}$ zu berechnen. Es werden QED Korrekturen des g-Faktors von lithium- und borartigen Ionen für einen weiten Bereich der Kernladungen vorgestellt. Vielelektronen-Beiträge sowie Strahlungseffekte werden auf der Ein-Schleifen-Ebene berechnet. Beiträge, die durch die im Rahmen der QED abgeleiteten Wechselwirkung zwischen den Elektronen resultieren und die meisten Terme des Vakuumpolarisationseffekts werden für alle Ordungen in der Kernkopplungsstärke $Z\alpha$ ausgewertet. Unsicherheiten aufgrund von Kerngrößeneffekten, numerischen Berechnungen und nicht berechneten Effekten werden diskutiert. Schließlich wird ein neuer Ansatz zur Bestimmung der Feinstrukturkonstante α unter Verwendung einer gewichteten Differenz des g-Faktors und der Energie des gebundenen Elektrons in wasserstoffartigen Systemen vorgestellt. Es wird gezeigt, dass Kernstruktureffekte hinreichend gut unterdrückt werden, während die Empfindlichkeit gegenüber α in dieser gewichteten Differenz im Vergleich zum g-Faktor zunimmt.

Abstract

In this thesis, quantum electrodynamic (QED) effects in few-electron highly charged ions are investigated. The interaction of the electron with the nucleus is taken into account in a nonperturbative manner. A versatile approach to accurately calculate self-energy corrections combining finite basis sets with analytical methods is presented. The approach is applicable to many-electron ions using the screening-potential approximation. The method is applied to calculate self-energy corrections to the energy level of the electron in the $4d_{3/2}$ state of $^{131}\mathrm{Xe}^{17+}$ and to the excitation energy of the $4d \to 4f$ excitation in $^{187}\mathrm{Re}^{29+}$. QED corrections to the g factor of lithiumlike and boronlike ions in a wide range of nuclear charges are presented. Many-electron contributions as well as radiative effects on the one-loop level are calculated. Contributions resulting from the interelectronic interaction, derived in a QED framework, and most of the terms of the vacuum polarization effect are evaluated to all orders in the nuclear coupling strength $Z\alpha$. Uncertainties resulting from nuclear size effects, numerical calculations, and uncalculated effects are discussed. Finally, a new approach to determine the fine-structure constant α using a weighted difference of the bound-electron g factor and energy in hydrogenlike systems is put forward. It is shown that nuclear structural effects are sufficiently well suppressed while sensitivity to α is enhanced in this weighted difference, as compared to the g factor.

In the course of this thesis, the following articles have been published or accepted for publication in a peer-reviewed journal:

- H. Cakir, V. A. Yerokhin, N. S. Oreshkina, B. Sikora, I. I. Tupitsyn, C. H. Keitel, and Z. Harman
  QED corrections to the g factor of Li- and B-like ions
  Phys. Rev. A, in print (2020) (Ref. [1])
- R. X. Schüssler, H. Bekker, M. Braß, H. Cakir, J. R. Crespo López-Urrutia, M. Door, P. Filianin, Z. Harman, M. W. Haverkort, W. J. Huang, P. Indelicato, C. H. Keitel, C. M. König, K. Kromer, M. Müller, Y. N. Novikov, A. Rischka, C. Schweiger, S. Sturm, S. Ulmer, S. Eliseev, and K. Blaum
  Detection of metastable electronic states by Penning trap mass spectrometry
  Nature, in print (2020) (Ref. [2])
- N. S. Oreshkina, H. Cakir, B. Sikora, V. A. Yerokhin, V. Debierre, Z. Harman, and C. H. Keitel
  Self-energy-corrected Dirac wave functions for advanced QED calculations in highly charged ions
  Phys. Rev. A **101**, 032511 (2020) (Ref. [3])
- A. Rischka, H. Cakir, M. Door, P. Filianin, Z. Harman, W. J. Huang, P. Indelicato, C. H. Keitel, C. M. König, K. Kromer, M. Müller, Y. N. Novikov, R. X. Schüssler, C. Schweiger, S. Eliseev, and K. Blaum
  Mass-Difference Measurements on Heavy Nuclides with an eV/c^2 *Accuracy in the PENTATRAP Spectrometer*
  Phys. Rev. Lett. **124**, 113001 (2020) (Ref. [4])
- B. Sikora, V. A. Yerokhin, N. S. Oreshkina, H. Cakir, C. H. Keitel, and Z. Harman
  Theory of the two-loop self-energy correction to the g factor in nonperturbative Coulomb fields
  Phys. Rev. Research **2**, 012002(R) (2020) (Ref. [5])
- I. Arapoglou, A. Egl, M. Höcker, T. Sailer, B. Tu, A. Weigel, R. Wolf, H. Cakir, V. A. Yerokhin, N. S. Oreshkina, V. A. Agababaev, A. V. Volotka, D. V. Zinenko, D. A. Glazov, Z. Harman, C. H. Keitel, S. Sturm, and K. Blaum
  g Factor of Boronlike Argon $^{40}\mathrm{Ar}^{13+}$
  Phys. Rev. Lett. **122**, 253001 (2019) (Ref. [6])
- B. Sikora, H. Cakir, N. Michel, V. Debierre, N. S. Oreshkina, N. A. Belov, V. A. Yerokhin, C. H. Keitel, and Z. Harman
  Improving the accuracy of the muon mass and magnetic moment anomaly via the bound-muon g factor
  Phys. Rev. D **97**, 111301(R) (2018) (Ref. [7])

The following article has been submitted to a peer-reviewed journal:

- H. Cakir, N. S. Oreshkina, I. A. Valuev, V. Debierre, V. A. Yerokhin, C. H. Keitel, and Z. Harman
  Improved access to the fine-structure constant with the simplest atomic systems
  Phys. Rev. Lett., submitted (Ref. [8])

The following contribution to a conference proceeding has been published:

- Z. Harman, B. Sikora, V. A. Yerokhin, H. Cakir, V. Debierre, N. Michel, N. S. Oreshkina, N. A. Belov, J. Zatorski, and C. H. Keitel
  The g factor of highly charged ions
  J. Phys. Conf. Ser. **1138**, 012002 (2018) (Ref. [9])

The following article is in preperation:

- S. Breidenbach, E. Dizer, H. Cakir, Z. Harman
  Hadronic vacuum polarization correction to atomic energy levels
  in preparation (Ref. [10])

Contents

Introduction

The interaction of charged particles with photons is described by quantum electrodynamics (QED). Due to its predictive success, it is considered to be the most successful instance of a quantum field theory. Highly charged ions provide an ideal testing ground for QED effects in strong fields. These strong fields are naturally achieved by stripping all but a few electrons from heavy elements up to Pb or U. The expactation value of the electric field strength for hydrogenlike (H-like) Pb^{81+}, for example, is of the order of 10^{16} Vcm^{-1} [11]. These strengths constitute the strongest ones achievable in laboratory experiments and pose a challange to theoretical calculations, as these field strength make perturbative approaches unfeasible. Rapid experimental developments allow for ever increasing accuracy in measurements which in turn stimulates theoretical investigations of highly charged ions.

The g factor of an electron is a measure of the strength of the interaction between the magnetic moment of the electron and an external magnetic field and belongs to the most accurately measured observables. Measurements of the free-electron magnetic anomaly are on the level of 10^{-10} fractional uncertainty [9] and theoretical calculations of the free-electron g factor include terms up to fifth order [12] in the fine-structure constant α. Measurements of the free-electron g factor, besides providing stringent tests of the theoretical framework of QED, have been combined with theoretical calculations to determine the value of the fine-structure constant α. Currently, the fractional uncertainty of α determined in this manner is on the level of 10^{-10}. For some more details on the measurements and theory, we refer to Ref. [12]. Recently, the uncertainty of α has been improved in measurements of the recoil velocity of an atom when it absorbs a photon [13, 14].

Recent high-precision measurements of the bound-electron g factor together with correspondingly accurate theoretical calculations allow detailed tests of QED in strong fields. Measurements of the bound-electron g factor have been performed for different types of atomic systems. The simplest ones are H-like ions, where all electrons but one are stripped from the atom. The g factors of H-like $^{12}C^{5+}$ [15, 16], $^{16}O^{7+}$ [17], and $^{28}Si^{13+}$ [18, 19] have been measured. More complicated systems are lithiumlike (Li-like) and boronlike (B-like) systems, where there are additional interactions between electrons as compared to H-like ions. The g factors of Li-like $^{28}Si^{11+}$ [20], and isotopes $^{40}Ca^{17+}$ and $^{48}Ca^{17+}$ [21] have been measured. Recently, the first high-precision measurement of the g factor of B-like $^{40}Ar^{13+}$ has been per-

formed with the ALPHATRAP Penning-trap setup [22] at the Max Planck Institute for Nuclear Physics [6], improving the previous experimental value [23] by several orders of magnitude, and the experiment is aiming to perform measurements in the near future on heavier systems and with a relative uncertainty of 10^{-11} or better [24].

Theoretical calculations of the bound-electron g factor follow two approaches in treating the interaction between the electron and the nucleus. One is the nonrelativistic QED treatment where expansions in the nuclear coupling strength $Z\alpha$, with Z being the nuclear charge number, are performed. These types of calculations typically allow for analytical expressions. However, they are not feasible for highly charged ions as the nuclear coupling strength is of order one for these systems. The other approach is to include the interaction between the electron and the nucleus in a fully relativistic, nonperturbative manner. This approach is suitable for a broad range of nuclear charge numbers but typically requires numerical methods for practical calculations, which, especially in case of light systems, are often associated with larger numerical uncertainties.

The leading contribution to the ground-state bound-electron g factor in a H-like system was first calculated by Breit in 1928 [25]. Today, many more contributions resulting from different types of effects have been calculated. Radiative corrections due to interactions of the bound electron with itself by the emission and reabsorption of a virtual photon (the self-energy effect) have been calculated to one-loop order perturbatively in the nuclear coupling strength up to order $(Z\alpha)^5$ [26–31] and to all orders [32–36]. Radiative corrections due to the interaction of the bound electron with the nucleus through the creation and annihilation of virtual electron-positron pairs (the vacuum polarization effect) have been calculated [11, 37–43]. The perturbative expansion of two-loop radiative corrections to order $(Z\alpha)^4$ [30, 44–46] has been recently extended to order $(Z\alpha)^5$ [47, 48], which has improved the theoretical uncertainty for low nuclear charges Z, and first milestones have been achieved in the non-perturbative calculation of two-loop corrections to the bound-electron g factor of H-like ions [5, 49].

Beyond testing QED effects in strong fields, these high-precision measurements of the g factor of highly charged ions with Penning trap experiments, together with a correspondingly accurate theoretical description, allow the determination of fundamental physical constants. This has already been demonstrated for the electron mass in Ref. [16]. A precise measurement of the magnetic moment of a single electron bound to a carbon nucleus has been combined with theoretical calculations of the g factor of the bound electron to obtain a value for the mass of the electron in atomic mass units which is by a factor of 13 more precise than the best previous measurements and the 2010 CODATA value [50].

The principle of the electron mass determination is as follows: A single electron is bound to a bare carbon nucleus and the ratio between the Larmor frequency ν_L

and the cyclotron frequency ν_{cyc} is measured. The mass of the electron is then given by [16]

$$m_{\mathrm{e}} = -\frac{g}{2}\frac{e}{q_{\mathrm{ion}}}\frac{\nu_{\mathrm{cyc}}}{\nu_{\mathrm{L}}}m_{\mathrm{ion}}\,,$$

where $e < 0$ is the charge of the electron, q_{ion} is the charge of the ion (i.e. q_{ion}/e is an integer) and m_{ion} is the mass of the ion (i.e. the mass of $^{12}\mathrm{C}^{5+}$). Using the theoretically predicted value for the bound-electron g factor, one obtains [16]

$$m_{\mathrm{e}} = 0.000\,548\,579\,909\,067(14)(9)(2)$$

in atomic mass units, where the first two uncertainties are the statistical and systematic ones, and the third uncertainty represents the uncertainty of the theoretical prediction of the g factor and the electron binding energies. For more details, we refer to Ref. [16]. In this context, a similar scheme to determine the mass of the muon or the free-muon g factor has been suggested [7].

A promising way of obtaining a value for the fine-structure constant α is by using the bound-electron g factor in H-like ions (as explained in, e.g., Ref. [51]). To this end, one subtracts from the experimental value of the bound-electron g factor all the corrections (e.g. QED and nuclear effects) to the Dirac value. Equating the result to the Dirac value, which is in the case of H-like ions given by [25]

$$g_{\mathrm{D}} = \frac{2}{3}\left(1 + 2\sqrt{1-(Z\alpha)^2}\right) = 2 - \frac{2}{3}(Z\alpha)^2 + \cdots\,,$$

gives an equation for α. The resulting relative uncertainty of α determined this way is approximately given by [52]

$$\frac{\delta\alpha}{\alpha} \propto \frac{1}{(Z\alpha)^2}\sqrt{(\delta g_{\mathrm{exp}})^2 + (\delta g_{\mathrm{theo}})^2}\,,$$

where δg_{exp}, and δg_{theo} denote the experimental and theoretical uncertainties of the g factor, respectively. This formula suggests that heavy highly charged ions are more suitable for the determination of the fine-structure constant α than light ions. However, nuclear effects like the charge distribution and polarizabilities are not well understood for such highly charged ions and, thus, pose a limitation on δg_{theo} and on the accurate determination of the g factor.

To overcome this obstacle, an idea was developed to construct observables out of g factors which are less sensitive to nuclear effects. In particular, the idea of forming a weighted (or specific) difference of the g factors of H- and Li-like ions with the same nuclear species was put forward [53]. The weight is chosen such that nuclear size effects are suppressed in the weighted difference. This method turned out to be unsuccessful for heavy highly charged ions because in the weighted difference not only the nuclear size effects are suppressed but also the leading dependence of the

bound-electron g factor on $Z\alpha$ [52]. In the same Ref. [52], it was proposed to use a weighted difference between g factors of H- and B-like systems with the same nuclear species as in this case the weight could be chosen such that nuclear size effects are suppressed without significantly suppressing the sensitivity to $Z\alpha$. It was shown that this allows to suppress the nuclear size effect down to 4×10^{-10} for heavy ions such as Pb and was smaller than the uncertainty due to α at that time. In addition, it was shown in Refs. [51, 54] that for low-Z ions one can obtain an even stronger suppression of nuclear effects and this weighted difference of g factors of H- and Li-like ions lead to relative uncertainties of α which were competitive with the value of α according to CODATA 2010 [50].

While the ALPHATRAP experiment performs high-precision bound-electron g factor measurements, another Penning trap setup at the Max Planck Institute for Nuclear Physics aims to perform high-precision mass measurements. The PENTATRAP experiment [55] is able to measure masses of ions on the eV scale and aims to perform high-precision mass measurements on heavy ions with a relative uncertainty below 10^{-11}. Mass measurements enable the determination of binding energies as well as allowing to test relativistic effects in atomic theory. In highly charged ions, besides many-body correlation effects, QED corrections become important as these scale strongly with $Z\alpha$. In particular, the binding energy of the valence electron in rubidiumlike $^{131}Xe^{17+}$ has been directly measured recently with an uncertainty of a few eV [4] and a long-lived metastable electronic state in $^{187}Re^{29+}$ was observed [2]. In future experiments, the binding energy of s-level electrons in highly charged ions is planed to be measured. These electrons strongly interact with the nuclear field since their wave functions have large overlaps with the nucleus. Therefore, QED effects will be strongly enhanced even in many-electron ions, which calls for accurate theoretical calculations of the leading radiative correction given by the self-energy contribution.

In this context, we developed a code base for numerical evaluations of QED effects in atomic systems. In our calculations, we use state-of-the-art numerical methods [56] to solve the radial Dirac equation. We use a nonperturbative approach in the nuclear coupling strength $Z\alpha$, allowing us to perform calculations for a broad range of nuclear charges. In particular, we perform calculations for highly charged ions. We use this code base to calculate radiative corrections to the binding energies of single- and multi-electron systems by combining different approaches of evaluating the self-energy effect [57, 58]. Many-electron systems are treated in the screening-potential approximation. We calculated the correction to the binding energy of the valuence electron in $^{131}Xe^{17+}$ [4] and to the excitation energy of the $4d \to 4f$ excitation in $^{187}Re^{29+}$ [2]. The self-energy correction to the bound-electron wave function has been investigated [3, 5]. We performed calculations of the bound-electron g factor of the Li- and B-like isoelectronic series for a broad range of nuclear charges [1, 6].

Interelectronic and radiative effects on the one-loop level to the ground-state g factor of Li-like and B-like ions are systematically calculated. These calculations for B-like ions have been extended to heavy elements for the first time. Our calculations for Li-like ions establish an independent confirmation of previous results [59, 60], and for B-like ions, we improve the accuracy of previous theoretical predictions [61–64]. The interelectronic interaction on the level of one-photon exchange and vacuum polarization effects have been calculated using QED perturbation theory. In particular, the leading-order screening effect for vacuum polarization corrections has been calculated explicitly including electric and magnetic loop effects. Estimated theoretical uncertainties have been supplemented for each value and our calculations are compared to existing experimental results. We also investigate a new approach to the determination of α using a weighted difference of the bound-state g factor and energy of H-like ions [8], thus avoiding many-electron effects, where we show that for a suitable choice of the weighting factor, nuclear structural effects can be effectively suppressed.

This thesis is organized as follows. In Chapter 1, we give an overview of the QED theory of atomic systems. It is shown that for highly charged ions, the nucleus can be treated as a source of a classical external field to which the bound electrons are exposed. This interaction can be separated from the photonic quantum field and be treated nonperturbatively by solving the Dirac equation in the presence of the external field, while remaining interactions are treated perturbatively. We outline the two-time Green's function formalism (TTGF) of Ref. [65] which allows to relate N-point functions, which are calculated perturbatively using Feynman diagram techniques, to energy shifts.

In Chapter 2, we start by outlining the reduction of the Dirac equation in the presence of an external field to a system of ordinary differential equations in the radial variable assuming a spherically symmetric nuclear potential. The basis set approach solving this radial Dirac equation using B-spline basis functions is discussed. We conclude the chapter by presenting our implementation of the dual kinetic balance (DKB) approach of Ref. [56].

In Chapter 3, we discuss the calculation of the self-energy correction in detail. Our approach, based on finite basis sets constructed using the DKB approach, combines methods of Refs. [57, 58]. Results for self-energy calculations in single- as well as multi-electron systems are presented. In particular, we present the self-energy contributions to the binding energy of the valence electron in $^{131}Xe^{17+}$ and to the difference of the energies of the ground and metastable states in $^{187}Re^{29+}$, both measured by the PENTATRAP experiment [2, 4].

In Chapter 4, we present our calculations of the g factor of Li- and B-like ions accepted for publication in Ref. [1]. We systematically discuss all effects contributing to the g factor of Li- and B-like ions calculated in the scope of this thesis. Results for

a broad range of nuclear charge numbers are presented and compared to previous theoretical studies and recent experimental results. In particular, we present our calculation of the g factor of B-like $^{40}Ar^{13+}$ which has been published separately in our collaborative work with the ALPHATRAP experiment in Ref. [6].

In Chapter 5, we propose a new approach of determining the fine-structure constant α based solely on observables of H-like systems [8]. We introduce a weighted difference of the bound-electron g factor and energy in units of the electron mass, which we call reduced g factor, and investigate the suppression of nuclear structural effects by a particular choice of the weight. We further investigate the sensivity of this new observable with respect to the uncertainty of the fine-structure constant.

We conclude this thesis by an overall discussion of the different QED effects considered and provide an outlook for future research opportunities.

We use a unit system in which the reduced Planck constant $\hbar$, the vacuum speed of light c, and the vacuum permittivity ε_0 are set to unity (i.e. $\hbar = c = \varepsilon_0 = 1$). The charge of the electron is denoted by $e < 0$ and the fine-structure constant is given by $\alpha = e^2/(4\pi)$ in this system of units. In Chapter 4, we additionally set the mass of the electron m_e to one (i.e. $m_\mathrm{e} = 1$). Indices of four-vectors are labeled as usual by Greek letters, for example, a^μ where $\mu = 0, 1, 2, 3$, and we use Einstein's summation convention, where $a_\mu b^\mu$ indicates a sum over the index μ. The metric $g_{\mu\nu}$ is diagonal, with elements $g_{00} = 1$ and $g_{11} = g_{22} = g_{33} = -1$.

1. Theory of Atomic Systems

A first approximation of the energy levels of atomic systems, where electrons are bound to a positively charged nucleus due to its static electric field, can be calculated by solving the stationary Schrödinger equation. For a hydrogen-like (H-like) system, where only one electron is bound to the nucleus, the equation reads

$$\left(-\frac{1}{2m_\mathrm{e}}\Delta - \frac{Ze^2}{4\pi r}\right)\psi_{n\ell m}(\boldsymbol{x}) = E_n\psi_{n\ell m}(\boldsymbol{x})\,. \tag{1.1}$$

In this equation m_e denotes the electron mass, $e < 0$ is the electron charge, Z denotes the nuclear charge number such that $-Ze$ is the charge of the nucleus, $\psi_{n\ell m}$ are the solutions of the stationary Schrödinger equation and E_n are the corresponding energy eigenvalues. While the states are characterized by the principal quantum number n, the orbital angular momentum ℓ, and the magnetic quantum number m, the binding energies depend only on n and are given by

$$E_n = -\frac{1}{2}\left(\frac{Z\alpha}{n}\right)^2 m_\mathrm{e}\,, \tag{1.2}$$

where $\alpha = e^2/(4\pi)$ denotes the fine-structure constant.

The stationary Schrödinger equation describes nonrelativistic electrons bound to the nucleus. However, as the nuclear charge Z increases, relativistic effects become more and more important and need to be taken into account. An easy way to see this is to estimate roughly the velocity of the electron bound to the nucleus. We know from the solution of Eq. (1.1) that the most probable position of an electron in its ground state is at $r_0 = a_0/Z$, with

$$a_0 = \frac{1}{m_\mathrm{e}\alpha} \tag{1.3}$$

denoting the Bohr radius. If we adapt a classical picture and imagine the electron to orbit the nucleus, we obtain using the formula for centripetal forces, that

$$\frac{m_\mathrm{e}v_0^2}{r_0} = \frac{Ze^2}{4\pi r_0^2}\,, \tag{1.4}$$

where v_0 is the velocity of the electron. Solving this equation for v_0 gives

$$v_0 = Z\alpha\,. \tag{1.5}$$

The value of v_0 thus approaches unity as the nuclear charge number Z increases. In particular for highly charged ions, relativistic effects are nonnegligible.

The leading contributions to the energy levels of a relativistic electron bound to the nucleus are given by the solutions of the stationary Dirac equation

$$\left(-i\boldsymbol{\alpha}\cdot\nabla + m_\mathrm{e}\beta - \frac{Ze^2}{4\pi r}\right)\psi_{n\kappa m}(\boldsymbol{x}) = E_{n\kappa}\psi_{n\kappa m}(\boldsymbol{x})\,, \tag{1.6}$$

where $\boldsymbol{\alpha} = (\alpha^1, \alpha^2, \alpha^3)$ and β are the Dirac matrices (we refer to Ref. [66] for an explicit representation of them), $\psi_{n\kappa m}$ are the spinor-valued solutions of the stationary Dirac equation, and $E_{n\kappa}$ are the corresponding eigenvalues. The solutions are again characterized by three quantum numbers as in the nonrelativistic case. However, instead of the orbital angular momentum quantum number ℓ we have now a relativistic angular momentum quantum number κ which takes nonzero integer values and is related to the total angular momentum j and the orbital angular momentum ℓ by $\kappa = (-1)^{j+\ell+1/2}(j+1/2)$. The energy levels of the bound electron are given by

$$E_{n\kappa} = m_\mathrm{e}\left[1 + \left(\frac{Z\alpha}{n - |\kappa| + \sqrt{\kappa^2 - (Z\alpha)^2}}\right)^2\right]^{-\frac{1}{2}}. \tag{1.7}$$

Expanding this expression in the nuclear coupling constant $Z\alpha$ gives

$$E_{n\kappa} = m_\mathrm{e}\left[1 - \frac{1}{2}\left(\frac{Z\alpha}{n}\right)^2 - \frac{1}{2}\left(\frac{Z\alpha}{n}\right)^4\left(\frac{n}{j+\frac{1}{2}} - \frac{3}{4}\right) + \cdots\right]. \tag{1.8}$$

The first term is the electron's rest energy and the second term is the nonrelativistic energy level from Eq. (1.2) obtained by solving Eq. (1.1). The leading relativistic correction to Eq. (1.2) is given by a term which depends on the total angular momentum quantum number j. Thus, the degeneracy in the total angular momentum of Eq. (1.2) is lifted. For example, while according to the nonrelativistic formula in Eq. (1.2) the electron in the states $2p_{1/2}$ and $2p_{3/2}$ has the same energy, there is a splitting between the levels $2p_{1/2}$ and $2p_{3/2}$ which is called the fine-structure splitting.

The Dirac equation only accounts for the leading relativistic effect which is the binding of the electron by the nucleus. There are additionally QED effects which result in corrections to Eq. (1.7). The electron can interact with itself by emitting and reabsorbing virtual photons. The electron can interact with the nucleus through the creation and annihilation of virtual electron-positron pairs. In a multi-electron system, electrons interact among each other by exchanging virtual photons. All these effects imply that we need a QED treatment of relativistic systems.

The idea is thus to treat the binding of the electron by the nucleus nonperturbatively while all other QED effects are treated perturbatively. In this chapter, we

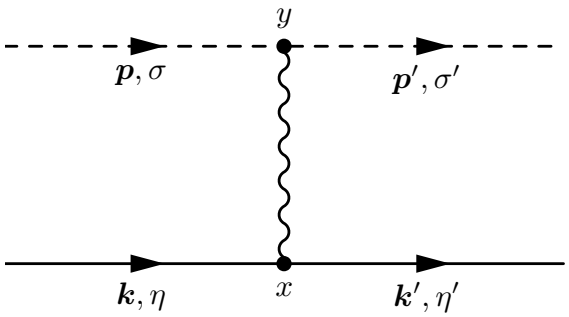

Figure 1.1.: Leading-order contribution to the electron-nucleus scattering amplitude. The dashed line corresponds to the nucleus while the thin line is the electron. The wavy line represents a virtual photon. The labels denote the momenta and spins of the electron and the nucleus.

will introduce the formalism necessary for a QED treatment of bound electrons. We begin by arguing that the interaction of the electron with the nucleus needs to be treated nonperturbatively for bound states to arise and show that this can be done by treating the nucleus as the source of a classical external field following the arguments and derivations of Ref. [67]. This will ultimately lead to the so-called Furry picture of QED [68] where the electron is considered to be exposed to this external field of the nucleus. We then introduce the two-time Green's function (TTGF) formalism of Ref. [65] to relate the perturbative expansion in terms of Feynman diagrams to corrections of the electronic energy levels. We close this chapter by considering some exemplary calculations.

1.1. The external field approximation

Let us consider a H-like system. The energy levels are the poles of the electron-nucleus scattering amplitude as a function of the center-of-mass energy. Within the formalism of QED, this amplitude is calculated perturbatively to some finite order in the nuclear coupling constant $Z\alpha$. However, no term in the perturbative series has these poles. Therefore, the poles arise only from the full sum which means that the interaction of the electron with the nucleus needs to be taken into account nonperturbatively.

When solving the stationary Schrödinger equation (1.1) or the stationary Dirac equation (1.6), the nucleus is assumed to be the source of a classical static external field since the nucleus is much heavier than the electron. We will show in the following that this assumption allows us to include the interaction between the electron and the nucleus into the QED Lagrangian and account for this effect in a nonperturbative manner. In doing so, we follow the derivations of Ref. [67].

The leading contribution to the electron-nucleus scattering amplitude is given by the Feynman diagram depicted in Fig. 1.1. The corresponding matrix element is

$$\begin{aligned}(-i)^2 \int d^4x \int d^4y \, \langle \boldsymbol{p}'\sigma' N; \boldsymbol{k}'\eta' e| \, T\left[A_\mu(x) J_e^\mu(x) A_\nu(y) J_N^\nu(y)\right] |\boldsymbol{p}\sigma N; \boldsymbol{k}\eta e\rangle \\ = (-i)^2 \int d^4x \int d^4y \, \langle \boldsymbol{k}'\eta' e| \, J_e^\mu(x) \, |\boldsymbol{k}\eta e\rangle \, \langle \boldsymbol{p}'\sigma' N| \, J_N^\nu(y) \, |\boldsymbol{p}\sigma N\rangle \, D_{\mu\nu}(x-y) \,, \quad (1.9)\end{aligned}$$

where e and N label the electron and the nucleus, respectively. The operators $J_e^\mu(x)$ and $J_N^\nu(y)$ denote the corresponding four-currents, the function

$$D_{\mu\nu}(x-y) = \int \frac{d^4q}{(2\pi)^4} \frac{-ig_{\mu\nu}}{q^2 + i0^+} e^{-iq\cdot(x-y)} \quad (1.10)$$

is the photon propagator in Feynman gauge, and 0^+ denotes a small positive number which is taken to be zero in the final result. The symbol T in Eq. (1.9) denotes the time-ordering operator which orders the operators in decreasing order of their time variables, taking into account possible minus signs that arise when commuting fermionic operators. We focus on the part of Eq. (1.9) involving the nucleus N and write the nuclear Green's function

$$\mathcal{G}^\nu_{\sigma'\sigma}(q;p) = -i \int d^4y \, e^{iq\cdot y} \, \langle \boldsymbol{p}'\sigma' N| \, J_N^\nu(y) \, |\boldsymbol{p}\sigma N\rangle \,. \quad (1.11)$$

The matrix element of the nuclear current operator is

$$\langle \boldsymbol{p}'\sigma' N| \, J_N^\nu(y) \, |\boldsymbol{p}\sigma N\rangle = -Ze \frac{\bar{u}^N_{\sigma'}(\boldsymbol{p}')\gamma^\nu u^N_\sigma(\boldsymbol{p})}{\sqrt{2p'^0}\sqrt{2p^0}} e^{i(p'-p)\cdot y} \,, \quad (1.12)$$

where the energies p'^0 and p^0 are on-shell, γ^μ denote the Dirac gamma matrices [66], and $\bar{\psi} = \psi^\dagger\gamma^0$ for a spinor ψ. The spinors $u^f_\sigma(\boldsymbol{p})$ denote the positive energy solutions of the stationary free Dirac equation

$$(-i\boldsymbol{\alpha}\cdot\nabla + \beta m_f)\psi(\boldsymbol{x}) = E\psi(\boldsymbol{x}) \,, \quad (1.13)$$

for a fermion of type f. Explicitly, they read [66]

$$u^f_\sigma(\boldsymbol{p}) = \sqrt{m_f + p^0} \begin{pmatrix} \xi_\sigma \\ \frac{\boldsymbol{\sigma}\cdot\boldsymbol{p}}{m_f + p^0}\xi_\sigma \end{pmatrix} , \quad (1.14)$$

where $p^0 = \sqrt{m_f^2 + \boldsymbol{p}^2}$ is on-shell, $\boldsymbol{\sigma} = (\sigma^1, \sigma^2, \sigma^3)$ are the Pauli matrices, and σ takes the values $\pm 1/2$ with

$$\xi_{+1/2} = \begin{pmatrix} 1 \\ 0 \end{pmatrix} \quad \text{and} \quad \xi_{-1/2} = \begin{pmatrix} 0 \\ 1 \end{pmatrix} . \quad (1.15)$$

Integrating over y in Eq. (1.11), we obtain

$$\mathcal{G}^{\nu}_{\sigma'\sigma}(q;p) = (2\pi)^4\delta^{(4)}(p'-p+q)\frac{iZe\bar{u}^N_{\sigma'}(\boldsymbol{p}')\gamma^{\nu}u^N_{\sigma}(\boldsymbol{p})}{\sqrt{2p'^0}\sqrt{2p^0}}\,. \tag{1.16}$$

In the limit $q \to 0$, we have that $p' \approx p$ and

$$\frac{\bar{u}^N_{\sigma'}(\boldsymbol{p}')\gamma^{\nu}u^N_{\sigma}(\boldsymbol{p})}{\sqrt{2p'^0}\sqrt{2p^0}} \to \frac{2p^{\nu}\delta_{\sigma'\sigma}}{2p^0}\,. \tag{1.17}$$

In the same limit, the delta function in Eq. (1.16) may be expanded to leading order in q using the identity $|t|\delta(tx) = \delta(x)$ and that $\boldsymbol{q} = \boldsymbol{p} - \boldsymbol{p}'$, with the result

$$\delta^{(4)}(p'-p+q) \approx p^0\delta(p\cdot q)\delta^{(3)}(\boldsymbol{p}'-\boldsymbol{p}+\boldsymbol{q})\,. \tag{1.18}$$

Substituting Eqs. (1.17) and (1.18) in Eq. (1.16) gives

$$\mathcal{G}^{\nu}_{\sigma'\sigma}(q;p) \to (2\pi)^3\delta^{(3)}(\boldsymbol{p}'-\boldsymbol{p}+\boldsymbol{q})2\pi iZep^{\nu}\delta_{\sigma'\sigma}\delta(p\cdot q)\,, \tag{1.19}$$

in the limit $q \to 0$.

At this point, we use our assumption that the nucleus is a nonrelativistic heavy particle with $|\boldsymbol{p}| \ll p^0$. Again, using the identity $|t|\delta(tx) = \delta(x)$ for the delta function, we can write

$$\delta(p\cdot q) \approx \frac{\delta(q^0)}{p^0}\,. \tag{1.20}$$

Substituting this into Eq. (1.19) gives

$$\mathcal{G}^{\nu}_{\sigma'\sigma}(q;p) \to (2\pi)^3\delta^{(3)}(\boldsymbol{p}'-\boldsymbol{p}+\boldsymbol{q})2\pi iZen^{\nu}\delta_{\sigma'\sigma}\delta(q^0)\,, \tag{1.21}$$

where n^{ν} is a unit time-like vector with $n^0 = 1$ and $\boldsymbol{n} = 0$. We assume that the nucleus has some momentum space wave function $\chi_{\sigma}(\boldsymbol{p})$ such that

$$\phi_{\sigma}(\boldsymbol{x}) = \int \frac{d^3p}{(2\pi)^3}\,\chi_{\sigma}(\boldsymbol{p})e^{i\boldsymbol{p}\cdot\boldsymbol{x}} \tag{1.22}$$

is its position space wave function. Then, we obtain that

$$\int \frac{d^3p'}{(2\pi)^3}\sum_{\sigma'}\int \frac{d^3p}{(2\pi)^3}\sum_{\sigma}\chi^*_{\sigma'}(\boldsymbol{p}')\mathcal{G}^{\nu}_{\sigma'\sigma}(q;p)\chi_{\sigma}(\boldsymbol{p}) \to \int d^3z\sum_{\sigma}|\phi_{\sigma}(\boldsymbol{z})|^2 2\pi iZen^{\nu}\delta(q^0)e^{-i\boldsymbol{q}\cdot\boldsymbol{z}} \tag{1.23}$$

Turning back to Eq. (1.9), the electronic part reads

$$-i\int d^4x e^{-iq\cdot x}\left\langle \boldsymbol{k}'\eta' e\right| J^{\mu}_e(x)\left|\boldsymbol{k}\eta e\right\rangle = (2\pi)^4\delta^{(4)}(k'-k-q)\frac{-ie\bar{u}^e_{\eta'}(\boldsymbol{k}')\gamma^{\mu}u^e_{\eta}(\boldsymbol{k})}{\sqrt{2k'^0}\sqrt{2k^0}}\,, \tag{1.24}$$

where k'^0 and k^0 are on-shell. Combining all the results, we see that including a nonrelativistic heavy nucleus is the same as adding a new vertex to the Feynman rules, where the electrons couple to an external field and the corresponding vertex reads

$$-\int \frac{d^4q}{(2\pi)^4} \frac{-2\pi Zen_\mu \delta(q^0)}{q^2+i0^+} e^{-i\boldsymbol{q}\cdot\boldsymbol{z}}(-ie)\gamma^\mu(2\pi)^4\delta^{(4)}(k'-k-q)\,. \tag{1.25}$$

The scattering amplitude then needs to be averaged by the nuclear distribution function $\sum_\sigma |\phi_\sigma(\boldsymbol{z})|^2$. This is the same contribution to the scattering amplitude that would result from an additional interaction term in the QED Lagrangian given by

$$\mathcal{L}_{\text{ext}}(x) = \mathcal{A}_\mu(x) J_e^\mu(x)\,, \tag{1.26}$$

where $\mathcal{A}^\mu(x)$ is an classical external field given by

$$\mathcal{A}^\mu(x) = \int \frac{d^4q}{(2\pi)^4} \frac{-2\pi Zen^\mu \delta(q^0)}{q^2+i0^+} e^{-i\boldsymbol{q}\cdot\boldsymbol{z}} e^{-iq\cdot x}\,. \tag{1.27}$$

Performing the Fourier transform in Eq. (1.27) gives

$$\mathcal{A}^0(x) = -\frac{Ze}{4\pi|\boldsymbol{x}-\boldsymbol{z}|}\,, \tag{1.28}$$

and the vector components $\mathcal{A}^i(x)$ vanish. This is the expression for the Coulomb potential of a point-like nucleus centered at the position $\boldsymbol{z}$.

The question arises whether this reasoning can be generalized to an arbitrary number of exchanged photons between the electron and the nucleus. The contribution coming from the nucleus to the electron-nucleus scattering diagrams involving n exchanged photons[1] is

$$\begin{aligned}\mathcal{G}^{\mu_1\cdots\mu_n}_{\sigma'\sigma}(q_1,\ldots,q_n;p) = (-i)^n \int d^4x_1\, e^{iq_1\cdot x_1}\cdots\int d^4x_n\, e^{iq_n\cdot x_n} \\ \times \langle \boldsymbol{p}'\sigma' N|\, T\left[J_N^{\mu_1}(x_1)\cdots J_N^{\mu_n}(x_n)\right]|\boldsymbol{p}\sigma N\rangle\,.\end{aligned} \tag{1.29}$$

We consider the next-to-leading order (i.e. $n=2$ in Eq. (1.29)) contribution to the scattering amplitude explicitly. The corresponding diagrams are depicted in Fig. 1.2. The contribution coming from the nucleus is given by

$$\begin{aligned}\mathcal{G}^{\mu_1\mu_2}_{\sigma'\sigma}(q_1,q_2;p) = (-i)^2 \int d^4x_1\, e^{iq_1\cdot x_1}\int d^4x_2\, e^{iq_2\cdot x_2} \\ \times \langle \boldsymbol{p}'\sigma' N|\, T\left[J_N^{\mu_1}(x_1)J_N^{\mu_2}(x_2)\right]|\boldsymbol{p}\sigma N\rangle\,.\end{aligned} \tag{1.30}$$

[1] This n is not to be confused with the principal quantum number introduced earlier.

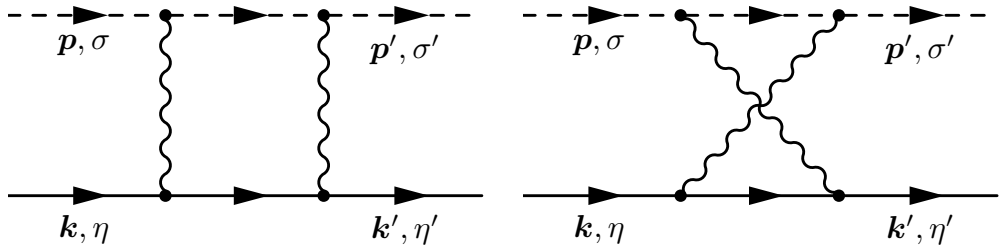

Figure 1.2.: Contributions to the electron-nucleus scattering amplitude involving two exchanged photons. Labels denote the momenta and spins of the incoming and outgoing particles.

We separate the time ordering in Eq. (1.30) into two pieces as

$$T\left[J_N^{\mu_1}(x_1)J_N^{\mu_2}(x_2)\right] = \Theta(x_1^0-x_2^0)J_N^{\mu_1}(x_1)J_N^{\mu_2}(x_2)+\Theta(x_2^0-x_1^0)J_N^{\mu_2}(x_2)J_N^{\mu_1}(x_1)\,. \quad (1.31)$$

We consider the first term where $x_1^0 > x_2^0$. Inserting the spectral resolution of the identity operator in between the current operators, we obtain

$$\begin{aligned}&\Theta(x_1^0-x_2^0)\left\langle \boldsymbol{p}'\sigma' N\right| J_N^{\mu_1}(x_1)J_N^{\mu_2}(x_2)\left|\boldsymbol{p}\sigma N\right\rangle \\ &\quad = \Theta(x_1^0-x_2^0)\sum_\eta \int \frac{d^3k}{(2\pi)^3}\left\langle \boldsymbol{p}'\sigma' N\right| J_N^{\mu_1}(x_1)\left|\boldsymbol{k}\eta N\right\rangle \left\langle \boldsymbol{k}\eta N\right| J_N^{\mu_2}(x_2)\left|\boldsymbol{p}\sigma N\right\rangle + \cdots\,,\end{aligned} \quad (1.32)$$

where we separated out the contribution resulting from the same type of intermediate states as the initial and final states and the dots denote omitted terms of the spectral resolution of the identity. Since the four-momentum operator is the generator of space-time translations, we can write

$$\left\langle \boldsymbol{p}'\sigma' N\right| J_N^{\mu}(x)\left|\boldsymbol{p}\sigma N\right\rangle = \left\langle \boldsymbol{p}'\sigma' N\right| J_N^{\mu}(0)\left|\boldsymbol{p}\sigma N\right\rangle e^{i(p'-p)\cdot x}\,. \quad (1.33)$$

We also use the integral representation of the Heaviside function given by [69]

$$\Theta(t) = \frac{i}{2\pi}\int d\omega\,\frac{1}{\omega+i0^+}e^{-i\omega t}\,. \quad (1.34)$$

Substituting Eqs. (1.33) and (1.34) into Eq. (1.32) and calculating the integrals over x_1 and x_2 from Eq. (1.30) as well as integrating over k and ω, we obtain that

$$\begin{aligned}(-i)^2\int d^4x_1\,e^{iq_1\cdot x_1}\int d^4x_2\,e^{iq_2\cdot x_2}\Theta(x_1^0-x_2^0)\left\langle \boldsymbol{p}'\sigma' N\right| J_N^{\mu_1}(x_1)J_N^{\mu_2}(x_2)\left|\boldsymbol{p}\sigma N\right\rangle \\ \to -i(2\pi)^4\delta^{(4)}(p'-p+q_1+q_2)\frac{1}{2p^0}\sum_\eta \frac{\mathcal{G}^{\mu_1}_{\sigma'\eta}(p)\mathcal{G}^{\mu_2}_{\eta\sigma}(p)}{2p\cdot q_1+i0^+}\,,\end{aligned} \quad (1.35)$$

as $q_1, q_2 \to 0$, where

$$\frac{\mathcal{G}^{\mu}_{\sigma'\sigma}(p)}{2p^0} = \langle \boldsymbol{p}\sigma' N| \, J^{\mu}_N(0) \, |\boldsymbol{p}\sigma N\rangle \, . \tag{1.36}$$

Eq. (1.17) implies that

$$\mathcal{G}^{\mu}_{\sigma'\sigma}(p) = -2Zep^{\mu}\delta_{\sigma'\sigma} \, . \tag{1.37}$$

For the second term in Eq. (1.31), we need to exchange q_1 and q_2 as well as μ_1 and μ_2 in the above expressions. Putting everything together, we obtain that

$$\begin{aligned}\mathcal{G}^{\mu_1\mu_2}_{\sigma'\sigma}(q_1, q_2; p) \to (2\pi)^4\delta(p' - p + q_1 + q_2)\frac{i}{p^0}(iZe)^2 p^{\mu_1}p^{\mu_2}\delta_{\sigma'\sigma} \\ \times \left(\frac{1}{p\cdot q_1 + i0^+} + \frac{1}{p\cdot q_2 + i0^+}\right) \, ,\end{aligned} \tag{1.38}$$

in the limit $q_1, q_2 \to 0$. Using Eq. (1.18) results in

$$\begin{aligned}\mathcal{G}^{\mu_1\mu_2}_{\sigma'\sigma}(q_1, q_2; p) \to (2\pi)^3\delta(\boldsymbol{p}' - \boldsymbol{p} + \boldsymbol{q}_1 + \boldsymbol{q}_2)2\pi i(iZe)^2 p^{\mu_1}p^{\mu_2}\delta_{\sigma'\sigma} \\ \times \delta(p\cdot(q_1 + q_2))\left(\frac{1}{p\cdot q_1 + i0^+} + \frac{1}{p\cdot q_2 + i0^+}\right) \, .\end{aligned} \tag{1.39}$$

Since $p\cdot(q_1 + q_2) = 0$, we have that

$$\frac{1}{p\cdot q_1 + i0^+} + \frac{1}{p\cdot q_2 + i0^+} = \frac{1}{p\cdot q_1 + i0^+} + \frac{1}{-p\cdot q_1 + i0^+} \, . \tag{1.40}$$

Using the identity

$$\delta(x) = \frac{i}{2\pi}\left(\frac{1}{x + i0^+} + \frac{1}{-x + i0^+}\right) \tag{1.41}$$

for the delta function in Eq. (1.40) and substituting it in Eq. (1.39) gives

$$\mathcal{G}^{\mu_1\mu_2}_{\sigma'\sigma}(q_1, q_2; p) \to (2\pi)^3\delta^{(3)}(\boldsymbol{p}' - \boldsymbol{p} + \boldsymbol{q}_1 + \boldsymbol{q}_2)(2\pi iZe)^2 p^{\mu_1}p^{\mu_2}\delta_{\sigma'\sigma}\delta(p\cdot q_1)\delta(p\cdot q_2) \, . \tag{1.42}$$

This equation is the equivalent for two exchanged photons of Eq. (1.19) and applying the same derivation which lead to Eq. (1.21), we obtain that

$$\mathcal{G}^{\mu_1\mu_2}_{\sigma'\sigma}(q_1, q_2; p) \to (2\pi)^3\delta^{(3)}(\boldsymbol{p}' - \boldsymbol{p} + \boldsymbol{q}_1 + \boldsymbol{q}_2)(2\pi iZe)^2 n^{\mu_1}n^{\mu_2}\delta_{\sigma'\sigma}\delta(q_1^0)\delta(q_2^0) \, . \tag{1.43}$$

That is, assuming a heavy nonrelativistic nucleus, the next-to-leading order contribution to the electron-nucleus scattering amplitude is obtained by inserting two Coulomb potentials.

This reasoning can in fact be generalized to an arbitrary number of exchanged photons. The derivation is analogous to the $n = 2$ case. For details, we refer to Ref. [67]. That is, in the limit $q_1, \ldots, q_n \to 0$, we obtain that

$$\mathcal{G}^{\mu_1\cdots\mu_n}_{\sigma'\sigma}(q_1, \ldots, q_n; p) \to (2\pi)^3\delta^{(3)}(\boldsymbol{p}' - \boldsymbol{p} + \boldsymbol{q}_1 + \cdots + \boldsymbol{q}_n)\delta_{\sigma'\sigma}\prod_{j=1}^{n} 2\pi iZen^{\mu_j}\delta(q_j^0) \, . \tag{1.44}$$

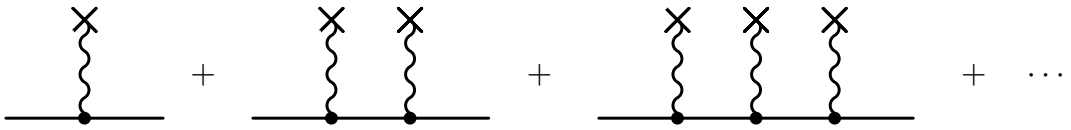

Figure 1.3.: Scattering of the electron of the static field of the nucleus. Photon lines ending with a cross correspond to interactions with the external field.

This in turn means that diagrams involving the exchange of n photons between the electron and the heavy nucleus in all possible orders can, effectively, be approximated by diagrams of the kind depicted in Fig. 1.3 where then n vertices resulting from the interaction term in Eq. (1.26) are inserted between electron propagators. In particular, the first diagram in Fig. 1.3 corresponds to the diagram in Fig. 1.1, and the second one to the diagrams in Fig. 1.2. The electron propagator in the external field of the nucleus has then the expansion

$$\begin{aligned} S(x,y) = S_0(x-y) &+ \int d^4z_1\, S_0(x-z_1) e\gamma^\mu \mathcal{A}_\mu(z_1) S_0(z_1-y) \\ &+ \int d^4z_1 \int d^4z_2\, S_0(x-z_1) e\gamma^\mu \mathcal{A}_\mu(z_1) S_0(z_1-z_2) e\gamma^\nu \mathcal{A}_\nu(z_2) S_0(z_2-y) + \cdots , \end{aligned} \tag{1.45}$$

where S_0 denotes the (free) electron propagator

$$S_0(x-y) = \int \frac{d^4p}{(2\pi)^4} \frac{i(\gamma^\mu p_\mu + m_\mathrm{e})}{p^2 - m_\mathrm{e}^2 + i0^+} e^{-ip\cdot(x-y)} . \tag{1.46}$$

Perturbative calculations are done using S instead of S_0 for electrons bound to the nucleus.

In general, S depends separately on x and y as the external potential $\mathcal{A}^\mu(x)$ breaks translational invariance. In the case of the static nuclear potential, since the external potential is time-independent, translational invariance with respect to time is preserved and S depends on x^0 and y^0 through $x^0 - y^0$. In the following, we will derive an expression for S in terms of the solutions of the stationary Dirac equation.

1.2. QED in the Furry picture

As our discussion so far shows, the interaction of electrons with the nucleus can be taken into account by adding the interaction term in Eq. (1.26) to the QED Lagrangian. It is this interaction with the Coulomb field of the nucleus that needs to be taken into account nonperturbatively. For this purpose, we rewrite the QED Lagrangian with the external potential in the form

$$\mathcal{L}_\mathrm{QED+ext} = -\frac{1}{4} F_{\mu\nu} F^{\mu\nu} + \bar{\psi}(i\gamma^\mu \partial_\mu - m_\mathrm{e} - e\gamma^\mu \mathcal{A}_\mu)\psi - eA_\mu \bar{\psi}\gamma^\mu \psi , \tag{1.47}$$

where we shifted the new interaction term into the Dirac part of the Lagrangian. In this Lagrangian, ψ is the electronic quantum field, A^μ is the quantum field operator of the photon, whereas $\mathcal{A}^\mu$ denotes the classical vector field representing the effect of the nucleus, and $F^{\mu\nu} = \partial^\mu A^\nu - \partial^\nu A^\mu$ is the electromagnetic field operator.

In the following, we consider just the part of the Lagrangian containing the Dirac term in the presence of an external field, given by

$$\mathcal{L}_{\mathrm{D+ext}} = \bar{\psi}(i\gamma^\mu \partial_\mu - m_\mathrm{e} - e\gamma^\mu \mathcal{A}_\mu)\psi \,, \tag{1.48}$$

and neglect the terms involving the quantum field A^μ of the photon. The field ψ is the electronic quantum field in the Heiseberg picture in which the time-dependence is determined by the Hamiltonian arising from the Lagrangian in Eq. (1.48). The interaction with the nucleus is taken into account nonperturbatively by solving the Dirac equation for the electronic quantum field ψ in the presence of the nuclear potential

$$(i\gamma^\mu \partial_\mu - m_\mathrm{e} - e\gamma^\mu \mathcal{A}_\mu(x))\psi(x) = 0 \,. \tag{1.49}$$

This is referred to as QED in the Furry picture [68].

We are mainly interested in static nuclear potentials. Therefore, we will assume in the following that only the component $\mathcal{A}^0$ of the external field is nonvanishing and that it is time-independent. We denote by $V(\boldsymbol{x}) = e\mathcal{A}^0(\boldsymbol{x})$ the potential energy. We can then expand the electronic field operator as

$$\psi(t, \boldsymbol{x}) = \sum_n^{\varepsilon_n > 0} a_n \psi_n(\boldsymbol{x}) e^{-i\varepsilon_n t} + \sum_n^{\varepsilon_n < 0} b_n^\dagger \psi_n(\boldsymbol{x}) e^{-i\varepsilon_n t} \,, \tag{1.50}$$

where the ψ_n are solutions of the stationary Dirac equation in the presence of the static field of the nucleus

$$(-i\boldsymbol{\alpha} \cdot \nabla + \beta m_\mathrm{e} + V(\boldsymbol{x}))\psi_n(\boldsymbol{x}) = \varepsilon_n \psi_n(\boldsymbol{x}) \,, \tag{1.51}$$

and ε_n are the corresponding eigenvalues. The index n denotes here all quantum numbers necessary to characterize the states and these quantum numbers may be continuous, in which case the sums in Eq. (1.50) need to be interpreted as integrals with proper normalizations. The operators $a_n^\dagger, a_n$ and $b_n^\dagger, b_n$ are creation and annihilation operators for electrons and positrons, respectively. That is, single electron and positron states are given by

$$a_n^\dagger |0\rangle = |n, e^-\rangle \,, \tag{1.52}$$

$$b_n^\dagger |0\rangle = \left|n, e^+\right\rangle \,, \tag{1.53}$$

respectively, where $|0\rangle$ denotes the vacuum in the presence of the external field.

The propagator of the electron in the external field of the nucleus is given by

$$S(x,y) = \langle 0|\, T\left[\psi(x)\bar{\psi}(y)\right] |0\rangle \ . \tag{1.54}$$

Writing the time-ordering operator explicitly in terms of Heaviside functions, using the expansion of the electronic quantum field from Eq. (1.50) and integral representations of the Heaviside functions, we obtain

$$S(x,y) = \frac{i}{2\pi}\int_{-\infty}^{+\infty} d\omega \sum_n \frac{\psi_n(\boldsymbol{x})\bar{\psi}_n(\boldsymbol{y})}{\omega - \varepsilon_n(1-i0^+)} e^{-i\omega(x^0-y^0)} \ . \tag{1.55}$$

We see that the propagator depends on the time variables x^0 and y^0 through their difference $x^0 - y^0$. Thus, we may perform the Fourier transform with respect to the time variable and express the propagator as a function of energy and coordinates. The expression reads

$$\frac{i}{2\pi} S(\omega, \boldsymbol{x}, \boldsymbol{y}) = \frac{i}{2\pi}\sum_n \frac{\psi_n(\boldsymbol{x})\bar{\psi}_n(\boldsymbol{y})}{\omega - \varepsilon_n(1-i0^+)} \ . \tag{1.56}$$

This expression has poles at the bound states of the electron and branch cuts from $(-\infty, -m_\mathrm{e}]$ and $[m_\mathrm{e}, +\infty)$. As it was argued in the beginning of the previous section, the unperturbed energy levels of the bound electron can be obtained from the poles of this propagator which corresponds to the electron-nucleus scattering amplitude with the interaction between the electron and the nucleus summed up to all orders.

Note however, that the poles of the propagator in Eq. (1.56) only give the leading relativistic expression for the energy levels of bound electrons resulting from the stationary Dirac equation as it was derived starting from the Lagrangian in Eq. (1.48). To obtain the radiative corrections to these leading values, one needs to consider the propagator derived from the full Lagrangian in Eq. (1.47) including the interaction with the quantum field of the photon. More generally, the energy levels including QED effects for atomic systems with N electrons can be obtained from the poles of the spectral representation of N-point functions. This will be the topic of the following section.

1.3. Energy levels of atomic systems

Consider an atomic system with N electrons. We now use the full theory defined by the Lagrangian in Eq. (1.47). The energy levels can be obtained from the spectral representation of the N-point Green's function [65]

$$G(x_1', \ldots, x_N'; x_1, \ldots, x_N) = \langle \Omega_0|\, T\left[\psi(x_1')\cdots\psi(x_N')\bar{\psi}(x_N)\cdots\bar{\psi}(x_1)\right] |\Omega_0\rangle \ , \tag{1.57}$$

where $|\Omega_0\rangle$ is the full vacuum state and where ψ now denotes the electronic field in the Heisenberg picture in which the time-dependence is governed by the full Hamiltonian arising from the Lagrangian in Eq. (1.47).

As usual, this N-point function is computed perturbatively by passing to the interaction picture using the Gell-Mann-Low formula [65]

$$G(x_1', \ldots, x_N'; x_1, \ldots, x_N) = \frac{\langle 0| T\left[\psi_I(x_1') \cdots \psi_I(x_N') \bar{\psi}_I(x_N) \cdots \bar{\psi}_I(x_1) e^{-i\int d^4z\, \mathcal{H}_I(z)}\right] |0\rangle}{\langle 0| T\left[e^{-i\int d^4z\, \mathcal{H}_I(z)}\right] |0\rangle}, \quad (1.58)$$

where the label I denotes the corresponding field in the interaction picture and $\mathcal{H}_I(z)$ is the interaction Hamiltonian given by

$$\mathcal{H}_I(z) = e\bar{\psi}_I(z)\gamma_\mu\psi_I(z)A_I^\mu(z) - \delta m_\mathrm{e}\bar{\psi}_I(z)\psi_I(z). \quad (1.59)$$

Note that we include from now on the mass renormalization counterterm δm_e in the interaction. The interaction of the electronic field with the nucleus is part of the unperturbed Hamiltonian resulting from Eq. (1.48). This is then computed perturbatively using the Feynman diagram technique.

Since time translations are not broken by the static electric field of the nucleus, it is convenient to perform the Fourier transforms of Eq. (1.57) with respect to the time variables:

$$G((E_1', \boldsymbol{x}_1'), \ldots, (E_N', \boldsymbol{x}_N'); (E_1, \boldsymbol{x}_1), \ldots, (E_N, \boldsymbol{x}_N)) = \int \frac{dx_1'^0}{2\pi} e^{iE_1'x_1'^0} \cdots \int \frac{dx_N'^0}{2\pi} e^{iE_N'x_N'^0} \int \frac{dx_1^0}{2\pi} e^{-iE_1x_1^0} \cdots \int \frac{dx_N^0}{2\pi} e^{-iE_Nx_N^0} \times G(x_1', \ldots, x_N'; x_1, \ldots, x_N). \quad (1.60)$$

The Feynman rules in position space to compute this N-point function are the same as for usual QED except that instead of the free-electron propagator we need to use the electron propagator in the Furry picture from Eq. (1.56).

The energy levels of the atomic system can be obtained from the spectral representation of the Fourier transformed N-point function given in Eq. (1.60). However, it is hard to extract these levels from this expression directly as it depends on $2(N-1)$ relative energies. It turns out that the spectral representation of the two-time Green's function defined by

$$\tilde{G}(t', \boldsymbol{x}_1', \ldots, \boldsymbol{x}_N'; t, \boldsymbol{x}_1, \ldots, \boldsymbol{x}_N) = G((t', \boldsymbol{x}_1'), \ldots, (t', \boldsymbol{x}_N'); (t, \boldsymbol{x}_1), \ldots, (t, \boldsymbol{x}_N)) \quad (1.61)$$

can be used instead to extract the energy levels of the atomic system. This is shown in Ref. [65]. In the following, we present the derivation from Ref. [65].

To obtain the spectral representation of Eq. (1.61), we first Fourier transform with respect to the time variables

$$2\pi i\delta(E'-E)\mathcal{G}(E,\boldsymbol{x}',\boldsymbol{x}) = \frac{1}{N!}\int dt'\, e^{iE't'}\int dt\, e^{-iEt}\tilde{G}(t',\boldsymbol{x}';t,\boldsymbol{x})\,, \tag{1.62}$$

where $\boldsymbol{x}'$ and $\boldsymbol{x}$ denote the collections of all $\boldsymbol{x}'_1,\ldots,\boldsymbol{x}'_N$ and $\boldsymbol{x}_1,\ldots,\boldsymbol{x}_N$, respectively. Let H denote the Hamiltonian of the full theory and let $|\Omega_n\rangle$ denote eigenstates of H with energies E_n. That is

$$H\,|\Omega_n\rangle = E_n\,|\Omega_n\rangle\ . \tag{1.63}$$

Without loss of generality, we assume for the vacuum energy $E_0 = 0$. Using that the Heisenberg picture operators can be written as

$$\psi(t,\boldsymbol{x}) = e^{iHt}\psi(0,\boldsymbol{x})e^{-iHt}\,, \tag{1.64}$$

and inserting resolutions of the identity operator in terms of the states $|\Omega_n\rangle$ in Eq. (1.62), we obtain

$$\begin{aligned}
&2\pi i\delta(E'-E)\mathcal{G}(E,\boldsymbol{x}',\boldsymbol{x})\\
&\quad= \frac{1}{N!}\int dt'\, e^{iE't'}\int dt\, e^{-iEt}\left[\Theta(t'-t)\sum_n \Phi_n(\boldsymbol{x}')\bar{\Phi}_n(\boldsymbol{x})e^{-iE_n(t'-t)}\right.\\
&\qquad\left.+(-1)^N\Theta(t-t')\sum_n \Xi_n(\boldsymbol{x}')\bar{\Xi}_n(\boldsymbol{x})e^{-iE_n(t-t')}\right]\,,
\end{aligned} \tag{1.65}$$

where

$$\Phi_n(\boldsymbol{x}_1,\ldots,\boldsymbol{x}_N) = \frac{1}{\sqrt{N!}}\,\langle\Omega_0|\,\psi(0,\boldsymbol{x}_1)\cdots\psi(0,\boldsymbol{x}_N)\,|\Omega_n\rangle\ , \tag{1.66}$$

$$\Xi_n(\boldsymbol{x}_1,\ldots,\boldsymbol{x}_N) = \frac{1}{\sqrt{N!}}\,\langle\Omega_n|\,\psi(0,\boldsymbol{x}_1)\cdots\psi(0,\boldsymbol{x}_N)\,|\Omega_0\rangle\ . \tag{1.67}$$

Using the integral representations of the Heaviside functions in Eq. (1.65), we obtain that

$$\mathcal{G}(E,\boldsymbol{x}',\boldsymbol{x}) = \sum_n \frac{\Phi_n(\boldsymbol{x}')\bar{\Phi}_n(\boldsymbol{x})}{E-E_n+i0^+} - (-1)^N\sum_n \frac{\Xi_n(\boldsymbol{x}')\bar{\Xi}_n(\boldsymbol{x})}{E+E_n-i0^+} \tag{1.68}$$

The energy levels of the bound states are the poles of $\mathcal{G}(E)$ on the right-hand real axis. If we neglect the interaction between the electronic field and the photon field, then these poles are isolated. However, the presence of the interaction transforms these poles into branch points, since photons have vanishing mass [65, 70]. In order to isolate these poles from the branch cuts, we introduce a non-zero photon mass which is assumed to be larger than the energy shift of the level under consideration

but smaller than the distance to other levels. The photon mass is then taken to be zero in the final expression.

Let the label $a = (a_1, \ldots, a_N)$ denote the state of the atomic system under consideration, i.e., the reference state, with the energy level E_a. The unperturbed energy level (i.e. the energy level neglecting the quantum interaction between the electron-positron and the photon fields) is given by the sum of the solutions of the Dirac equation in the presence of the external field in Eq. (1.51) as

$$E_a^{(0)} = \varepsilon_{a_1} + \cdots + \varepsilon_{a_N} \,. \tag{1.69}$$

The corresponding unperturbed wave function is the Slater determinant of the solutions of Eq. (1.51)

$$u_a(\boldsymbol{x}_1, \ldots, \boldsymbol{x}_N) = \frac{1}{\sqrt{N!}} \sum_\sigma \operatorname{sign} \sigma \psi_{\sigma(a_1)}(\boldsymbol{x}_1) \cdots \psi_{\sigma(a_N)}(\boldsymbol{x}_N) \,, \tag{1.70}$$

where σ denotes the permutation of the labels $a_1, \ldots, a_N$. We define the function

$$g_{aa}(E) = \langle u_a | \, \mathcal{G}(E) \gamma_1^0 \cdots \gamma_N^0 \, | u_a \rangle \,. \tag{1.71}$$

Explicitly, Eq. (1.71) reads

$$g_{aa}(E) = \int d^{3N}x' \int d^{3N}x \, u_a^\dagger(\boldsymbol{x}') \mathcal{G}(E, \boldsymbol{x}', \boldsymbol{x}) \gamma_1^0 \cdots \gamma_N^0 u_a(\boldsymbol{x}) \,. \tag{1.72}$$

Using the spectral representation of $\mathcal{G}(E)$ given in Eq. (1.68), we see that

$$g_{aa}(E) = \frac{A_a}{E - E_a} + \text{terms regular at } E = E_a \,, \tag{1.73}$$

where the residue A_a is given by

$$A_a = \frac{1}{N!} \int d^{3N}x' \int d^{3N}x \, u_a^\dagger(\boldsymbol{x}') \Phi_a(\boldsymbol{x}') \Phi_a^\dagger(\boldsymbol{x}) u_a(\boldsymbol{x}) \,. \tag{1.74}$$

From this pole, we obtain the energy level E_a by using complex integration theory. Namely, let Γ be a small contour around the isolated pole at $E = E_a$. Then, we have that

$$\frac{1}{2\pi i} \oint_\Gamma dE \, E \, g_{aa}(E) = E_a A_a \,, \tag{1.75}$$

and that

$$\frac{1}{2\pi i} \oint_\Gamma dE \, g_{aa}(E) = A_a \,. \tag{1.76}$$

Thus, the energy level is given by

$$E_a = \frac{\dfrac{1}{2\pi i} \oint_\Gamma dE \, E \, g_{aa}(E)}{\dfrac{1}{2\pi i} \oint_\Gamma dE \, g_{aa}(E)} \,. \tag{1.77}$$

It is convenient to write an expression for the energy shift $\Delta E_a = E_a - E_a^{(0)}$. To this end, we define

$$\Delta g_{aa}(E) = g_a(E) - g_{aa}^{(0)}(E)\,, \tag{1.78}$$

where the leading contribution is given by

$$g_{aa}^{(0)}(E) = \frac{1}{E - E_a^{(0)}}\,. \tag{1.79}$$

Introducing the notation $\Delta E = E - E_a^{(0)}$, we have that

$$\Delta E_a = \frac{\dfrac{1}{2\pi i}\oint_\Gamma dE\,\Delta E \Delta g_{aa}(E)}{1 + \dfrac{1}{2\pi i}\oint_\Gamma dE\,\Delta g_{aa}(E)}\,. \tag{1.80}$$

The function $\Delta g_{aa}(E)$ and the shift ΔE_a are expanded order by order in a perturbation series in the fine-structure constant α as

$$\Delta E_a = \Delta E_a^{(1)} + \Delta E_a^{(2)} + \cdots\,, \tag{1.81}$$

$$\Delta g_{aa}(E) = \Delta g_{aa}^{(1)}(E) + \Delta g_{aa}^{(1)}(E) + \cdots\,. \tag{1.82}$$

We obtain expressions for $\Delta E^{(1)}, \Delta E^{(2)}, \ldots$ by expanding Eq. (1.80) in a geometric series, substituing the expressions in Eqs. (1.81) and (1.82) and comparing terms order by order in α. For the first two terms in the expansion, we have that

$$\Delta E_a^{(1)} = \frac{1}{2\pi i}\oint_\Gamma dE\,\Delta E \Delta g_{aa}^{(1)}(E)\,, \tag{1.83}$$

$$\Delta E_a^{(2)} = \frac{1}{2\pi i}\oint_\Gamma dE\,\Delta E \Delta g_{aa}^{(2)}(E) - \Delta E_a^{(1)}\frac{1}{2\pi i}\oint_\Gamma dE\,\Delta g_{aa}^{(1)}(E)\,. \tag{1.84}$$

For practical calculations, it is convenient to express the function $g_{aa}(E)$ in terms of the Fourier transformed N-point function in Eq. (1.60). We have that

$$\begin{aligned} g_{aa}(E)\delta(E'-E) = -\frac{2\pi i}{N!}\int dE_1' \cdots \int dE_N' \int dE_1 \cdots \int dE_N\, \delta(E' - E_1' - \cdots - E_N') \\ \times \delta(E - E_1 - \cdots - E_N)\,\langle u_a|\, G(E_1', \ldots, E_N'; E_1, \ldots, E_N)\gamma_1^0 \cdots \gamma_N^0\,|u_a\rangle\,, \end{aligned} \tag{1.85}$$

where

$$\begin{aligned} \langle u_a|\, G(E_1', \ldots, E_N'; E_1, \ldots, E_N)\gamma_1^0 \cdots \gamma_N^0\,|u_a\rangle = \int d^3x_1' \cdots \int d^3x_N' \\ \int d^3x_1 \cdots \int d^3x_N\, u_a^\dagger(\boldsymbol{x}_1', \ldots, \boldsymbol{x}_N') G((E_1', \boldsymbol{x}_1'), \ldots, (E_N', \boldsymbol{x}_N'); (E_1, \boldsymbol{x}_1), \ldots, (E_N, \boldsymbol{x}_N)) \\ \times \gamma_1^0 \cdots \gamma_N^0 u_a(\boldsymbol{x}_1, \ldots, \boldsymbol{x}_N)\,. \end{aligned} \tag{1.86}$$

The Fourier transform of the N-point function is then perturbatively calculated using the Feynman diagram technique (see Appendix A for the Feynman rules).

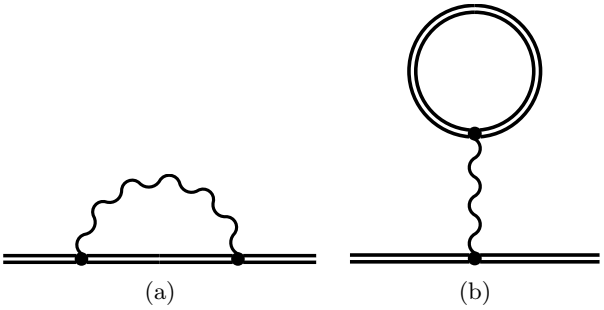

Figure 1.4.: The Furry-picture Feynman diagrams of the leading order QED corrections to the energies of a single-electron atomic system. A double line represents an electron in the static field of the nucleus. The Figure (a) corresponds to the self-energy and (b) to the vacuum-polarization correction.

1.4. Exemplary calculations

We first consider the leading order corrections to the energy levels of a H-like system with just one electron bound to the nucleus. The corresponding Feynman diagrams are shown in Fig. 1.4. The diagram in Fig. 1.4a corresponds to the self-energy correction where the bound electron emits and reabsorbs a virtual photon. The diagram in Fig. 1.4b corresponds to the vacuum polarization effect where the bound electron interacts with the nucleus by the creation and subsequent annihilation of a virtual electron-positron pair. In the following, we derive formal expressions for these two contributions using the TTGF formalism presented in the previous section. We will use from now on a notation where $|a\rangle$ corresponds to the solution ψ_a of the stationary Dirac equation in Eq. (1.51) and $|ab\rangle$ corresponds to the tensor product $\psi_a \otimes \psi_b$. The following calculations can be found in Ref. [65].

We first consider the self-energy contribution in Fig. 1.4a. The corresponding contribution to the Fourier transformed Green's function is obtained using the Feynman rules and reads

$$\begin{aligned} G((E', \boldsymbol{x}'); (E, \boldsymbol{x})) \sim \int d^3 z_1 \int d^3 z_2 \int d\eta \int d\omega \, \frac{i}{2\pi} S(E', \boldsymbol{x}', \boldsymbol{z}_2)(-2\pi i) e\gamma^\mu \\ \times \delta(E' - \eta - \omega) \frac{i}{2\pi} S(\eta, \boldsymbol{z}_2, \boldsymbol{z}_1)(-2\pi i) e\gamma^\nu \delta(\eta + \omega - E) \frac{i}{2\pi} S(E, \boldsymbol{z}_1, \boldsymbol{x}) \\ \times \frac{i}{2\pi} D_{\mu\nu}(\omega, \boldsymbol{z}_1 - \boldsymbol{z}_2) \,, \quad (1.87) \end{aligned}$$

where S is the propagator of the electron in the field of the nucleus given in Eq. (1.56), $D_{\mu\nu}$ is the propagator of the photon, for which an expression in Feynman gauge is given in Eq. (1.10), $\boldsymbol{z}_1$ and $\boldsymbol{z}_2$ denote the vertices in position space, η is the energy

of the virtual fermion, and ω is the energy of the virtual photon. Integrating over η and simplifying the resulting expression, we have that

$$G((E', \boldsymbol{x}'); (E, \boldsymbol{x})) \sim \left(\frac{i}{2\pi}\right)^2 \int d^3z_1 \int d^3z_2 \int d\omega\, S(E', \boldsymbol{x}', \boldsymbol{z}_2) e\gamma^\mu S(E-\omega, \boldsymbol{z}_2, \boldsymbol{z}_1) \times e\gamma^\nu S(E, \boldsymbol{z}_1, \boldsymbol{x}) D_{\mu\nu}(\omega, \boldsymbol{z}_1 - \boldsymbol{z}_2)\delta(E'-E)\,. \quad (1.88)$$

If the electron is in a state a, we obtain that

$$\langle a|\, G(E'; E)\gamma_1^0\, |a\rangle \sim \left(\frac{i}{2\pi}\right)^2 \frac{1}{E' - \varepsilon_a(1-i0^+)} \frac{1}{E - \varepsilon_a(1-i0^+)} \times \int d\omega \sum_n \frac{\langle an|\, I(\omega)\, |na\rangle}{E - \omega - \varepsilon_n(1-i0^+)} \delta(E'-E)\,, \quad (1.89)$$

where the kernel operator

$$I(\omega, \boldsymbol{x}, \boldsymbol{y}) = e^2 \alpha_1^\mu \alpha_2^\nu D_{\mu\nu}(\omega, \boldsymbol{x} - \boldsymbol{y})\,, \quad (1.90)$$

is the photon interaction operator and $\alpha^\mu = \gamma^0\gamma^\mu$. We introduce the self-energy operator

$$\langle a|\, \Sigma(E)\, |b\rangle = \frac{i}{2\pi} \int d\omega \sum_n \frac{\langle an|\, I(\omega)\, |nb\rangle}{E - \omega - \varepsilon_n(1-i0^+)}\,. \quad (1.91)$$

With this notation, we have

$$\Delta g_{aa}^{(1)}(E) \sim \frac{\langle a|\, \Sigma(E)\, |a\rangle}{(E-\varepsilon_a)^2}\,. \quad (1.92)$$

Using Eq. (1.83), we obtain for the self-energy correction to the energy level as

$$\Delta E_a^{(1,\mathrm{SE})} = \langle a|\, \Sigma(\varepsilon_a)\, |a\rangle\,. \quad (1.93)$$

This expression corresponds to the result neglecting the mass counterterm in Eq. (1.59). If one considers the mass counterterm explicitly, the self-energy correction is given by

$$\Delta E_a^{(1,\mathrm{SE})} = \langle a|\, \left(\Sigma(\varepsilon_a) - \delta m_\mathrm{e}\gamma^0\right) |a\rangle\,. \quad (1.94)$$

Next, we consider the vacuum-polarization contribution in Fig. 1.4b. The term contributing to the Fourier transformed Green's function is

$$G((E', \boldsymbol{x}'); (E, \boldsymbol{x})) \sim -\int d^3z_1 \int d^3z_2 \int d\eta \int d\omega\, \frac{i}{2\pi} S(E', \boldsymbol{x}', \boldsymbol{z}_1) \times (-2\pi i) e\gamma^\mu \delta(E - E' - \omega) \frac{i}{2\pi} S(E, \boldsymbol{z}_1, \boldsymbol{x}) \frac{i}{2\pi} D_{\mu\nu}(\omega, \boldsymbol{z}_1 - \boldsymbol{z}_2) \times \mathrm{Tr}\left(\frac{i}{2\pi} S(\eta, \boldsymbol{z}_2, \boldsymbol{z}_2)\gamma^\nu\right)(-2\pi i) e\delta(\omega)\,. \quad (1.95)$$

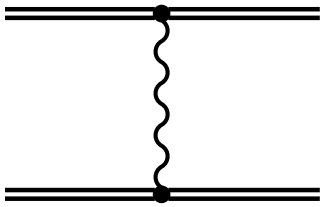

Figure 1.5.: The Furry-picture Feynman diagram of the interelectronic-interaction contribution to the energy shift.

Integrating over ω and simplifying the resulting expression gives

$$G((E',\boldsymbol{x}');(E,\boldsymbol{x})) \sim -\left(\frac{i}{2\pi}\right)^2 \int d^3z_1 \int d^3z_2 \int d\eta\, S(E',\boldsymbol{x}',\boldsymbol{z}_1) e\gamma^\mu S(E,\boldsymbol{z}_1,\boldsymbol{x}) \times eD_{\mu\nu}(0,\boldsymbol{z}_1-\boldsymbol{z}_2)\,\mathrm{Tr}\left(S(\eta,\boldsymbol{z}_2,\boldsymbol{z}_2)\gamma^\nu\right)\delta(E'-E)\,. \quad (1.96)$$

We introduce the vacuum polarization potential

$$U_{\mathrm{VP}}(\boldsymbol{x}) = \frac{e^2}{2\pi i}\int d^3y\,\alpha^\mu D_{\mu\nu}(0,\boldsymbol{x}-\boldsymbol{y}) \int d\eta\ \mathrm{Tr}\left(\sum_n \frac{\psi_n(\boldsymbol{y})\psi_n^\dagger(\boldsymbol{y})}{\eta-\varepsilon_n(1-i0^+)}\gamma^\nu\right). \quad (1.97)$$

Assuming that the electron is in the state a, we obtain that

$$\langle a|\, G(E';E)\gamma_1^0\,|a\rangle \sim \frac{i}{2\pi}\frac{1}{E'-\varepsilon_a(1-i0^+)}\frac{1}{E-\varepsilon_a(1-i0^+)}\,\langle a|\, U_{\mathrm{VP}}\,|a\rangle\,\delta(E'-E)\,, \quad (1.98)$$

for the matrix elements of the Fourier transformed Green's function and

$$\Delta g_{aa}^{(1)}(E) \sim \frac{\langle a|\, U_{\mathrm{VP}}\,|a\rangle}{(E-\varepsilon_a)^2}\,. \quad (1.99)$$

Using Eq. (1.83), we obtain for the vacuum-polarization correction

$$\Delta E_a^{(1,\mathrm{VP})} = \langle a|\, U_{\mathrm{VP}}\,|a\rangle\ . \quad (1.100)$$

So far we only considered single-electron systems. In many-electron systems, one needs to also take into account the interactions between the electons. In the following, we calculate the leading contribution due to interelectronic interactions for a two-electron system.

Let $n=(a,b)$ denote the level of the two-electron system under consideration. The leading interelectronic-interaction contribution is given by the Feynman diagram depicted in Fig. 1.5. The electronic wave function is given by the Slater determinant for $N=2$ in Eq. (1.70). Using Eq. (1.85), we obtain

$$\Delta g_{nn}^{(1)}(E) = \left(\frac{i}{2\pi}\right)^2 \int dE_1' \int dE_1 \sum_\sigma \mathrm{sign}\,\sigma \frac{1}{E_1'-\varepsilon_{\sigma(a)}+i0^+}\frac{1}{E-E_1'-\varepsilon_{\sigma(b)}+i0^+} \times \frac{1}{E_1-\varepsilon_a+i0^+}\frac{1}{E-E_1-\varepsilon_b+i0^+}\,\langle\sigma(a)\sigma(b)|\, I(E_1'-E_1)\,|ab\rangle\ , \quad (1.101)$$

where σ denotes permutations of the labels a and b. We can rewrite the product of propagators as

$$\frac{1}{E_1-\varepsilon_{\sigma(a)}+i0^+}\frac{1}{E-E_1'-\varepsilon_{\sigma(b)}+i0^+}= \frac{1}{\Delta E}\left(\frac{1}{E_1'-\varepsilon_{\sigma(a)}+i0^+}+\frac{1}{E-E_1'-\varepsilon_{\sigma(b)}+i0^+}\right), \quad (1.102)$$

$$\frac{1}{E_1-\varepsilon_{a}+i0^+}\frac{1}{E-E_1-\varepsilon_{b}+i0^+}= \frac{1}{\Delta E}\left(\frac{1}{E_1-\varepsilon_{a}+i0^+}+\frac{1}{E-E_1-\varepsilon_{b}+i0^+}\right). \quad (1.103)$$

Substituting these expressions into Eq. (1.101) and using Eq. (1.83), we obtain

$$\begin{aligned}\Delta E_n^{(1,\mathrm{int})} = \frac{1}{2\pi i}\oint_\Gamma dE\,\frac{1}{\Delta E}\Bigg[\left(\frac{i}{2\pi}\right)^2\int dE_1'\int dE_1\sum_\sigma \mathrm{sign}\,\sigma \\ \times\left(\frac{1}{E_1'-\varepsilon_{\sigma(a)}+i0^+}+\frac{1}{E-E_1'-\varepsilon_{\sigma(b)}+i0^+}\right) \\ \times\left(\frac{1}{E_1-\varepsilon_{a}+i0^+}+\frac{1}{E-E_1-\varepsilon_{b}+i0^+}\right)\langle\sigma(a)\sigma(b)|\,I(E_1'-E_1)\,|ab\rangle\Bigg]. \quad (1.104)\end{aligned}$$

The expression in the brackets is a regular function of E in the contour Γ. Thus, we obtain after integrating over E the expression

$$\begin{aligned}\Delta E_n^{(1,\mathrm{int})} = \left(\frac{i}{2\pi}\right)^2\int dE_1'\int dE_1\sum_\sigma \mathrm{sign}\,\sigma\,\langle\sigma(a)\sigma(b)|\,I(E_1'-E_1)\,|ab\rangle \\ \times\left(\frac{1}{E_1'-\varepsilon_{\sigma(a)}+i0^+}+\frac{1}{-(E_1'-\varepsilon_{\sigma(a)})+i0^+}\right) \\ \times\left(\frac{1}{E_1-\varepsilon_{a}+i0^+}+\frac{1}{-(E_1-\varepsilon_{a})+i0^+}\right). \quad (1.105)\end{aligned}$$

Using the identity for the delta function in Eq. (1.41) and integrating over E_1' and E_1, we obtain the final expression

$$\Delta E_n^{(1,\mathrm{int})} = \langle ab|\,I(0)\,|ab\rangle - \langle ba|\,I(\varepsilon_b-\varepsilon_a)\,|ab\rangle\,. \quad (1.106)$$

Note that this formula contains the direct and exchange matrix elements of the interaction. These matrix elements can be calculated in the Coulomb or Feynman gauge as explained in Appendix B.

2. Numerical Methods

In Chapter 1, we presented and discussed the theoretical foundations of atomic systems. Thereby, we realized that the stationary Dirac equation in the presence of an external field (see Eq. (1.51)) plays an important role, as its solutions provide the basis for perturbative QED in the Furry picture. Therefore, in this chapter, we present a numerical algorithm to solve the Dirac equation in the presence of an external field and discuss our implementation of the algorithm. For that purpose, we assume that the static field of the nucleus is spherically symmetric resulting in a radial potential energy function $V(r)$.

2.1. The radial Dirac equation

The Dirac-Hamiltonian in the presence of a spherically symmetic external field reads

$$H = -i\boldsymbol{\alpha} \cdot \nabla + \beta m_\mathrm{e} + V(r)\,. \tag{2.1}$$

Since the field of the nucleus is spherically symmetric, the total angular momentum $\boldsymbol{J}$ and the parity operator P commute with the Hamiltonian H. This means that solutions of the stationary Dirac equation $H\psi = \varepsilon\psi$ are characterized by definite energy, angular momentum, and parity values.

To solve the stationary Dirac equation in the presence of an spherically symmetric external field, one makes the ansatz [66]

$$\psi(\boldsymbol{r}) = \begin{pmatrix} \varphi(\boldsymbol{r}) \\ \chi(\boldsymbol{r}) \end{pmatrix}\,, \tag{2.2}$$

where φ and χ are two-component spinors. Since the solution has definite parity, we have

$$P\psi = \lambda\psi\,, \tag{2.3}$$

where $|\lambda| = 1$. The action of the parity operator on a spinor ψ is given by [66, 67]

$$P\psi(\boldsymbol{r}) = \eta\beta\psi(-\boldsymbol{r})\,, \tag{2.4}$$

where η is either -1 or $+1$. For the ansatz in Eq. (2.2), this implies

$$P\psi(\boldsymbol{r}) = \begin{pmatrix} \eta\varphi(-\boldsymbol{r}) \\ -\eta\chi(-\boldsymbol{r}) \end{pmatrix}\,. \tag{2.5}$$

That is, the two-component spinors φ and χ have opposite parities.

Eigenfunctions of total angular momentum and parity are two-component spherical spinors $\Omega_{\kappa m}$. For definitions and details on these functions, we refer to Refs. [66, 71]. The spherical spinors are functions of the angles and are indexed by the integer-valued relativistic angular momentum quantum number κ, and the magnetic quantum number m. The parity of $\Omega_{\kappa m}$ is $(-1)^\ell$ where $\ell = |\kappa + 1/2| - 1/2$ is the orbital angular momentum quantum number. The quantum number κ is related to the total and orbital angular momentum quantum numbers by $\kappa = (-1)^{j+\ell+1/2}(j + 1/2)$ and is the eigenvalue $K\Omega_{\kappa m} = \kappa\Omega_{\kappa m}$ of the operator [66, 71]

$$K = -1 - 2\boldsymbol{L} \cdot \boldsymbol{S} \,. \tag{2.6}$$

Note that $\Omega_{\kappa m}$ and $\Omega_{-\kappa m}$ have opposite parities.

The Dirac equation in the presence of a spherically symmetric external field is then reduced to a ordinary differential equation for the radial variable r by making the separation ansatz [66]

$$\psi(\boldsymbol{r}) = \frac{1}{r} \begin{pmatrix} G(r)\Omega_{\kappa m}(\boldsymbol{n}) \\ iF(r)\Omega_{-\kappa m}(\boldsymbol{n}) \end{pmatrix} , \tag{2.7}$$

where G and F denote radial wave functions, and $\boldsymbol{n} = \boldsymbol{r}/r$. The resulting coupled system of ordinary differential equations for the radial wave functions are given by

$$G'(r) + \frac{\kappa}{r} G(r) - [\varepsilon + m_\mathrm{e} - V(r)]F(r) = 0 \,, \tag{2.8}$$

$$F'(r) - \frac{\kappa}{r} F(r) + [\varepsilon - m_\mathrm{e} - V(r)]G(r) = 0 \,. \tag{2.9}$$

This coupled system of ordinary differential equations can be brought into a matrix form given by

$$\begin{pmatrix} V(r) + m_\mathrm{e} & \frac{\kappa}{r} - \frac{d}{dr} \\ \frac{\kappa}{r} + \frac{d}{dr} & V(r) - m_\mathrm{e} \end{pmatrix} \begin{pmatrix} G(r) \\ F(r) \end{pmatrix} = \varepsilon \begin{pmatrix} G(r) \\ F(r) \end{pmatrix} , \tag{2.10}$$

which is called the radial Dirac equation.

The spectrum consists of normalizable solutions with discrete energy eigenvalues corresponding to bound-state solutions and continuum solutions with eigenvalues ranging from $(-\infty, m_\mathrm{e}]$ and $[m_\mathrm{e}, +\infty)$. The discrete bound-state solutions are given by

$$\psi_{n\kappa m}(\boldsymbol{r}) = \frac{1}{r} \begin{pmatrix} G_{n\kappa}(r)\Omega_{\kappa m}(\boldsymbol{n}) \\ iF_{n\kappa}(r)\Omega_{-\kappa m}(\boldsymbol{n}) \end{pmatrix} , \tag{2.11}$$

with corresponding energy eigenvalues $\varepsilon_{n\kappa}$, where n is the principal quantum number. Continuum solutions are labeled by the real-valued eigenvalue in the continuous spectrum instead of n.

In the case of a point-like nucleus, for which $V(r) = -Z\alpha/r$, the bound-state and continuum solutions of the radial Dirac equation can be given explicitly (see, e.g., Ref. [66]). For extended nuclei, the radial Dirac equation needs to be solved numerically.

2.2. Finite basis sets

Solutions of the stationary Dirac equation in the presence of the external field are the basis for perturbative calculation in Furry-picture QED (see the discussion in Chapter 1). Typically, in calculations of higher-order perturbative effects, infinite sums over discrete and integrals over continuum parts of the spectrum arise [72]. For example, a second order correction to the energy level of an bound electron in the reference state $|a\rangle$ due to an external potential U (see, e.g., the vacuum-polarization effect discussed in Section 1.4) is given by

$$\Delta E = \sum_{n}^{\varepsilon_n \neq \varepsilon_a} \frac{\langle a| U |n\rangle \langle n| U |a\rangle}{\varepsilon_n - \varepsilon_a} \,. \tag{2.12}$$

These type of expressions will later arise in Chapter 4, when we consider vacuum-polarization corrections to the Zeeman splitting. Also, we evaluated such expressions in Refs. [7, 10]. In Eq. (2.12), the label n represents the collection of all quantum numbers of the intermediate state, which can have discrete and continuous components, and the sum over n corresponds to a sum over discrete and an appropriately normalized integral over the continuous quantum numbers. In the remainder of this section, we will present a method to approximate these kinds of spectral sums. The discussion follows Ref. [56].

The radial Dirac equation given in Eq. (2.10) can be written in the form

$$H_\kappa \phi = \varepsilon \phi \,, \tag{2.13}$$

where

$$H_\kappa = \begin{pmatrix} V(r) + m_\mathrm{e} & \frac{\kappa}{r} - \frac{d}{dr} \\ \frac{\kappa}{r} + \frac{d}{dr} & V(r) - m_\mathrm{e} \end{pmatrix} , \tag{2.14}$$

and ϕ is the vector of radial functions

$$\phi(r) = \begin{pmatrix} G(r) \\ F(r) \end{pmatrix} . \tag{2.15}$$

For any ϕ_1 and ϕ_2 of such vectors not necessarily satisfying the radial Dirac equation, we define the scalar product

$$\langle \phi_1 | \phi_2 \rangle = \int_0^\infty dr \, [G_1(r) G_2(r) + F_1(r) F_2(r)] \,. \tag{2.16}$$

The radial Dirac equation can then be derived from the variation of the action

$$S(\phi) = \langle\phi| H_\kappa |\phi\rangle - \varepsilon \langle\phi|\phi\rangle \ , \tag{2.17}$$

assuming proper boundary conditions for the components G and F.

The system under consideration is confined to a spherical cavity of radius R_{cav} and appropriate boundary conditions are imposed at $r = 0$ and $r = R_{\text{cav}}$. Through this restriction of the system to a cavity, the continuous part of the spectrum becomes discrete as well. In practical calculations, the cavity radius R_{cav} is chosen large enough such that results do not depend on it. The idea is now to approximate radial wave functions by a finite set of functions. This reduces the radial Dirac equation, which is an ordinary differential equation, to an algebraic equation with a numerically generated spectrum of finite size. This numerically determined spectrum and functions are then used to calculate spectral sums of the kind given in Eq. (2.12).

The function ϕ is approximated by a finite linear combination given by

$$\phi(r) = \sum_{i=1}^{2N} c_i u_i(r) \, , \tag{2.18}$$

where the u_i are assumed to be basis functions of a suitable space of functions chosen to approximate the radial wave functions and which satisfy proper boundary conditions. Substituting Eq. (2.18) into Eq. (2.17), the action becomes a multivaried function of the coefficients c_i. Since physical wave functions, i.e. solutions satisfying the radial Dirac equation, are stationary points of the action, this now corresponds to determining the set of coefficients for which the derivate of S with respect to the coefficients vanish. This leads to a generalized eigenvalue equation for the vector $\boldsymbol{c}$ of coefficients $c_1, \ldots, c_{2N}$ given by

$$\boldsymbol{A} \cdot \boldsymbol{c} = \varepsilon \, \boldsymbol{B} \cdot \boldsymbol{c} \, , \tag{2.19}$$

where the components of the $2N \times 2N$ symmetric matrices $\boldsymbol{A}$ and $\boldsymbol{B}$ are

$$A_{ij} = \frac{\langle u_i| H_\kappa |u_j\rangle + \langle u_j| H_\kappa |u_i\rangle}{2} \, , \tag{2.20}$$

and

$$B_{ij} = \langle u_i | u_j \rangle \ . \tag{2.21}$$

Solving the generalized eigenvalue equation in Eq. (2.19) for a given κ generates $2N$ eigenvalues $\varepsilon_{n\kappa}$ and coefficients $\boldsymbol{c}(n\kappa)$ where $n = 1, 2, \ldots, 2N$. The first N solutions approximate the negative continuum and the remaining N solutions approximate the bound states and the positive continuum.

The key message is that radial wave functions can now be represented on the computer by the set of coefficients $\boldsymbol{c}(n\kappa)$. To appreciate this fact, let us consider again the energy shift in Eq. (2.12). We can rewrite it as

$$\Delta E = \langle a| U |\delta a\rangle \ , \tag{2.22}$$

where

$$|\delta a\rangle = \sum_{n}^{\varepsilon_n \neq \varepsilon_a} \frac{\langle n| U |a\rangle}{\varepsilon_n - \varepsilon_a} |n\rangle \ . \tag{2.23}$$

Now, if the potential U is spherically symmetric, then its matrix elements are

$$\langle a| U |b\rangle = \int_0^\infty dr\, U(r)[G_{n_a\kappa_a}(r)G_{n_b\kappa_b}(r) + F_{n_a\kappa_a}(r)F_{n_b\kappa_b}(r)]\delta_{\kappa_a,\kappa_b}\delta_{m_a,m_b} \ , \tag{2.24}$$

that is, they preserve the relativistic angular momentum and magnetic quantum numbers. This implies that $|\delta a\rangle$ is represented by

$$\delta\psi_{n_a\kappa_a m_a}(\boldsymbol{r}) = \frac{1}{r}\begin{pmatrix} \delta G_{n_a\kappa_a}(r)\Omega_{\kappa_a m_a}(\boldsymbol{n}) \\ i\delta F_{n_a\kappa_a}(r)\Omega_{-\kappa_a m_a}(\boldsymbol{n}) \end{pmatrix} \ , \tag{2.25}$$

where

$$\begin{pmatrix} \delta G_{n_a\kappa_a}(r) \\ \delta F_{n_a\kappa_a}(r) \end{pmatrix} = \sum_{n}^{\varepsilon_{n\kappa_a} \neq \varepsilon_{n_a\kappa_a}} \frac{U_{n;n_a\kappa_a}}{\varepsilon_{n\kappa_a} - \varepsilon_{n_a\kappa_a}} \begin{pmatrix} G_{n\kappa_a}(r) \\ F_{n\kappa_a}(r) \end{pmatrix} \ , \tag{2.26}$$

where

$$U_{n;n_a\kappa_a} = \int_0^\infty dr\, U(r)[G_{n\kappa_a}(r)G_{n_a\kappa_a}(r) + F_{n\kappa_a}(r)F_{n_a\kappa_a}(r)] \, . \tag{2.27}$$

Substituting the approximation given in Eq. (2.18) into Eq. (2.26), we see that the corrections of the radial wave functions are given by corrections to the coefficients, namely

$$\delta\boldsymbol{c}(n_a\kappa_a) = \sum_{n}^{\varepsilon_{n\kappa_a} \neq \varepsilon_{n_a\kappa_a}} \frac{U_{n;n_a\kappa_a}}{\varepsilon_{n\kappa_a} - \varepsilon_{n_a\kappa_a}} \boldsymbol{c}(n\kappa_a) \, . \tag{2.28}$$

So, operations on the radial wave functions can be translated to operations on the coefficients representing them.

2.3. Finite basis sets constructed from B-splines

Different approaches using finte basis sets differ in their choice of the basis functions u_i and the implementation of boundary conditions. In Ref. [73], finite basis sets were constructed from B-splines. We give a short summary of the definition and properties of B-splines necessary in the context of this thesis. We follow the discussion of Ref. [73]. A more detailed review of the use of B-splines in atomic physics calculation can be found in Ref. [74].

A B-spline of order K is a piecewise polynomial function of maximum degree $K-1$ defined on a partition of the cavity interval $[0, R_{\text{cav}}]$ into subintervals. The endpoints of these subintervals are given by the knot sequence t_i, where $i = 1, 2, \ldots, N+K$, where N is the number of B-splines. The ith B-spline functions of order K denoted by with respect to the knot sequence (t_i), denoted by B_{iK}, is defined recursively by

$$B_{i,1}(r) = \begin{cases} 1, & t_i \leq r < t_{i+1}\,, \\ 0, & \text{otherwise,} \end{cases} \tag{2.29}$$

and

$$B_{iK}(r) = \frac{r - t_i}{t_{i+K-1} - t_i} B_{i,K-1}(r) + \frac{t_{i+K} - r}{t_{i+K} - t_{i+1}} B_{i+1,K-1}(r)\,. \tag{2.30}$$

The B-spline B_{iK} vanishes everywhere except for $t_i \leq r < t_{i+K}$. On the subintervals where it does not vanish, it is a piecewise polynomial of degree $K-1$ at most. The sum of all B-splines that do not vanish at a given poin r is unity. B-splines form a basis of piecewise polynomials of degree $K-1$. For atomic physical calculations, the knots t_i are chosen such that their multiplicity at $r = 0$ and $r = R_{\text{cav}}$ is K, that is $t_1 = \cdots = t_K = 0$ and $t_{N+1} = \cdots = t_{N+K} = R_{\text{cav}}$, and the knots inbetween form a strictly increasing sequence. The distinct knots define a strictly increasing sequence $x_1, \ldots, x_M$ of breakpoints where $M = N - K + 2$ and the first and last breakpoints are $x_1 = 0$ and $x_M = R_{\text{cav}}$. For $K > 1$, which is the case for calculations in this thesis, all B-splines vanish at $r = 0$ and $r = R_{\text{cav}}$ except the first B-spline at $r = 0$ and the last B-spline at $r = R_{\text{cav}}$ where they take the value one. This fact is often used in the implementation of boundary conditions. Typically, for a fixed order K, the index for the order is dropped and the ith B-spline is denoted as B_i, which will be used in the following.

Using the notation of Section 2.2, the basis functions u_i were chosen in Ref. [73] as

$$u_i(r) = \begin{pmatrix} B_i(r) \\ 0 \end{pmatrix}, \tag{2.31}$$

for $i = 1, \ldots, N$, and as

$$u_i(r) = \begin{pmatrix} 0 \\ B_i(r) \end{pmatrix}, \tag{2.32}$$

for $i = N+1, \ldots, 2N$. The MIT bag-model boundary conditions were implemented adding boundary terms to the action in Eq. (2.17) which gave $G(0) = 0$ and $G(R_{\text{cav}}) = -F(R_{\text{cav}})$. The boundary terms added to the action were observed to eliminate the so-called spurious states, which are part of the numerical spectrum with nonphysical energies, that lie in the bound-state spectrum [72].

In Ref. [56], the basis set was chosen to be

$$u_i(r) = \begin{pmatrix} B_i(r) \\ \frac{1}{2m_{\text{e}}} \left(\frac{d}{dr} + \frac{\kappa}{r} \right) B_i(r) \end{pmatrix}, \tag{2.33}$$

for $i = 1, \ldots, N$, and

$$u_i(r) = \begin{pmatrix} \frac{1}{2m_e}\left(\frac{d}{dr} - \frac{\kappa}{r}\right) B_{i-N}(r) \\ B_{i-N}(r) \end{pmatrix} , \tag{2.34}$$

for $i = N+1, \ldots, 2N$, assuming that the nucleus is extended and not point-like, i.e. the nuclear potential is bounded from below. This choice was called the dual kinetic balance (DKB) approach [56]. It is argued in the reference that for this choice of the basis functions, no spurious states occur in the numerical spectrum. For numerical calculations in this thesis, we use the DKB approach.

In practical calculations, ommiting the first and last B-spline functions provides the boundary conditions at the origin for $|\kappa| = 1$. For $|\kappa| > 1$, it is also necessary to remove the second B-spline function as well. However, it is argued in Ref. [56] that this has no effect on the result. Similarly, removing the last two B-splines would give the boundary condition $G(R_{\mathrm{cav}}) = F(R_{\mathrm{cav}}) = 0$, which, according to Ref. [56], does not effect the result as well. The radial wave functions in terms of B-spline basis functions are given by

$$G_{n\kappa}(r) = \sum_{i=2}^{N-1} \left\{ c_i(n\kappa) B_i(r) + \frac{c_{N+i}(n\kappa)}{2m_e} \left[B_i'(r) - \frac{\kappa}{r} B_i(r) \right] \right\} , \tag{2.35}$$

$$F_{n\kappa}(r) = \sum_{i=2}^{N-1} \left\{ \frac{c_i(n\kappa)}{2m_e} \left[B_i'(r) + \frac{\kappa}{r} B_i(r) \right] + c_{N+i}(n\kappa) B_i(r) \right\} . \tag{2.36}$$

We will apply this basis set for the fully relativistic calculation of radiative corrections.

3. Self-Energy Calculations

In Chapter 1, we derived an expression for the correction to the energy level of a bound electron in a H-like system induced by the emission and reabsorption of a virtual photon using the TTGF formalism [65]. The result given in Eq. (1.94) was that this self-energy shift is the expectation value of the self-energy operator with respect to the atomic state minus a renormalization term. In general, this expression is complex valued due to the radiative decay of atomic energy levels. Only the real part of it contributes to the shift of the energy level. The imaginary part defines the radiative transition width of an excited state and vanishes for the ground state [67]. Thus, the self-energy shift is given by

$$\Delta E_{\mathrm{SE}} = \mathrm{Re}\,\langle a|\left(\Sigma(\varepsilon_a) - \delta m_{\mathrm{e}}\gamma^0\right)|a\rangle\ . \tag{3.1}$$

The matrix elements of the self-energy operator were introduced in Eq. (1.91). While Eq. (1.91) gives a formal expression for the operator, it needs to be further simplified. In particular, the divergencies of the operator need to be treated.

To this end, we reformulate the self-energy contribution from Eq. (1.93) in terms of propagators as

$$\langle a|\,\Sigma(\varepsilon_a)\,|a\rangle = 2i\alpha\int d\omega\int d^3x\int d^3y\,\psi_a^\dagger(\boldsymbol{x})\alpha^\mu G(\varepsilon_a-\omega,\boldsymbol{x},\boldsymbol{y})\alpha^\nu\psi_a(\boldsymbol{y})D_{\mu\nu}(\omega,\boldsymbol{x}-\boldsymbol{y})\,, \tag{3.2}$$

where ψ_a is the solutions of the statitonary Dirac equation in the presence of the nuclear field representing the electronic state with corresponding energy eigenvalue ε_a, $G(\omega) = S(\omega)\gamma^0$ is the propagator of the electron in the field of the nucleus (see Eq. (1.56)), $D_{\mu\nu}$ is the photon propagator (see Eq. (1.10)), and $\alpha^\mu = \gamma^0\gamma^\mu$.

The singularties of the self-energy operator in the frequency plane are depicted in Fig. 3.1. The integral over ω in Eq. (3.2) extends over the whole real axis. The photon propagator (with a ficticious photon mass to be taken to zero at the end) gives branch cuts which approach the origin. The propagator of the electron in the nuclear field has a branch cut from $-\infty$ to $-m_{\mathrm{e}}$ which is slightly shifted to the positive imaginary domain, poles for the bound states between 0 and m_{e} and a branch cut from m_{e} to $+\infty$, which are slightly shifted to the negative imaginary domain. This corresponds to the Feynman prescription of the integration contour. Since the argument of the electronic propagator in Eq. (3.2) is $\varepsilon_a - \omega$, these poles

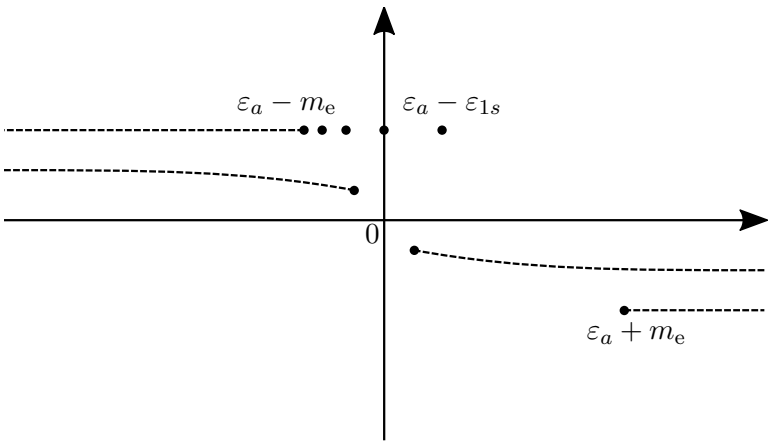

Figure 3.1.: Poles and cuts of the self-energy operator in the frequency plane.

and branch cuts are mirrored at the origin and shifted by ε_a. In particular, the pole corresponding to the reference state a lies on the imaginary axis.

The propagator G of the electron in the field of the nucleus can be writen as an operator equation as [58]

$$G(\omega) = \frac{1}{\omega - H}\,, \tag{3.3}$$

where the shifts into the imaginary plane of the poles and cuts are left out as they are only required for Feynman prescription of the frequency integral. In this formula, H denotes the Dirac Hamiltonian in the presence of the static nuclear field, which we will call Dirac-Coulomb Hamiltonian for brevity. The Dirac-Coulomb Hamiltonian is given by

$$H = H_0 + V\,, \tag{3.4}$$

where

$$H_0 = -i\boldsymbol{\alpha}\cdot\nabla + \beta m_\mathrm{e} \tag{3.5}$$

is the (free) Dirac Hamiltonian and where V is the potential energy resulting from the interaction of the electron with the nucleus. The propagator can then be separated as [58]

$$\frac{1}{\omega - H} = \frac{1}{\omega - H_0} + \frac{1}{\omega - H_0} V \frac{1}{\omega - H_0} + \frac{1}{\omega - H_0} V \frac{1}{\omega - H_0} V \frac{1}{\omega - H_0}\,. \tag{3.6}$$

The separation is diagrammatically depicted in Fig. 3.2 and contains a zero-potential contribution, where the intermediate electron is a free electron, a one-potential contribution, where the intermediate free electron interacts once with the nucleus, and a remaining many-potential contribution, corresponding to the first, second and third term on the right-hand side of Eq. (3.6), respectively. Correspondingly, we have that

$$\langle a|\,\Sigma(\varepsilon_a)\,|a\rangle = \langle a|\,\Sigma^{(0)}(\varepsilon_a)\,|a\rangle + \langle a|\,\Sigma^{(1)}(\varepsilon_a)\,|a\rangle + \langle a|\,\Sigma^{(2+)}(\varepsilon_a)\,|a\rangle\,, \tag{3.7}$$

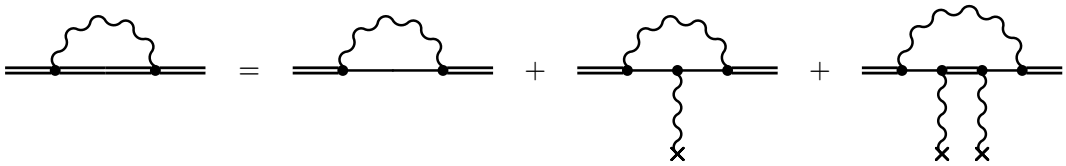

Figure 3.2.: The expansion of the self-energy diagram in terms of zero-, one-, and many-potential terms.

where $\Sigma^{(0)}$ denotes the zero-potential, $\Sigma^{(1)}$ denotes the one-potential, and $\Sigma^{(2+)}$ denotes the many-potential contribution. This separation allows to treat the divergences appearing in the expression for the self-energy contribution. The zero- and one-potential terms can be regularized using well-known regularized expressions for the self-energy and vertex functions in momentum space, while the many-potential term is finite, as can be seen from power counting. In the following, we discuss each of these terms separately. The derivation follows and combines the derivations and methods of Refs. [57, 58, 75].

We assume that the potential energy function V is spherically symmetric. Note that we will use in this chapter upright letters like p to denote four-momenta and p^μ for their components. The Feynman slash notation $\not{p} = \gamma^\mu p_\mu$ will be used.

3.1. The zero-potential contribution

The zero-potential contribution is given by the expression [58]

$$\langle a|\, \Sigma^{(0)}(\varepsilon_a)\, |a\rangle = \int \frac{d^3p}{(2\pi)^3}\, \widetilde{\psi}_a^\dagger(\boldsymbol{p})\gamma^0\Sigma_0(\mathrm{p})\widetilde{\psi}_a(\boldsymbol{p})\,, \tag{3.8}$$

where $p^0 = \varepsilon_a$, the wave function $\widetilde{\psi}_a$ denotes the Fourier transform of ψ_a given by

$$\widetilde{\psi}_a(\boldsymbol{p}) = \int d^3x\, \psi_a(\boldsymbol{x}) e^{-i\boldsymbol{p}\cdot\boldsymbol{x}}\,, \tag{3.9}$$

and Σ_0 denotes the free-electron self-energy function, formally given by

$$\Sigma_0(\mathrm{p}) = -4\pi i\alpha \int \frac{d^4k}{(2\pi)^4}\, \frac{1}{\mathrm{k}^2 + i0^+}\gamma_\mu \frac{\not{p} - \not{k} + m_\mathrm{e}}{(\mathrm{p}-\mathrm{k})^2 - m_\mathrm{e}^2 + i0^+}\gamma^\mu\,. \tag{3.10}$$

This expression is infrared finite and thus we do not need to introduce a ficticious photon mass. However, the expression is ultraviolet divergent.

The divergent parts are identified by regularizing the integral. We use dimensional regularization with the space-time dimension $d = 4 - 2\varepsilon$, for some small positive number ε. The result reads

$$\Sigma_0(\mathrm{p}) = \delta m_\mathrm{e} - \frac{\alpha}{\pi}\frac{\Delta}{4}(\not{p} - m_\mathrm{e}) + \Sigma_{0,\mathrm{R}}(\mathrm{p})\,, \tag{3.11}$$

where $\Sigma_{0,\mathrm{R}}$ denotes the finite remainder,

$$\delta m_\mathrm{e} = \frac{\alpha}{\pi}\left(\frac{3}{4}\Delta + 1\right) m_\mathrm{e}\,, \tag{3.12}$$

and

$$\Delta = \frac{1}{\varepsilon} - \gamma_\mathrm{E} + \ln\left(\frac{4\pi}{m_\mathrm{e}}\right)\,, \tag{3.13}$$

with γ_E being the Euler-Mascheroni constant. The divergent term δm_e is cancelled by the renormalization counterterm in Eq. (1.94). The divergence due to Eq. (3.13) is cancelled by the divergent part of the one-potential term discussed in the next section. Thus, we only need to take the expectation value with respect to the finite remainder

$$\Sigma_{0,\mathrm{R}}(\mathrm{p}) = \frac{\alpha}{\pi}\frac{m_\mathrm{e} a(\varrho) + \not{\mathrm{p}} b(\varrho)}{4}\,, \tag{3.14}$$

where (see, e.g., Ref. [58])

$$a(\varrho) = 2\left(1 + \frac{2\varrho}{1-\varrho}\ln\varrho\right)\,, \tag{3.15}$$

$$b(\varrho) = -\frac{2-\varrho}{1-\varrho}\left(1 + \frac{\varrho}{1-\varrho}\ln\varrho\right)\,, \tag{3.16}$$

and

$$\varrho = \frac{m_\mathrm{e}^2 - \mathrm{p}^2}{m_\mathrm{e}^2}\,. \tag{3.17}$$

Using Eq. (3.8), where we substitute $\Sigma_{0,\mathrm{R}}$ for Σ_0, an explicit expression for the zero-potential contribution can be obtained. To this end, note that the Fourier transformed wave function can be written as

$$\widetilde{\psi}_{n\kappa m}(\boldsymbol{p}) = \frac{(-i)^\ell}{p}\begin{pmatrix}\widetilde{G}_{n\kappa}(p)\Omega_{\kappa m}(\hat{\boldsymbol{p}})\\ \widetilde{F}_{n\kappa}(p)\Omega_{-\kappa m}(\hat{\boldsymbol{p}})\end{pmatrix}\,, \tag{3.18}$$

where $2\ell = |2\kappa+1|-1$, the variable $p = |\boldsymbol{p}|$, and $\hat{\boldsymbol{p}} = \boldsymbol{p}/|\boldsymbol{p}|$. The Fourier transformed radial wave functions read

$$\widetilde{G}_{n\kappa}(p) = 4\pi\int_0^\infty dr\, G_{n\kappa}(r) j_\ell(pr) pr\,, \tag{3.19}$$

and

$$\widetilde{F}_{n\kappa}(p) = -4\pi\frac{\kappa}{|\kappa|}\int_0^\infty dr\, F_{n\kappa}(r) j_{\bar{\ell}}(pr) pr\,, \tag{3.20}$$

where $2\bar{\ell} = |2\kappa - 1| - 1$, and j_k denotes the spherical Bessel function of first kind of order k [76]. With this, we have the expression for the matrix element [58]

$$\begin{aligned}\langle a|\,\Sigma_\mathrm{R}^{(0)}(\varepsilon_a)\,|a\rangle = \frac{\alpha}{\pi}\frac{1}{4(2\pi)^3}\int_0^\infty dp\,\Big\{&a(\varrho)[\widetilde{G}_a^2(p) - \widetilde{F}_a^2(p)]\\ &+b(\varrho)[\varepsilon_a(\widetilde{G}_a^2(p) + \widetilde{F}_a^2(p)) + 2\,p\,\widetilde{G}_a(p)\widetilde{F}_a(p)]\Big\}\,,\end{aligned} \tag{3.21}$$

with the subscript R indicating that this term corresponds to the regularized part.

3.2. The one-potential contribution

The one-potential contribution reads [58]

$$\langle a|\,\Sigma^{(1)}(\varepsilon_a)\,|a\rangle = \int \frac{d^3p'}{(2\pi)^3}\int \frac{d^3p}{(2\pi)^3}\,\widetilde{\psi}^{\dagger}_a(\boldsymbol{p}')\gamma^0\Gamma^0(\mathrm{p}',\mathrm{p})\widetilde{V}(|\boldsymbol{p}'-\boldsymbol{p}|)\widetilde{\psi}_a(\boldsymbol{p})\,, \tag{3.22}$$

where $p'^0 = p^0 = \varepsilon_a$, the function $\widetilde{V}$ is the Fourier transform of the potential energy function V, and Γ^μ denotes the free-electron vertex function formally given by the expression

$$\Gamma^\mu(\mathrm{p}',\mathrm{p}) = -4\pi i\alpha\int\frac{d^4k}{(2\pi)^4}\,\frac{1}{\mathrm{k}^2+i0^+}\gamma_\nu\frac{\not{\mathrm{p}}'-\not{\mathrm{k}}+m_\mathrm{e}}{(\mathrm{p}'-\mathrm{k})^2+m_\mathrm{e}^2+i0^+}\gamma^\mu \times\frac{\not{\mathrm{p}}-\not{\mathrm{k}}+m_\mathrm{e}}{(\mathrm{p}-\mathrm{k})^2+m_\mathrm{e}^2+i0^+}\gamma^\nu\,. \tag{3.23}$$

Again, this expression is infrared finite, but ultraviolet divergent and dimensional regularization gives [58]

$$\Gamma^\mu(\mathrm{p}',\mathrm{p}) = \frac{\alpha}{\pi}\frac{\Delta}{4}\gamma^\mu + \Gamma^\mu_\mathrm{R}(\mathrm{p}',\mathrm{p})\,, \tag{3.24}$$

where Δ is given in Eq. (3.13), and Γ^μ_R denotes the finite remainder.

The divergent term cancels the remaining divergent term of the zero-potential contribution. To see this, consider the Fourier transform of the stationary Dirac equation in the presence of the nuclear field, given in Eq. (1.51), for the wave function ψ_a. The Fourier transformed equation reads

$$(\not{p}-m_\mathrm{e})\widetilde{\psi}_a(\boldsymbol{p}) = \int\frac{d^3p'}{(2\pi)^3}\,\gamma^0\widetilde{V}(|\boldsymbol{p}-\boldsymbol{p}'|)\widetilde{\psi}_a(\boldsymbol{p}')\,, \tag{3.25}$$

which implies that the divergent part of the zero-potential contribution is cancelled by the divergent part of the one-potential contribution.

The finite remainder of the free-electron vertex function can be written in the form[58]

$$\Gamma^\mu_\mathrm{R}(\mathrm{p}',\mathrm{p}) = \frac{\alpha}{\pi}\frac{1}{4}[A\gamma^\mu+\not{\mathrm{p}}'(B_1p'^\mu+B_2p^\mu)+\not{\mathrm{p}}(C_1p'^\mu+C_2p^\mu)+D\not{\mathrm{p}}'\gamma^\mu\not{\mathrm{p}}+H_1p'^\mu+H_2p^\mu]\,, \tag{3.26}$$

where

$$A = C_{24}-2+\mathrm{p}'^2C_{11}+\mathrm{p}^2C_{12}+4(\mathrm{p}'\cdot\mathrm{p})(C_0+C_{11}+C_{12})+m_\mathrm{e}^2(C_{11}+C_{12}-2C_0)\,, \tag{3.27}$$

$$B_1 = -4(C_{11}+C_{21})\,, \tag{3.28}$$

$$B_2 = -4(C_0+C_{11}+C_{12}+C_{23})\,, \tag{3.29}$$

$$C_1 = -4(C_0 + C_{11} + C_{12} + C_{23})\,, \tag{3.30}$$

$$C_2 = -4(C_{12} + C_{22})\,, \tag{3.31}$$

$$D = 2(C_0 + C_{11} + C_{12})\,, \tag{3.32}$$

$$H_1 = 4m_\mathrm{e}(C_0 + 2C_{11})\,, \tag{3.33}$$

$$H_2 = 4m_\mathrm{e}(C_0 + 2C_{12})\,, \tag{3.34}$$

and

$$C_0 = \int_0^1 \frac{dy}{(y\mathrm{p}' + (1-y)\mathrm{p})^2}\,(-\ln X)\,, \tag{3.35}$$

$$\begin{pmatrix} C_{11} \\ C_{12} \end{pmatrix} = \int_0^1 \frac{dy}{(y\mathrm{p}' + (1-y)\mathrm{p})^2} \begin{pmatrix} y \\ 1-y \end{pmatrix} (1 - Y\ln X)\,, \tag{3.36}$$

$$\begin{pmatrix} C_{21} \\ C_{22} \\ C_{23} \end{pmatrix} = \int_0^1 \frac{dy}{(y\mathrm{p}' + (1-y)\mathrm{p})^2} \begin{pmatrix} y^2 \\ (1-y)^2 \\ y(1-y) \end{pmatrix} \left[Y(1 - Y\ln X) - \frac{1}{2}\right]\,, \tag{3.37}$$

$$C_{24} = -\int_0^1 dy\,\ln\left(1 - y(1-y)\frac{(\mathrm{p}'-\mathrm{p})^2}{m_\mathrm{e}^2}\right)\,, \tag{3.38}$$

with

$$X = 1 + \frac{1}{Y}\,, \tag{3.39}$$

and

$$Y = \frac{m_\mathrm{e}^2 - y\mathrm{p}'^2 - (1-y)\mathrm{p}^2}{(y\mathrm{p}' + (1-y)\mathrm{p})^2}\,. \tag{3.40}$$

In principal, the coefficients C_{ij} can be related to C_0, which in turn can be expressed in terms of the dilogarithm function [75]. However, we calculate these coefficients numerically, using numerical quadrature routines from the library Quadpack [77], since it is mentioned in Ref. [58] that this is safer. Note that the denominator $(y\mathrm{p}' + (1-y)\mathrm{p})^2$ has zeros in the interval of integration, which are cancelled by correspoding zeros of the numerators. These cancellations are taken into account explicitly in the numerical evaluation.

Using Eq. (3.26), we obtain that

$$\begin{aligned}\widetilde{\psi}_a^\dagger(\boldsymbol{p}')\gamma^0\Gamma_\mathrm{R}^0(\mathrm{p}',\mathrm{p})\widetilde{\psi}_a(\boldsymbol{p}) = \frac{\alpha}{\pi}\frac{1}{4}\Big[&\mathcal{F}_1(p',p,\xi)\Omega^\dagger_{\kappa_a m_a}(\hat{\boldsymbol{p}}')\Omega_{\kappa_a m_a}(\hat{\boldsymbol{p}}) \\ &+\mathcal{F}_2(p',p,\xi)\Omega^\dagger_{-\kappa_a m_a}(\hat{\boldsymbol{p}}')\Omega_{-\kappa_a m_a}(\hat{\boldsymbol{p}})\Big]\,,\end{aligned} \tag{3.41}$$

where

$$\begin{aligned}\mathcal{F}_1(p',p,\xi) &= A\widetilde{G}'_a\widetilde{G}_a + \varepsilon_a(B_1+B_2)(\varepsilon_a\widetilde{G}'_a + p'\widetilde{F}'_a)\widetilde{G}'_a + \varepsilon_a(C_1+C_2) \\ &\times \widetilde{G}'_a(\varepsilon_a\widetilde{G}_a + p\widetilde{F}_a) + D(\varepsilon_a\widetilde{G}'_a + p'\widetilde{F}'_a)(\varepsilon_a\widetilde{G}_a + p\widetilde{F}_a) + \varepsilon_a(H_1+H_2)\widetilde{G}'_a\widetilde{G}_a\,,\end{aligned} \tag{3.42}$$

$$\mathcal{F}_2(p',p,\xi) = A\widetilde{F}'_a\widetilde{F}_a + \varepsilon_a(B_1+B_2)(\varepsilon_a\widetilde{F}'_a + p'\widetilde{G}'_a)\widetilde{F}'_a + \varepsilon_a(C_1+C_2) \\ \times \widetilde{F}'_a(\varepsilon_a\widetilde{F}_a + p\widetilde{G}_a) + D(\varepsilon_a\widetilde{F}'_a + p'\widetilde{G}'_a)(\varepsilon_a\widetilde{F}_a + p\widetilde{G}_a) + \varepsilon_a(H_1+H_2)\widetilde{F}'_a\widetilde{F}_a\,, \quad (3.43)$$

where $\widetilde{G}'_a, \widetilde{F}'_a$ and $\widetilde{G}_a, \widetilde{F}_a$ are shorthand notations for $\widetilde{G}_a(p'), \widetilde{F}_a(p')$ and $\widetilde{G}_a(p), \widetilde{F}_a(p)$, respectively, and ξ denotes the cosine of the angle between $\boldsymbol{p}'$ and $\boldsymbol{p}$, that is

$$\xi = \frac{\boldsymbol{p}'\cdot\boldsymbol{p}}{p'p}\,. \quad (3.44)$$

The expression in Eq. (3.41) can be simplified by using the summation rule [58]

$$\frac{4\pi}{2|\kappa|}\sum_m \Omega^\dagger_{\kappa m}(\hat{\boldsymbol{p}}')\Omega_{\kappa m}(\hat{\boldsymbol{p}}) = P_\ell(\xi)\,, \quad (3.45)$$

where P_ℓ denotes the Legendre polynomial of order ℓ. With this, we obtain that [58]

$$\langle a|\,\Sigma^{(1)}_{\mathrm{R}}(\varepsilon_a)\,|a\rangle = \frac{\alpha}{\pi}\frac{1}{4(2\pi)^5}\int_0^\infty dp'\,p'\int_0^\infty dp\,p\int_{-1}^{+1}d\xi\,\widetilde{V}(q) \\ \times\left[\mathcal{F}_1(p',p,\xi)P_\ell(\xi) + \mathcal{F}_2(p',p,\xi)P_{\bar{\ell}}(\xi)\right], \quad (3.46)$$

where

$$q = |\boldsymbol{p}'-\boldsymbol{p}| = \sqrt{p'^2+p^2-2p'p\xi}\,. \quad (3.47)$$

3.3. The many-potential contribution

The many-potential contribution is given by

$$\langle a|\,\Sigma^{(2+)}(\varepsilon_a)\,|a\rangle = 2i\alpha\int d\omega\int d^3x\int d^3y\,\psi^\dagger_a(\boldsymbol{x})\alpha^\mu G^{(2+)}(\varepsilon_a-\omega,\boldsymbol{x},\boldsymbol{y})\alpha^\nu\psi_a(\boldsymbol{y}) \\ \times D_{\mu\nu}(\omega,\boldsymbol{x}-\boldsymbol{y})\,, \quad (3.48)$$

which is obtained from Eq. (3.2) by replacing the propagator G of the electron in the field of the nucleus by the many-potential contribution $G^{(2+)}$ to the propagator, which is the last term in Eq. (3.6). That is, we have as an operator equation

$$G^{(2+)}(\omega) = \frac{1}{\omega-H_0}V\frac{1}{\omega-H}V\frac{1}{\omega-H_0}\,. \quad (3.49)$$

The spectral representation of this expression is given by

$$G^{(2+)}(\omega) = \sum_{\alpha,\beta,i}\frac{|\alpha\rangle\langle\alpha|\,V\,|i\rangle\langle i|\,V\,|\beta\rangle\langle\beta|}{(\omega-\varepsilon_\alpha)(\omega-\varepsilon_i)(\omega-\varepsilon_\beta)}\,, \quad (3.50)$$

where $|\alpha\rangle$ and $|\beta\rangle$ represents eigenstates of the free Dirac Hamiltonian H_0 with eigenvalues ε_α and ε_β, respectively, and $|i\rangle$ represents eigenstates of the Dirac-Coulomb

Hamiltonian H with eigenvalues ε_i. Substituting this spectral representation into Eq. (3.48), we obtain that [57]

$$\langle a|\,\Sigma^{(2+)}(\varepsilon_a)\,|a\rangle = \frac{i}{2\pi}\int d\omega \sum_{\alpha,\beta,i} \frac{\langle i|\,V\,|\beta\rangle\,\langle a\beta|\,I(\omega)\,|\alpha a\rangle\,\langle\alpha|\,V\,|i\rangle}{(\varepsilon_a-\omega-\varepsilon_\alpha u^+)(\varepsilon_a-\omega-\varepsilon_i u^+)(\varepsilon_a-\omega-\varepsilon_\beta u^+)}\,, \tag{3.51}$$

where we introduced the notation $u^+ = 1 - i0^+$ for brevity.

Compared to the self-energy operator Σ in Eq. (3.2), we have the appearance of free-electron propagators which contribute cuts from $-\infty$ to $-m_\mathrm{e}$ and from m_e to $+\infty$. Thus, the many-potential contribution Σ^{2+} has the same poles and cuts as Σ, which are depicted in Fig. 3.1.

We can further simplify the expression in Eq. (3.51) by introducing frequency-dependent effective basis functions [57, 58]

$$\left|\phi_i^{(\pm)}(\omega)\right\rangle = \sum_\alpha \frac{\langle\alpha|\,V\,|i\rangle}{\omega-\varepsilon_\alpha(1\mp i0^+)}\,|\alpha\rangle\ . \tag{3.52}$$

With this definition, Eq. (3.51) takes the form

$$\langle a|\,\Sigma^{(2+)}(\varepsilon_a)\,|a\rangle = \frac{i}{2\pi}\int d\omega \sum_i \frac{\left\langle a\phi_i^{(-)}(\varepsilon_a-\omega)\right|\,I(\omega)\,\left|\phi_i^{(+)}(\varepsilon_a-\omega)a\right\rangle}{\varepsilon_a-\omega-\varepsilon_i(1-i0^+)}\,. \tag{3.53}$$

Assuming that the nuclear potential is spherically symmetric, the matrix elements of the potential energy are given by

$$\langle a|\,V\,|b\rangle = \int_0^\infty dr\,V(r)[G_a(r)G_b(r)+F_a(r)F_b(r)]\delta_{\kappa_a\kappa_b}\delta_{m_a m_b}\,, \tag{3.54}$$

that is, they are diagonal in the relativistic angular momentum and magnetic quantum numbers. This implies that the effective basis functions in Eq. (3.52) have the same angular dependence as the eigenstate $|i\rangle$, and the expression in Eq. (3.52) only amounts to a correction of the radial wave functions.

We can further simplify Eq. (3.53) by performing the angular integrations explicitly. This will leave only radial integrations for numerical evaluation. To this end, the photon interaction operator is expanded in a partial-wave series. The resulting expressions are given in Appendix B. The expression in Eq. (3.53) becomes

$$\begin{aligned}\langle a|\,\Sigma^{(2+)}(\varepsilon_a)\,|a\rangle = \frac{i\alpha}{2\pi}\sum_{\kappa_i,n_i}\frac{(-1)^{j_i-j_a}}{2j_a+1}\int d\omega \\ \times\sum_L(-1)^L\frac{R_L\left(\omega;a\phi_i^{(-)}(\varepsilon_a-\omega)\phi_i^{(+)}(\varepsilon_a-\omega)a\right)}{\varepsilon_a-\omega-\varepsilon_i(1-i0^+)}\,,\end{aligned} \tag{3.55}$$

where the sum over L runs from $|j_a - j_i|$ to $j_a + j_i$, and the function R_L defined in Eq. (B.5) of the Appendix B involves radial integrals.

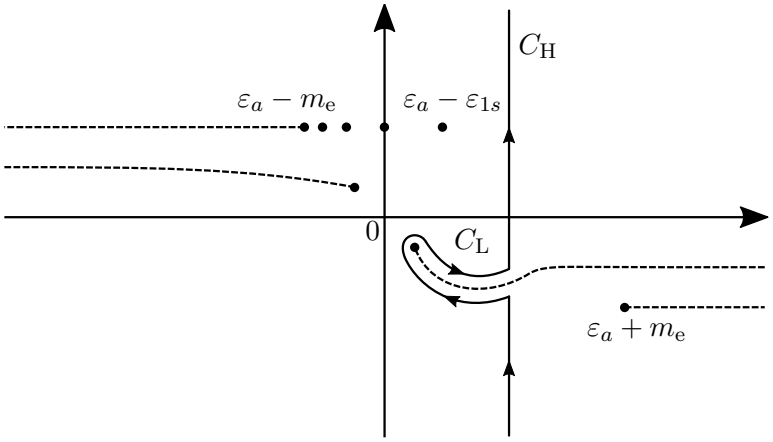

Figure 3.3.: Contour of integration for the many-potential term in the frequency plane. The contour of integration is comprised of a low-energy part C_L and a high-energy part C_H.

To perform the frequency integration, we use a Wick rotation to rotate the contour of integration from the real axis to the complex plane. This allows to avoid oscillatory integrals in favor of strongly decaying functions. We use the contour from Ref. [58]. The contour is depicted in Fig. 3.3. It is comprised of a low-energy part C_L and a high-energy part C_H. The contour C_L is chosen such that the poles from the bound-electron propagator coming from bound states n with $\varepsilon_n < \varepsilon_a$ are avoided. This makes the calculation applicable to an arbitrary initial bound state without the necessity to subtract residues due to poles arising from bound states n with $\varepsilon_n < \varepsilon_a$. The contour C_H connects to the contour C_L at points on the plane with real part ε_0 and goes vertically to $\pm\infty$.

In practical calculations, after taking all limits, the contour C_H extends from $\varepsilon_0 - i\infty$ to $\varepsilon_0 + i\infty$. The contour C_L is given by the parametrization of an elipse

$$\omega = \frac{\varepsilon_0}{2}\left(1 + \frac{\delta e^{-i\varphi}}{\sqrt{\delta^2\cos^2\varphi + \sin^2\varphi}}\right), \tag{3.56}$$

where the parameter φ runs from 0 to π for the lower part and from π to 0 for the upper part of the contour. The parameters are ε_0 and δ are free parameters which are adjusted to achieve optimal numerical efficiency. We use the values $\varepsilon_0 = \varepsilon_a - 0.9\varepsilon_{1s}$ and $\delta = \varepsilon_a/(5n_a^{1/3})$ from Ref. [58] for these parameters, where ε_{1s} is the ground-state Dirac energy and n_a is the principal quantum number of the reference state.

3.4. Numerical calculations

One sees from the formulas in Eq. (3.21) and Eq. (3.46) that we need the Fourier transforms of the reference state wave function to calculate the zero- and one-potential contributions. According to Eq. (3.18), this amounts to calculating spherical Bessel transforms given in Eqs. (3.19) and (3.20) of the radial wave functions.

In our numerical treatment, the radial wave functions are determined in a cavity of radius R_{cav} using the DKB approach (see Chapter 2). Therefore, the integral in Eqs. (3.19) and (3.20) extends only up to R_{cav}, that is

$$\widetilde{G}_{n\kappa}(p) = 4\pi \int_0^{R_{\mathrm{cav}}} dr\, G_{n\kappa}(r) j_\ell(pr) pr\,, \tag{3.57}$$

and

$$\widetilde{F}_{n\kappa}(p) = -4\pi \frac{\kappa}{|\kappa|} \int_0^{R_{\mathrm{cav}}} dr\, F_{n\kappa}(r) j_{\bar{\ell}}(pr) pr\,. \tag{3.58}$$

The interval from 0 to R_{cav} is divided into subintervals by the sequence of breakpoints $0 = x_1 < x_2 < \cdots < x_M = R_{\mathrm{cav}}$ and the integrals in Eqs. (3.57) and (3.58) are expressed as sums of integrals over each of the subintervals. Using the expansion of the radial wave functions in terms of B-spline basis function given in Eqs. (2.35) and (2.36) the fact that B-splines of order K are polynomials of degree at most $K-1$ on each of these subintervals, we can reduce the computation of the integrals over each of the subintervals to the computation of elementary integrals.

To this end, we note that a linear combination of B-spline basis functions can be expressed as

$$\sum_{i=1}^{N} c_i B_i(x) = \sum_{k=0}^{K-1} c_{kj} (x - x_j)^k\,, \tag{3.59}$$

for $x_j \le x < x_{j+1}$. The terms $(x-x_j)^k$ can be expanded using the binomial theorem to obtain

$$\sum_{k=0}^{K-1} c_{kj} (x - x_j)^k = \sum_{s=0}^{K-1} d_{sj} x^s\,, \tag{3.60}$$

where the coefficients d_{sj} are given by

$$d_{sj} = \sum_{k=s}^{K-1} \binom{k}{s} (-x_j)^{k-s} c_{kj}\,. \tag{3.61}$$

In this manner, we can write

$$x\, G_{n\kappa}(x) = \sum_{s=0}^{K} g_{sj}(n\kappa) x^s\,, \tag{3.62}$$

$$x\, F_{n\kappa}(x) = \sum_{s=0}^{K} f_{sj}(n\kappa) x^s\,, \tag{3.63}$$

for $x_j \le x < x_{j+1}$. The expansion coefficients $g_{sj}(n\kappa)$ and $f_{sj}(n\kappa)$ can be obtained from the expansion of the radial wave functions in terms of B-spline basis function in Eqs. (2.35) and (2.36) using Eqs. (3.59)-(3.61). With these definitions, the spherical Bessel transforms of the radial wave functions read

$$\widetilde{G}_{n\kappa}(p) = 4\pi \sum_{j=1}^{M-1} \sum_{s=0}^{K} g_{sj}(n\kappa) \frac{\mathcal{J}_{s\ell}(px_{j+1}) - \mathcal{J}_{s\ell}(px_j)}{p^s}\,, \tag{3.64}$$

$$\widetilde{F}_{n\kappa}(p) = -4\pi \frac{\kappa}{|\kappa|} \sum_{j=1}^{M-1} \sum_{s=0}^{K} f_{sj}(n\kappa) \frac{\mathcal{J}_{s\bar{\ell}}(px_{j+1}) - \mathcal{J}_{s\bar{\ell}}(px_j)}{p^s}\,, \tag{3.65}$$

where

$$\mathcal{J}_{s\ell}(x) = \int_0^x dt\, t^s j_\ell(t)\,. \tag{3.66}$$

The functions $\mathcal{J}_{s\ell}$ are calculated iteratively (see also Ref. [78]). For $\ell = 0$, we have that $j_0 = \operatorname{sinc} x$ and

$$\mathcal{J}_{s0}(x) = \int_0^x dt\, t^{s-1} \sin t\,. \tag{3.67}$$

For $s = 0$, we obtain $\mathcal{J}_{00}(x) = \operatorname{Si} x$, where Si is the sine integral function [76]. The values $\mathcal{J}_{s0}(x)$ for $s > 0$ are determined iteratively starting from $\mathcal{J}_{00}(x)$ and using partial integration. For $\ell > 0$ and $s = 0$, we use the recurrence relation [76]

$$(\ell+1) j_\ell(x) = x[j_{\ell-1}(x) - j'_\ell(x)]\,, \tag{3.68}$$

and partial integration to obtain

$$\mathcal{J}_{0\ell}(x) = \frac{\mathcal{J}_{1,\ell-1}(x) - x j_\ell(x)}{\ell}\,. \tag{3.69}$$

For $\ell > 0$ and $s > 0$, we use the recurrence relation [76]

$$j_\ell(x) = \frac{\ell-1}{x} j_{\ell-1}(x) - j'_{\ell-1}(x)\,, \tag{3.70}$$

and, again, partial integration to obtain

$$\mathcal{J}_{s\ell}(x) = (\ell+s-1)\mathcal{J}_{s-1,\ell-1}(x) - x^k j_{\ell-1}(x)\,. \tag{3.71}$$

The calculation of the zero-potential contribution using Eq. (3.21) is then straightforward. We use Quadpack [77] routines to perform the integration. For the calculation of the one-potential contribution using Eq. (3.46), we need to do some further simplification. First of all, if ϱ denotes the spherically symmetric nuclear charge density normalized to one, then we have for the Fourier transform of the potential energy function

$$\widetilde{V}(q) = -4\pi Z\alpha \frac{\widetilde{\varrho}(q)}{q^2}\,. \tag{3.72}$$

In particular, for a homogeneously charged sphere as the model for the nucleus, that is

$$\varrho(\boldsymbol{x}) = \frac{3}{4\pi R_{\mathrm{nucl}}^3}\Theta(R_{\mathrm{nucl}} - |\boldsymbol{x}|)\,, \tag{3.73}$$

where R_{nucl} denotes the nuclear radius, we obtain for its Fourier transform

$$\widetilde{\varrho}(q) = 3\,\frac{j_1(qR_{\mathrm{nucl}})}{qR_{\mathrm{nucl}}}\,. \tag{3.74}$$

Substituting Eq. (3.72) into the Eq. (3.46), we see that the one-potential term is of the form

$$\langle a|\,\Sigma^{(1)}(\varepsilon_a)\,|a\rangle = \int_0^\infty dp' \int_0^\infty dp \int_{-1}^{+1} d\xi\,\frac{p'p}{q^2}\,\widetilde{\varrho}(q) f(p', p, \xi)\,, \tag{3.75}$$

with an integrable singularity of the integral over ξ at $q = 0$. To remove the singularity, we perform a substitution similar to the one in Ref. [57] given by

$$\xi = \frac{p'^2 + p^2 - e^{-2v}}{2p'p}\,, \tag{3.76}$$

where the variable v runs from $v_{\mathrm{min}} = -\ln(p' + p)$ to $v_{\mathrm{max}} = -\ln(|p' - p|)$. This transforms Eq. (3.75) into

$$\langle a|\,\Sigma^{(1)}(\varepsilon_a)\,|a\rangle = \int_0^\infty dp' \int_0^\infty dp \int_{v_{\mathrm{min}}}^{v_{\mathrm{max}}} dv\,\widetilde{\varrho}(e^{-v}) f(p', p, \xi(p', p, v))\,. \tag{3.77}$$

This means, that the one-potential contribution takes the form

$$\langle a|\,\Sigma^{(1)}(\varepsilon_a)\,|a\rangle = \int_0^\infty dp' \int_0^\infty dp\, g(p', p)\,, \tag{3.78}$$

with a function g that satisfy $g(p', p) = g(p, p')$. This symmetry implies that we can transform the integral over p' and p into

$$\langle a|\,\Sigma^{(1)}(\varepsilon_a)\,|a\rangle = \int_0^\infty dx \int_0^x dy\, g\left(\frac{x+y}{2}, \frac{x-y}{2}\right)\,. \tag{3.79}$$

Finally, we transform the integral over x to the interval $0 \leq s < 1$ by substituting $x = \tan(\pi s/2)$. The integrals are numerically computed using routines from the library Quadpack [77].

For the calculation of the many-potential contribution using Eq. (3.55), we follow the finite basis set approach of Ref. [57]. However, we use basis sets obtained from the DKB approach rather than the ones used in Ref. [57]. We need basis sets for free electrons and for electrons in the static field of the nucleus. We use these basis sets to construct the frequency-dependent effective basis functions in Eq. (3.52). In practical calculations, we use twenty more basis functions for the electrons in the

Table 3.1.: Self-energy corrections for various H-like ions in terms of the dimensionless function F_{SE} defined in Eq. (3.80). The nucleus is modeled to be a homogeneously charged sphere. We compare our calculations to the results of Refs. [79, 80].

Ion	R_{RMS} [fm]	$1s_{1/2}$	$2s_{1/2}$	$2p_{1/2}$	Refs.
Fe^{26+}	3.730	2.783 8(1)	3.059(2)	−0.077(2)	
		2.783 766(1)	3.059 29(1)	−0.076 22(1)	[79, 80]
Xe^{53+}	4.826	1.781 9(2)	2.160(1)	0.025 6(2)	
		1.781 866(1)	2.160 775(1)	0.025 616(1)	[79, 80]
Pb^{81+}	5.505	1.487 3(2)	2.065 3(3)	0.205 6(2)	
		1.487 258(1)	2.065 327(1)	0.205 610(1)	[79, 80]
U^{91+}	5.863	1.472 4(1)	2.170 4(3)	0.316 9(1)	
		1.472 424(1)	2.170 404(2)	0.316 858(1)	[79, 80]

field of the nucleus as compared to the free electrons as this was observed to improve the calculation in Ref. [57]. The convergence of the calculated value for the many-potential contribution is tested by performing the calculation for increasing number of basis functions in the basis set.

The many-potential term is a series in the angular quantum number κ. We compute the sequence of terms and group them according to their angular momentum quantum number ℓ. That is, we have that $\kappa = -1$ for $\ell = 0$ and we have that $\kappa = \ell$ or $\kappa = -(\ell + 1)$ for $\ell > 0$. The terms involve an integral over the photon frequency ω along the contour C_{L} and C_{H}, for which we use again routines from the library Quadpack [77]. The series over ℓ is truncated at some maximal value ℓ_{max} and the remainder is extrapolated from the calculated terms by fitting polynomials in $1/\ell$ to these terms.

3.5. Results and summary

Following common notations, we express the self-energy correction in terms of a dimensionless function F_{SE} given by the equation

$$\Delta E_{\mathrm{SE}} = \frac{\alpha}{\pi} \frac{(Z\alpha)^4}{n_a^3} F_{\mathrm{SE}}(Z\alpha) m_{\mathrm{e}} \,, \tag{3.80}$$

where n_a is the principal quantum number of the reference state.

For calculations of the self-energy correction with an extended nucleus, we use the homogeneously charged sphere as the model for the nuclear charge distribution. In Table 3.1 we present numerical results for this correction for various H-like ions.

Table 3.2.: Self-energy corrections for H-like ions in terms of the dimensionless function F_{SE} for a point-like nucleus. The calculations are compared to results from Ref. [58].

Ion	$4f_{5/2}$	$5f_{5/2}$	$4f_{7/2}$	$4f_{7/2}$	Ref.
W^{73+}	−0.021(2)	−0.020(3)	0.022(3)	0.024(1)	
	−0.019 8(4)	−0.018 4(7)	0.023 1(4)	0.024 7(7)	[58]
U^{91+}	−0.019(2)	−0.019(2)	0.023(2)	0.03(2)	
	−0.018 9(2)	−0.017 5(5)	0.024 5(2)	0.026 2(5)	[58]

We compare our results to the ones of Refs. [79, 80], where an approach based on position-space expressions for the self-energy shift together with expansions in the nuclear coupling strength $Z\alpha$ has been employed. We use the same values for the nuclear RMS radii as given in Ref. [80]. We see that our calculations agree with the one of Refs. [79, 80] to the precision we achieve. There are even more precise results in Ref. [81], where an approach developed in Ref. [82] has been used. Within this approach, the many-potential contribution to the propagator of the electron in the field of the nucleus is separated into an approximate part, which can be treated explicitly without performing a partial-wave expansion, and a remainder term, which is expanded in a partial-wave series with enchanced convergence. However, our purpose is not to reach utmost numerical precision, but to provide a versatile method capable of yielding self-energy results for arbitrary bound-electron states. Uncertainties arising from the screening potential approximation to be introduced later in this chapter are larger than the numerical uncertainty of the self-energy calculations.

We are also interested in the quality of our method when the reference state is highly excited. To this end, we tabulate calculations for f ($\ell = 3$) states in Table 3.2 and compare our results to the ones of Ref. [58], where a method based on the evaluation of the many-potential contribution to the propagator of the electron in the field of the nucleus has been employed. As the calculations in Ref. [58] have been performed for point-like nuclei, we also treat the nucleus as effectively point-like by choosing the nuclear radius small enough. We see that our results are consistent with the results of Ref. [58] within the precision we achieve.

In a multi-electron configuration, where there is one valence electron over closed shells, we use the screening potential approximation to account for the interactions between the valence electron and the core electrons. In this approximation, the charge density of the core electrons generates a spherically symmetric potential which screens the potential of the nucleus. If V_{scr} denotes the resulting potential energy function, then self-energy corrections to the valence electron are obtained by using the methods detailed in this chapter with the substitution of $V + V_{\mathrm{scr}}$ instead of V.

Table 3.3.: Screened self-energy corrections for Na-like Pt^{67+} and Li-like U^{89+}. A core-Hartree potential is used for the screening. The results are expressed in eV and compared to the results of Ref. [57].

	Pt^{67+}		U^{89+}		
Term	$3s_{1/2}$	$3p_{3/2}$	$2s_{1/2}$	$2p_{1/2}$	Ref.
Zero-potential	−97.404 109(5)	−96.951 860 0(5)	−246.7831	−284.5500	
	−97.40	−96.95	−246.78	−284.55	[57]
One-potential	72.550 61(28)	67.051 58(28)	188.6148	169.0079	
	72.55	67.05	188.62	169.01	[57]
Many-potential	32.660(5)	30.912(5)	120.832(1)	124.115	
	32.64(6)	30.89(6)	120.80(6)	124.09(6)	[57]
Total	7.807(5)	1.011(5)	62.664(1)	8.573	
	7.79(6)	0.99(6)	62.64(6)	8.54(6)	[57]

In Table 3.3, we tabulate calculations of the screening effect using a core-Hartree (CH) potential as screening potential. That is, we set $V_{\mathrm{scr}} = V_{\mathrm{CH}}$, where the core-Hartree potential is given by

$$V_{\mathrm{CH}}(r) = 4\pi\alpha \int_0^\infty dr'\, r'^2 \frac{\varrho_{\mathrm{core}}(r')}{r_>}\,, \tag{3.81}$$

where $r_>$ is the larger one of r and r', and ϱ_{core} denotes the combined radial charge densities of the core electrons. Explicitly, we have that

$$\varrho_{\mathrm{core}}(r) = \frac{1}{4\pi r^2} \sum_{c\in\mathrm{core}} (2j_c+1)[G_c^2(r) + F_c^2(r)]\,. \tag{3.82}$$

The radial wave functions of the core electrons are obtained from Dirac-Fock calculations performed with the grasp2K atomic structure package [83]. We tabulate in Table 3.3 calculations for Na-like Pt^{67+} and Li-like U^{89+} and compare our calculations with the results of Ref. [57]. We list the zero-, one-, and many-potential contributions separately. We see that our results agree with the results of Ref. [57]. Our results are also more precise as we use more terms in the partial-wave expansion of the many-potential term.

Again, since we are interested in the quality of our calculations for highly-excited states, we compare our calculations to the results in Ref. [85]. There, a Kohn-Sham (KS) potential was used for the screening effect. That is, we have $V_{\mathrm{scr}} = V_{\mathrm{KS}}$, where

$$V_{\mathrm{KS}}(r) = 4\pi\alpha \int_0^\infty dr'\, r'^2 \frac{\varrho_{\mathrm{cv}}}{r_>} - \left[\frac{3}{\pi} r^3 \varrho_{\mathrm{cv}}(r)\right]^{\frac{1}{3}} \frac{\alpha}{r}\,, \tag{3.83}$$

Table 3.4.: Screened self-energy corrections for Cu-like ions in terms of the dimensionless function F_{SE}. A Kohn-Sham potential is used for the screening. The nucleus is modeled to be a homogeneously charged sphere in our calculations. The RMS radii are taken from Ref. [84]. We compare our calculations to the results of Refs. [85], where the nuclear charge distribution is of Fermi-Dirac type. The RMS radii used are not given in the reference.

Ion	R_{RMS} [fm]	$4d_{3/2}$	$4d_{5/2}$	Refs.
Sn^{21+}	4.6519	−0.012(2)	0.006(1)	
		−0.0117	0.0060	[85]
Nd^{31+}	4.9421	−0.0143(2)	0.011(1)	
		−0.0143	0.0109	[85]

where the density ϱ_{cv} also includes the valence electron and is given by

$$\varrho_{\mathrm{cv}}(r) = \varrho_{\mathrm{core}}(r) + \frac{G_v^2(r) + F_v^2(r)}{4\pi r^2}\,, \tag{3.84}$$

with G_v and F_v denoting the radial wave functions of the valence electron. The radial wave functions are again obtained from Dirac-Fock calculations [83]. Our results are consistent with the results of Ref. [85].

After establishing that our calculations accurately reproduce prior calculations of the self-energy contribution for single-electron systems as well in the screening approximation, we discuss the calculation of the self-energy correction to the binding energy of Rb-like $^{131}Xe^{17+}$. The ground state of $^{131}Xe^{18+}$ is a Kr-like configuration with $[\mathrm{Ar}]3d^{10}4s^24p^6$. The additional electron in Rb-like $^{131}Xe^{17+}$ is in the state $4d_{3/2}$. Note that the valence shell is filled according to Coulomb ordering. The leading single-electron contribution to the self-energy correction is −16(2) meV. We performed the screening calculation with the core-Hartree and Kohn-Sham potentials. For the prior, we obtained for the correction −4.3(1) meV and for the latter −4.7(1) meV. In our calculations, we model the nucleus as a homogeneously charged sphere and take the RMS radius from Ref. [84]. In total, the self-energy correction to the binding energy of $^{131}Xe^{17+}$ is approximately 21 meV. The measured value of the total binding energy in Ref. [4] is 432.4(1.3)(3.4) eV. Thus, the leading QED effect of self-energy correction is not visible at this level of precision, however, it will be relevant for projected experiments with xenon ions in higher ionization states employing the PENTARAP Penning-trap setup [86].

Recently, the PENTATRAP experiment observed a long-lived metastable electronic state in $^{187}Re^{29+}$ [2]. The electronic excitation energy was determined by measuring the mass difference between the ground and excited state of the ion. The

ground state is given by the configuration $[\mathrm{Kr}]4d^{10}$ with a total angular momentum of $J = 0$. The excited state is given by the configuration $[\mathrm{Kr}]4d^9 4f^1$ with a total angular momentum of $J = 5$, where an electron is excited from the $4d_{5/2}$ state to the $4f_{5/2}$ state. We calculate the self-energy shift by considering the electron in the $4d_{5/2}$ state for the ground state and in the $4f_{5/2}$ state for the excited state, while all remaining electrons screen the nucleus. We use again the core-Hartree and Kohn-Sham screening potentials. Our result for the ground-state self-energy contribution is 18.49(5) meV using the core-Hartree, and 20.35(8) meV using the Kohn-Sham potential. For the excited state, we obtain $-8.7(2)$ meV with the core-Hartree, and $-9.8(2)$ meV with the Kohn-Sham potential. Thus, the contribution to the electronic excitation energy is of approximately -30 meV. The measured value of the excitation energy in Ref. [2] is 202.2(1.7) eV. Thus, the self-energy effect is not yet visible at the current level of experimental precision.

Besides self-energy corrections to energy levels, we are also interested in corrections to the g factor. The first-order self-energy corrections to the g factor as well as second-order self-energy corrections to energy levels involve a subset of diagrams where the external wave functions are perturbed due to the self-energy effect. The self-energy correction of $|a\rangle$ is given by

$$|\delta_{\mathrm{SE}} a\rangle = \sum_{n}^{\varepsilon_n \neq \varepsilon_a} \frac{\langle n| \Sigma(\varepsilon_a) |a\rangle}{\varepsilon_n - \varepsilon_a} |n\rangle \ . \tag{3.85}$$

In contrast to our considerations in this chapter, one needs nondiagonal matrix elements of the self-energy operator in this case. The numerical calculations of these self-energy corrected wave functions were considered in Ref. [3] and used in Ref. [5]. In Ref. [3], besides implementing numerical Fourier transforms of the wave functions (albeit in a different way than explained in Section 3.4), we observed that the self-energy corrected wave functions admit an asymptotic form for large radii r, which is proportional to some power of r multiplied by the radial wave functions. Numerical calculations and analysis by N. S. Oreshkina showed, that [3]

$$\begin{pmatrix} \delta_{\mathrm{SE}} G_a(r) \\ \delta_{\mathrm{SE}} F_a(r) \end{pmatrix} \propto \frac{\alpha}{\pi} r \begin{pmatrix} G_a(r) \\ F_a(r) \end{pmatrix} , \tag{3.86}$$

for large r and fits to numerical calculations allowed to determine the proportionality constant. This then helped to improve the numerical calculations.

4. The g Factor of Lithium- and Boronlike Ions

The following discussion and the results have been accepted for publication (see Ref. [1]) and the text is to a large extent verbatim with some modifications and extensions to make it more accessible. The results for B-like $^{40}Ar^{13+}$ have been published separately in a collaborative work in Ref. [6]. Note that we are using units in which $m_e = 1$ in this chapter.

4.1. Relativistic g factor

We consider the Zeeman shift of an energy level of an atom with a spinless nucleus. The contribution to the Zeeman shift which is linear in the external magnetic field is parametrized in terms of the g factor of the atom by the equation

$$\Delta E = g\,\mu_B \langle \boldsymbol{J} \cdot \boldsymbol{B} \rangle\,, \tag{4.1}$$

where ΔE is the energy shift, $\boldsymbol{J}$ is the operator of the total angular momentum, $\boldsymbol{B}$ is the external magnetic field, $\mu_B = |e|/2$ denotes the Bohr magneton, and g is the g factor. The g factor is determined by computing the Zeeman energy splitting and solving Eq. (4.1) for g.

The relativistic interaction of an electron with the homogeneous external magnetic field is given by

$$V_{\rm mag}(\boldsymbol{r}) = -e\boldsymbol{\alpha} \cdot \boldsymbol{A}(\boldsymbol{r})\,, \tag{4.2}$$

where $\boldsymbol{A}$ is the vector potential $\boldsymbol{A}(\boldsymbol{r}) = (\boldsymbol{B} \times \boldsymbol{r})/2$. Assuming that the magnetic field is directed along the z axis, $V_{\rm mag}$ reduces to

$$V_{\rm mag}(\boldsymbol{r}) = \mu_B B_z \left(\boldsymbol{r} \times \boldsymbol{\alpha}\right)_z\,. \tag{4.3}$$

An *ab initio* QED theory of the g factor of an atom can be formulated e.g. within the two-time Green's function formalism [65]. Within this formalism, the Zeeman energy splitting is calculated.

To leading order (i.e. linear in the magnetic field and at the tree level), the Zeeman energy splitting of an atomic state $|a\rangle$ is given by the matrix element $\langle a|\, V_{\rm mag}\, |a\rangle$, where a labels the collection of quantum numbers n, κ, m defining an atomic state.

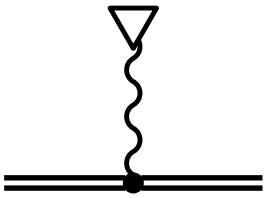

Figure 4.1.: The Feynman diagram representing the leading contribution to the bound-electron g factor. A wavy line with a triangle represents an interaction with the external magnetic field.

While we need only the diagonal matrix elements of the magnetic interaction potential $V_{\rm mag}$ for the g factor, it is useful to give a slightly more general expression for later considerations where the principal quantum numbers of the states differ. Namely

$$\langle n\kappa m|\, V_{\rm mag}\, |n'\kappa m\rangle = \mu_{\rm B} B_z m \frac{\kappa}{j(j+1)} \int_0^\infty dr\, r[G_{n\kappa}(r)F_{n'\kappa}(r) + F_{n\kappa}(r)G_{n'\kappa}(r)]\,, \tag{4.4}$$

where the functions $G_{n\kappa}$ and $F_{n\kappa}$ are the radial components of the electronic wave function given in Eq. (2.11).

4.1.1. Dirac value and nuclear size contribution

The leading contribution to the g factor of an alkali-like (or monovalent) atom or ion arises through the interaction of the valence electron with the external magnetic field. The corresponding Feynman diagram is depicted in Fig. 4.1. Within the approximation of non-interacting electrons, contributions resulting from the interaction of the closed-shell core electrons with the external magnetic field cancel in the final sum, since electrons with opposite spin projections induce contributions of the same magnitude but of opposite sign. Therefore, only the contribution of the valence electron remains. For this reason, the g factor of the whole alkali-like atom is often termed as the bound-electron g factor (assuming that of the valence electron).

The leading (Dirac) contribution to the bound-electron g factor of an alkali-like atom with the valence state characterized by the quantum numbers n and κ is

$$g_{\rm D} = \frac{2\kappa}{j(j+1)} \int_0^\infty dr\, r\, G_{n\kappa}(r)F_{n\kappa}(r)\,, \tag{4.5}$$

which is obtained from Eqs. (4.1) and (4.4).

For a point-like nucleus, the integral in Eq. (4.5) can be evaluated analytically, with the result [25, 87]

$$g_{\rm D}({\rm pnt}) = \frac{\kappa}{2j(j+1)} \left(2\kappa\varepsilon_{n\kappa} - 1\right)\,, \tag{4.6}$$

where $\varepsilon_{n\kappa}$ is the Dirac energy of the reference state. In particular, for the $2s$ and $2p_{1/2}$ states relevant for this chapter, they are

$$\varepsilon_{2s} = \varepsilon_{2p_{1/2}} = \sqrt{\frac{1+\gamma}{2}} \tag{4.7}$$

where $\gamma = \sqrt{1-(Z\alpha)^2}$.

The nuclear size correction to the point-nucleus Dirac value is determined as the difference of Eq. (4.5) evaluated numerically for an extended nuclear charge distribution and the point-nucleus result of Eq. (4.6). We mostly use the homogeneously charged sphere as the model for an extended nucleus with the RMS radii taken from Ref. [84]. We estimate the dependence on the model by also using the two-parameter Fermi distribution and find it to be insignificant compared to the uncertainties associated with other contributions.

4.1.2. First-order interelectronic interaction

Interactions among the electrons in a multi-electron ion result in a contribution to the bound-electron g factor. These interactions can be classified according to the number of exchanged photons and the associated perturbation parameter is $1/Z$, i.e., the ratio of the strength of the electron-electron Coulomb repulsion and the strength of the Coulomb interaction with the nucleus.

We calculate the leading one-photon exchange contribution, which corresponds to the first-order perturbation correction in the parameter $1/Z$. A typical contributing diagram is depicted in Fig. 4.2. As seen in the figure, the computation of the one-photon exchange contribution reduces the many-electron problem to a two-electron one, where one of the core electrons interacts with the valence electron in addition to the interaction with the external magnetic field. Analogous contributions from the exchange between core electrons vanish, again, identically after summing over the momentum projections of the closed-shell core states.

The one-photon exchange contribution to the Zeeman shift of an energy level can be expressed as the sum of an *irreducible* and a *reducible* part; the corresponding formulas were derived in Ref. [53] using the two-times Green's function formalism. Alternatively, one can start from the contribution of the interelectronic interaction to the level energy (see Section 1.4) and systematically consider the perturbations of each of the matrix elements. This approach has the additional advantage that it also provides a numerical algorithm to evaluate the contributions. We used this second approach to verify the formulas of Ref. [53] and to compute these contributions. The idea behind this approach is that diagrams of the kind depicted in Fig. 4.2 correspond to first-order contributions in diagrams corresponding to corrections to the level energy with the electronic states being solutions of the Dirac equation in

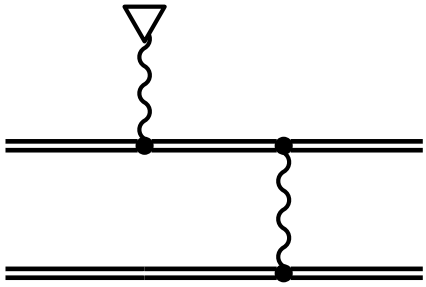

Figure 4.2.: A typical Feynman diagram representing the one-photon interelectronic-interaction contribution to the bound-electron g factor. Only diagrams where one of the electrons is the valence electron and the other one a core electron contribute.

the static nuclear field *and* in the external magnetic field. Then, the formula for the shift of the level energy is expanded perturbatively to obtain the contribution to the bound-electron g factor.

The irreducible part arises from the first-order perturbative correction to the bound-electron wave function $|a\rangle \mapsto |a\rangle + |\delta a\rangle$, with

$$|\delta a\rangle = \sum_{n}^{\varepsilon_n \neq \varepsilon_a} \frac{\langle n| V_{\rm mag} |a\rangle}{\varepsilon_a - \varepsilon_n} |n\rangle \ , \tag{4.8}$$

where a is either a core-electron state c or a valence-electron state v, and the summation label n runs over the whole electronic spectrum including all bound states except the reference state a. The irreducible contribution is then given by

$$\Delta E^{(1)}_{\rm int,irr} = 2 \sum_{c} \Big(\langle vc| I(0) |\delta vc\rangle - \langle cv| I(\Delta_{vc}) |\delta vc\rangle + \langle vc| I(0) |v\delta c\rangle - \langle cv| I(\Delta_{vc}) |v\delta c\rangle \Big) , \tag{4.9}$$

where the summation is carried out over all core states, $\Delta_{vc} = \varepsilon_v - \varepsilon_c$ is the difference between the unperturbed (Dirac) energy levels of the valence and core electrons, and I is the operator of the electron-electron interaction introduced in Eq. (1.90).

The reducible contribution arises from first-order perturbations of the energies of the core and valence electrons by the magnetic interaction, $\varepsilon_a \mapsto \varepsilon_a + \langle a| V_{\rm mag} |a\rangle$. It is given by

$$\Delta E^{(1)}_{\rm int,red} = \sum_{c} \langle cv| I'(\Delta_{vc}) |vc\rangle \Big(\langle c| V_{\rm mag} |c\rangle - \langle v| V_{\rm mag} |v\rangle \Big) , \tag{4.10}$$

where the prime on $I'(\omega)$ denotes the derivative with respect to ω.

For the numerical computation of the one-photon exchange correction we solve the radial Dirac equation using basis sets constructed from B splines within the dual

Table 4.1.: First-order interelectronic-interaction contribution to the bound-electron g factor of the ground state of Li- and B-like ions. The uncertainties account for uncertainties in the nuclear RMS radii and numerical errors.

	Electron correlation of order $(1/Z)^1$	
Z	Li-like	B-like
18	0.000 414 450 489 (3)	0.000 657 531 117 (1)
20	0.000 461 147 896 (3)	0.000 731 996 913 (1)
24	0.000 555 185 23 (1)	0.000 882 350 695 (5)
32	0.000 746 458 66 (1)	0.001 190 274 990 (5)
54	0.001 306 216 8 (4)	0.002 118 178 3 (3)
82	0.002 148 290 (1)	0.003 654 888 (2)
92	0.002 509 828 (7)	0.004 393 71 (1)

kinetic balance (DKB) approach [56, 73]. This approach is particularly suited for the computation of spectral sums as in Eq. (4.8). In our numerical treatment of the radial Dirac equation we take the nuclear size into account by using a homogeneously charged sphere as a nucleus with RMS radii taken from Ref. [84]. The contributions are calculated using the Feynman and Coulomb gauges (see Appendix B) in order to estimate the numerical uncertainty. We present our result in Table 4.1. Our calculations of the one-photon exchange correction reproduce previous results obtained in Ref. [53] for Li-like ions and Ref. [61, 88] for B-like ions.

4.1.3. Higher-order interelectronic interaction [1]

Besides the leading one-photon interelectronic-interaction of order $1/Z$, there are higher-order contribtution due to the interelectronic interaction which need to be taken into account. The exchange of just one photon reduced the leading interelectronic interaction to a two-electron contribution. In the higher-order contributions however, two or more photons are exchanged. Correspondingly, there are now diagrams involving two or more electrons.

Corrections of order $(1/Z)^2$, i.e. corrections involving two exchanged photons have been computed for Li-like ions in Ref. [59] using perturbation theory. Contributions of order $(1/Z)^3$ and higher were calculated there within the Breit approximation using the configuration-interaction Dirac-Fock-Sturm method [89, 90].

In Ref. [1], contributions of order $(1/Z)^2$ and higher were computed using the configuration-interaction Dirac-Fock-Sturm method. Thereby, Dirac-Hartree-Fock

[1] This section does not comprise work in relation with this thesis. The calculations described in this section have been performed by N. S. Oreshkina and I. I. Tupitsyn in Ref. [1].

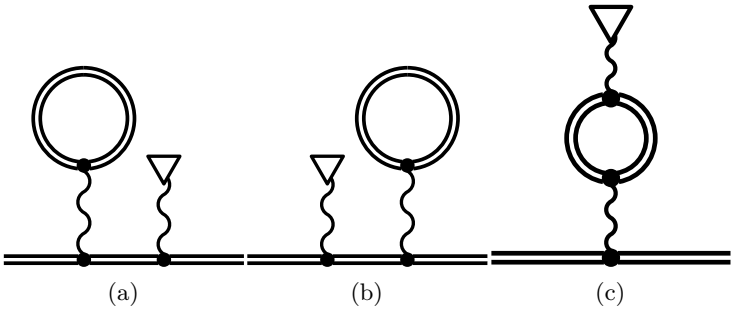

Figure 4.3.: Feynman diagrams corresponding to the vacuum polarization contributions arising from the interaction of the valence electron.

orbitals were used to describe the occupied states while relativistic Sturmian orbitals were employed for the virtual states as in Ref. [62]. Contributions of the negative energy part of the spectrum were found to be relevant in the calculation for Li-like ions in Ref. [20]. These contributions are also important in the B-like case and they were described by Sturmian orbitals as well.

4.2. Vacuum polarization

Besides relativistic contributions to the bound-electron g factor, there are contributions resulting from QED effects. These are the interaction of the electrons with themselves by emmitting and reabsorbing a virtual photon, which is called the self-energy (SE) effect, and the interactions of the electrons with the nucleus by creating and annihilating virtual electron-positron pairs, which is called the vacuum polarization (VP) effect.

In Ref. [1], both these effects were considered. The one-electron SE contribution was taken into account to all orders in $Z\alpha$. Screening effects of the SE contribution due to interelectronic interactions were taken into account through effective potentials. The calculation of the SE contributions have been performed by Prof. V. A. Yerokhin and are not part of this thesis. Thus, in the following, we will restrict ourselves to the description of the VP contributions and refer the reader to Ref. [1] for more details about the calculation of the SE effect.

4.2.1. One-electron vacuum polarization

In the independent electron approximation, i.e. without taking into account the interactions among the electrons, only the valence electron gives a vacuum polarization contribution to the Zeeman splitting. The corresponding diagrams are shown in Fig. 4.3. These diagrams are divided into two groups. The first group comprises the

diagrams in Fig. 4.3a and Fig. 4.3b. They arise due to perturbations of the external wave functions in the tadpole diagram. We call this group the electric loop (EL) contributions. The remaining diagram in Fig. 4.3c arises due to a loop correction to the propagator of the photon mediating the magnetic interaction. Accordingly, it is called the magnetic loop (ML) contribution. The total VP contribution to the Zeeman splitting can thus be written as

$$\Delta E_{\mathrm{VP}} = \Delta E_{\mathrm{VP,EL}} + \Delta E_{\mathrm{VP,ML}} \tag{4.11}$$

For the computation of the EL contribution, we note that the tadpole part of the EL diagrams is equivalent to the insertion of a potential function U_{EL} called EL potential. A detailed derivation of the formal expression for U_{EL} is given in Ref. [91]. It reads

$$U_{\mathrm{EL}}(\boldsymbol{x}) = \frac{i\alpha}{2\pi} \int d^3y \, \frac{1}{|\boldsymbol{x}-\boldsymbol{y}|} \int_{C_F} d\omega \, \mathrm{tr}(G(\omega, \boldsymbol{y}, \boldsymbol{y})) \,, \tag{4.12}$$

where, again, G denotes the Dirac Coulomb Green's function and C_F is the usual Feynman integration contour. The contribution to the energy shift is then

$$\Delta E_{\mathrm{VP,EL}} = 2 \langle v | \, U_{\mathrm{EL}} \, | \delta v \rangle \,, \tag{4.13}$$

where the first-order perturbation $|\delta v\rangle$ of the reference state is given by Eq. (4.8).

The expression in Eq. (4.12) is divergent and needs to be renormalized. To this end, the potential U_{EL} is expanded in powers of the nuclear coupling strength $Z\alpha$. This corresponds to an expansion of the loop in Fig. 4.3a and in Fig. 4.3b in terms of the free-electron propagator and interactions with the nucleus. Due to Furry's theorem, only odd powers of $Z\alpha$ contribute.

The leading term is of order $Z\alpha$ and is called the Uehling contribution. This term is charge divergent. After renormalization, it results in a finite potential called the Uehling potential and is given by [92]

$$U_{\mathrm{Ue}}(\boldsymbol{x}) = -\frac{2}{3}\frac{\alpha}{\pi} Z\alpha \int d^3y \, \frac{\varrho(\boldsymbol{y})}{|\boldsymbol{x}-\boldsymbol{y}|} K_1(2|\boldsymbol{x}-\boldsymbol{y}|) \,, \tag{4.14}$$

where ϱ denotes the nuclear charge distribution normalized to one and where

$$K_1(x) = \int_1^\infty dt \, e^{-xt} \left(1 + \frac{1}{2t^2}\right) \frac{\sqrt{t^2-1}}{t^2} \,. \tag{4.15}$$

For our computations of the Uehling potential, we use analytical formulas resulting from a homogeneously charged sphere as nucleus which have been derived in Ref. [93].

The contribution of higher order in $Z\alpha$ to the EL potential is called the Wichmann-Kroll potential U_{WK} [94]. We use the expressions in Ref. [91] to obtain a partial-wave

expansion for the contributions to the g factor from the partial-wave expansion of the Wichmann-Kroll potential given by

$$U_{\mathrm{WK}}(\boldsymbol{x}) = \sum_{|\kappa|=1}^{\infty} U_{\mathrm{WK}}^{|\kappa|}(\boldsymbol{x})\,. \tag{4.16}$$

We truncate the partial-wave expansion of the g factor at a finite value of $|\kappa|$, typically $|\kappa| = 11$, and estimate the remainder by fitting polynomials in $1/|\kappa|$ to the tail of the partial-wave contributions. In Ref. [91] the nucleus is taken to be a spherical shell and analytical solutions for the Dirac-Coulomb Green's function are used in the calculations. We, however, use a homogeneously charged sphere as a nucleus and, thus, compute the Dirac-Coulomb Green's function numerically, much in the spirit of Refs. [81, 95]. The numerical calculation is performed using the method of Refs. [96, 97] for solving the stationary Dirac equation. We also use approximate expressions for this potential derived in Ref. [98] for point-like nuclei to check our numerical calculations. The total EL potential is then

$$U_{\mathrm{EL}} = U_{\mathrm{Ue}} + U_{\mathrm{WK}}\,. \tag{4.17}$$

In the case of the ML contribution, the effect of the loop can be expressed as a modification of the vector potential of the external magnetic field. This results in a modification of V_{mag} to V_{ML} and the contribution to the Zeeman splitting is given by

$$\Delta E_{\mathrm{VP,ML}} = \langle v|\, V_{\mathrm{ML}}\, |v\rangle\ , \tag{4.18}$$

where $V_{\mathrm{ML}} = -e\boldsymbol{\alpha}\cdot\boldsymbol{A}_{\mathrm{ML}}$ and $\boldsymbol{A}_{\mathrm{ML}}$ is the modified vector potential.

In order to compute the modified vector potential, the loop is, again, expanded in terms of the free-electron propagator and interactions with the nuclear field. The leading order term for a point-like nucleus is $\propto (Z\alpha)^2$ and has been derived in Refs. [42, 43]. We call this term the Delbrück contribution. We only take this leading order term into account and neglect higher order contributions as we expect them to be small compared to the uncertainties of other contributions to the g factor. We obtain

$$\boldsymbol{A}_{\mathrm{ML}}(\boldsymbol{r}) = \boldsymbol{A}(\boldsymbol{r})\Pi_{\mathrm{De}}(|\boldsymbol{r}|)\,, \tag{4.19}$$

where the polarization function Π_{De} is given by

$$\Pi_{\mathrm{De}}(x) = \frac{\alpha}{\pi}(Z\alpha)^2\frac{4}{x^2}\int_0^\infty dq\, F_{\mathrm{De}}(q) j_1(qx) qx\,. \tag{4.20}$$

In this formula, j_1 is the spherical Bessel function of order one and the function F_{De} is taken from Ref. [43]. In Tables 4.4 and 4.5 we estimate the uncertainty of the ML contribution due to higher-order contributions conservatively to be $(Z\alpha)^2\ln\big((Z\alpha)^{-2}\big)$ times the Delbrück contribution and include this into the calculation of the uncertainty of the one-electron VP contribution.

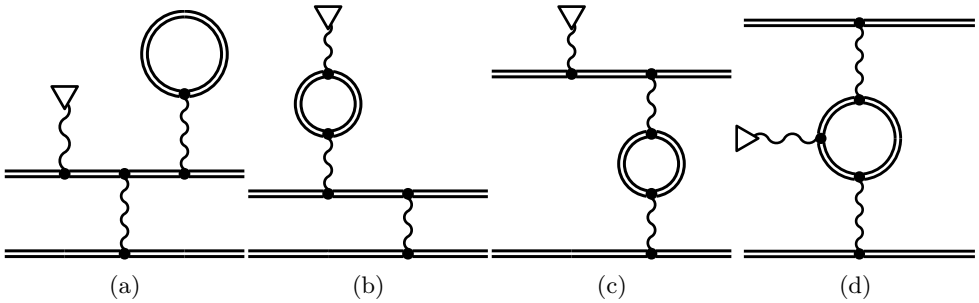

Figure 4.4.: Vacuum polarization contributions to the two-electron interaction. Each of the diagrams shown represents one type of contribution. Contributions represented by the first diagram are called electric loop (EL), by the second diagram magnetic loop (ML), by the third diagram electric loop propagator (ELP), and by the forth magnetic loop propagator (MLP) contributions.

4.2.2. First-order screened vacuum polarization

Apart from single-electron VP contributions to the bound-electron g factor, we calculated the leading order interelectronic-interaction correction to the VP effect. Typical examples of the corresponding Feynman diagrams are depicted in Fig. 4.4. Each of these diagrams represents one of four groups of contributions.

The first group of contributions is again called electric loop contributions. The diagram in Fig. 4.4a depicts one of the diagrams belonging to this group. These EL contributions arise due to first order perturbative corrections to the wave functions of the external and the intermediate states and to the energy levels of the electronic states. Again, there are reducible and irreducible contributions to the Zeeman splitting. Expressions for these contributions have been derived for Li-like systems in Ref. [99] using the two-time Green's function formalism [65], which can be readily generalized to the B-like case. Alternatively, one can start from Eq. (4.9) and Eq. (4.10) and, again, systematically consider the perturbations of each of the matrix elements and Dirac energy levels by the EL potential. However, there is an additional complication due to the appearance of states $|\delta v\rangle$ and $|\delta c\rangle$ already perturbed by the magnetic potential. One way to tackle this issue is to note that

$$|\delta a\rangle = \hat{G}(\varepsilon_a) V_{\mathrm{mag}} |a\rangle \ , \tag{4.21}$$

where a denotes either a valence state v or a core state c and

$$\hat{G}(\varepsilon_a) = \sum_n^{\varepsilon_n \neq \varepsilon_a} \frac{|n\rangle \langle n|}{\varepsilon_a - \varepsilon_n} \tag{4.22}$$

is the reduced Green's function and perturb the reduced Green's function. For this, we use the formula

$$\hat{G}(\varepsilon_a) = \frac{\partial}{\partial\varepsilon}\left[(\varepsilon-\varepsilon_a)G(\varepsilon)\right]\Big|_{\varepsilon=\varepsilon_a}, \tag{4.23}$$

where

$$G(\varepsilon) = \frac{1}{\varepsilon - H} = \sum_n \frac{|n\rangle\langle n|}{\varepsilon-\varepsilon_n}, \tag{4.24}$$

denotes the Green's function of the electron in the static electric field of the nucleus and H is the Dirac-Coulomb Hamiltonian and perturb the Dirac energy levels and the (full) Green's function. To first order in the EL potential, we obtain

$$\varepsilon_a \mapsto \varepsilon_a + \langle a| U_{\mathrm{EL}} |a\rangle ,$$

and

$$\sum_n \frac{|n\rangle\langle n|}{\varepsilon-\varepsilon_n} \mapsto \sum_n \frac{|n\rangle\langle n|}{\varepsilon-\varepsilon_n} + \sum_m\sum_n \frac{|m\rangle\langle m| U_{\mathrm{EL}} |n\rangle\langle n|}{(\varepsilon-\varepsilon_m)(\varepsilon-\varepsilon_n)} .$$

Plugging these expressions into Eq. 4.23 and taking only into account terms of first order in the EL potential U_{EL}, we obtain for the reduced Green's function

$$\begin{aligned}
&\sum_n^{\varepsilon_n\neq\varepsilon_a} \frac{|n\rangle\langle n|}{\varepsilon_a-\varepsilon_n} \mapsto \sum_n^{\varepsilon_n\neq\varepsilon_a} \frac{|n\rangle\langle n|}{\varepsilon_a-\varepsilon_n} + \sum_m^{\varepsilon_m\neq\varepsilon_a}\sum_n^{\varepsilon_n\neq\varepsilon_a} \frac{|m\rangle\langle m| U_{\mathrm{EL}} |n\rangle\langle n|}{(\varepsilon_a-\varepsilon_m)(\varepsilon_a-\varepsilon_n)} \\
&- \sum_n^{\varepsilon_n\neq\varepsilon_a} \frac{|a\rangle\langle a| U_{\mathrm{EL}} |n\rangle\langle n|}{(\varepsilon_a-\varepsilon_n)^2} - \sum_m^{\varepsilon_m\neq\varepsilon_a} \frac{|m\rangle\langle m| U_{\mathrm{EL}} |a\rangle\langle a|}{(\varepsilon_a-\varepsilon_m)^2} - \langle a| U_{\mathrm{EL}} |a\rangle \sum_n^{\varepsilon_n\neq\varepsilon_a} \frac{|n\rangle\langle n|}{(\varepsilon_a-\varepsilon_n)^2} .
\end{aligned}$$

The second group of contributions, represented by the diagram in Fig. 4.4b with a loop on the photon mediating the magnetic interaction, is correspondingly called the magnetic loop contributions. To compute these contributions, we need to substitute the magnetic potential V_{mag} in Eq. (4.8) by the magnetic loop potential V_{ML} which arises from the modified vector potential in Eq. (4.19).

The third group of contributions, represented by Fig. 4.4c, arises from a loop correction to the photon propagator mitigating the interaction between the electrons. Accordingly, we call it the electric loop propagator (ELP) contributions. We expand the loop in terms of the free-electron propagator and interactions with the nuclear potential. We take again only the leading order term into account, which is just the free-electron loop, since higher-order contributions are expected to be smaller than the uncertainties of other contributions. This modifies the photon interaction operator I from Eq. (1.90) into [100]

$$\tilde{I}(\varepsilon, \boldsymbol{r}_1, \boldsymbol{r}_2) = \frac{2}{3}\frac{\alpha}{\pi}\int_1^\infty dt \left(1+\frac{1}{2t^2}\right)\frac{\sqrt{t^2-1}}{t^2} I\left(\sqrt{\varepsilon^2-(2t)^2}, \boldsymbol{r}_1, \boldsymbol{r}_2\right) . \tag{4.25}$$

The contribution is then obtained by using $\tilde{I}$ instead of I in Eq. (4.9) and Eq. (4.10).

The fourth group of contributions is called magnetic loop propagator (MLP) contributions. The diagram in Fig. 4.4d represents one of the contributing diagrams. If we expand this diagram in terms of the free-electron propagator and interactions with the nuclear field, then, due to Furry's theorem, the leading order contribution will have four vertices. As such, its leading contribution is of higher order than the ELP contribution. Thus, we neglect these terms anticipating that their contribution will be small.

Higher order interaction-effects (i.e. of order $1/Z^2$ or higher) have been estimated and given as an uncertainty of the first-order screened vacuum polarization result. For Li-like ions, this effect has been calculated using a screening potential approach. For B-like ions, we expect these terms of higher order to be too small to be visible compared to the uncertainties of the other contributions for most of the ions considered in this work. Thus, we estimate the uncertainty due to higher-order contributions to be 10% of the first-order contributions.

4.2.3. Vacuum polarization results

We present our results of the single-electron VP correction for the ground state of Li-like and B-like ions in Table 4.2. The contributions are divided into EL and ML contributions according to our discussion above. The Uehling and Wichmann-Kroll contributions to the EL term are listed separately. Both contributions are calculated taking the nuclear size into account. The uncertainties result from the quoted uncertainties of the RMS radii in Ref. [84]. Compared to the uncertainties of the other contributions to the g factor, we expect the dependence on the nuclear model of higher-order corrections to be of no relevance. In the case of the Wichmann-Kroll contributions, the uncertainties additionally include the uncertainties from the truncation of the partial-wave expansion. The Delbrück contribution has been calculated for a point-like nucleus using the formulas of Refs. [42, 43]. We observe that the Uehling terms are the largest contributions in magnitude for both the Li-like and B-like case. In the Li-like case, we see that while the Delbrück contribution is larger than the Wichmann-Kroll contribution for low nuclear charges, this changes for higher nuclear charges. We also observe that in the B-like case the Uehling and Delbrück contributions cancel each other to a significant degree for low nuclear charges.

The results for the first-order screened VP corrections for the ground state of Li-like and B-like ions are listed in Table 4.3. The contributions are divided according to the groups of diagrams discussed above. Compared to the single-electron case, we have additionally the ELP contribution. This has been calculated using the leading free-electron contribution.

Table 4.2.: Single-electron VP corrections to the g factor of the ground state of Li-like and B-like ions, in units of ppm. The uncertainty of the Uehling contribution results from the uncertainty of the nuclear RMS taken from Ref. [84]. The uncertainty of the Wichmann-Kroll contribution is the combined uncertainty due to the nuclear RMS and the extrapolation of the partial-wave series.

Z	EL, Uehling	EL, Wichmann-Kroll	ML, Delbrück
Li-like:			
18	−0.080 041 83 (2)	0.000 244 93 (4)	0.001 102 6
20	−0.120 944 51 (3)	0.000 448 74 (4)	0.001 850 7
24	−0.247 384 1 (2)	0.001 275 7 (1)	0.004 524 6
32	−0.771 498 4 (4)	0.006 605 (4)	0.018 438
54	−6.622 35 (5)	0.134 88 (1)	0.234 30
82	−46.814 5 (4)	1.754 1(1)	1.796 6
92	−87.661 (4)	3.796 7(3)	3.168
B-like:			
18	−0.000 418 694 19 (2)	0.000 002 44 (3)	0.000 413 11
20	−0.000 789 094 95 (4)	0.000 005 49 (5)	0.000 706 75
24	−0.002 372 519 (1)	0.000 022 4 (1)	0.001 797 2
32	−0.013 710 925 (2)	0.000 209 (3)	0.007 950 5
54	−0.376 778 (1)	0.012 93 (2)	0.128 97
82	−7.250 91 (4)	0.444 58(5)	1.410 8
92	−18.394 5 (3)	1.289 7(1)	2.881 5

Table 4.3.: First-order VP screening correction to the g factor of the ground state of Li-like and B-like ions, in units of ppm. The uncertainty of the Uehling contribution results from the uncertainty of the nuclear RMS taken from Ref. [84]. The uncertainty of the Wichmann-Kroll contribution is the combined uncertainty due to the nuclear RMS and the extrapolation of the partial-wave series.

Z	EL, Uehling	EL, Wichmann-Kroll	ELP, Uehling	ML, Delbrück
Li-like:				
18	0.012 746 390(3)	−0.000 038 987 (5)	−0.000 085 6	−0.000 163 3
20	0.017 346 904(4)	−0.000 064 318 (7)	−0.000 118	−0.000 246 8
24	0.029 614 54(3)	−0.000 152 52 (1)	−0.000 205	−0.000 503 0
32	0.069 500 41(3)	−0.000 593 2 (3)	−0.000 499	−0.001 537
54	0.356 946(3)	−0.007 203 3(5)	−0.002 71	−0.011 5
82	1.676 36(2)	−0.061 650 (4)	−0.014	−0.056
92	2.800 2(2)	−0.118 67 (2)	−0.024	−0.085
B-like:				
18	0.006 522(2)	−0.000 021 16 (1)	0.000 003 6	−0.000 134 1
20	0.008 987(2)	−0.000 035 59 (2)	0.000 011	−0.000 207
24	0.015 766(2)	−0.000 088 00 (7)	0.000 044	−0.000 443
32	0.039 435(5)	−0.000 374 (2)	0.000 26	−0.001 499
54	0.257 1(2)	−0.006 256 (7)	0.005 0	−0.015 5
82	1.853(2)	−0.088 1 (1)	0.059	−0.126
92	3.728(2)	−0.206 8 (3)	0.13	−0.24

4.3. Other effects

4.3.1. Nuclear recoil

In Furry picture calculations, the nucleus is taken to be a source of a classical background electric field. This corresponds to taking the nuclear mass M to be infinite. While this often gives a reasonably accurate first approximation, one needs to take the finite mass of the nucleus into account for more precise computations of the bound-electron g factor. This is done in a perturbative expansion in the small parameter $1/M$.

In this paper, we include for completeness results for the nuclear-recoil effect to order $1/M$ calculated and tabulated in Ref. [101] for Li-like ions, and in Refs. [102, 103] for B-like ions. We note that the calculations of the nuclear recoil effect for B-like ions have been improved very recently in Ref. [104]. No values were tabulated for Li-like Xe^{51+} and B-like Cr^{19+}, Ge^{27+} and Xe^{49+} in the given references. For these ions, we obtained values and corresponding uncertainties by fitting functions to the tabulated values, as explained in the following.

For Li- as well as B-like ions, the nuclear recoil correction to the g factor is written as the sum of a Breit term $\Delta g_{\mathrm{Breit}}$ and a QED term Δg_{QED}. For Li-like ions, the Breit term is parametrized in Ref. [101] as

$$\Delta g_{\mathrm{rec,Breit}} = \frac{(Z\alpha)^2}{M}\left[A(Z\alpha) + \frac{B(Z\alpha)}{Z} + \frac{C(Z\alpha, Z)}{Z^2}\right], \tag{4.26}$$

where the coefficients $A(Z\alpha)$ and $B(Z\alpha)$ denote contributions of zeroth and first order in $1/Z$, respectively, and $C(Z\alpha, Z)$ denotes contributions of second and higher order in $1/Z$. The coefficient $A(Z\alpha)$ was calculated analytically while $B(Z\alpha)$ and $C(Z\alpha, Z)$ were calculated and tabulated numerically in the given reference. The QED part is parametrized as

$$\Delta g_{\mathrm{rec,QED}} = \frac{1}{M}\frac{(Z\alpha)^5}{8}P(Z\alpha)\,. \tag{4.27}$$

Interelectronic interaction corrections were included using screening potential approximations. To obtain values for Xe^{51+}, we proceeded as follows: We calculated $A(Z\alpha)$ using the analytical formula given in Ref. [101]. For $B(Z\alpha)$ and $C(Z\alpha, Z)$, we fitted polynomials in $Z\alpha$ to the tabulated values in the reference. We use the $a + b\,(Z\alpha)^2 + c\,(Z\alpha)^4$ to fit $B(Z\alpha)$ and $a + b\,(Z\alpha) + c\,(Z\alpha)^2 + d\,(Z\alpha)^3$ to fit $Z\alpha\,C(Z\alpha, Z)$. For the QED part, given by $Z\alpha\,P(Z\alpha)$, we used the function $a\,\ln(Z\alpha) + b + c\,(Z\alpha) + d\,(Z\alpha)^5$.

For B-like ions, the Breit term is parametrized in Refs. [102, 103] as

$$\Delta g_{\mathrm{rec,Breit}} = \frac{1}{M}\left[A_{\mathrm{L}}(Z\alpha) + \frac{B(Z\alpha)}{Z}\right], \tag{4.28}$$

where the coefficients $A_{\mathrm{L}}(Z\alpha)$ and $B(Z\alpha)$ again denote contributions of zeroth and first order in $1/Z$, respectively. The subscript L on the coefficient denotes that only lower-order terms in $Z\alpha$ are included. The QED part is given as

$$\Delta g_{\mathrm{rec,QED}} = \frac{1}{M}\left[A_{\mathrm{H}}^{\mathrm{2el}}(Z\alpha) + \frac{(Z\alpha)^3}{8}P(Z\alpha)\right], \tag{4.29}$$

where the subscript H denotes higher-order terms in $Z\alpha$ and the superscript 2el denotes two-electron contributions to the recoil correction. Again, interelectronic interactions are included using screening potential approximations. To obtain the recoil correction for Ca^{15+}, Cr^{19+}, and Xe^{49+}, we fit the function $a + b\,(Z\alpha)^2 + c\,(Z\alpha)^3 + d\,(Z\alpha)^7$ to the data for $Z\alpha\,[A_{\mathrm{L}}(Z\alpha) + B(Z\alpha)/Z]$ tabulated in Refs. [102, 103], the function $a+b\,(Z\alpha)^2+c\,(Z\alpha)^4+d\,(Z\alpha)^6$ to the values for $A_{\mathrm{H}}^{\mathrm{2el}}(Z\alpha)$, and the function $a+b\,Z\alpha+c\,(Z\alpha)^2$ to the data for $Z\alpha\,P(Z\alpha)$ for small values of Z tabulated in Ref. [103].

4.3.2. Two-loop effects

For the calculation of two-loop contributions in the independent electron approximation, we use formulas from Refs. [53, 105]. These formulas assume a point-like nucleus and are perturbative in the nuclear-coupling strength $Z\alpha$.

In the Li-like case, the formula includes terms up to order order $(Z\alpha)^2$ and reads [53]

$$g_{2s,\mathrm{two-loop}} = -2\left[1 + \frac{1}{24}(Z\alpha)^2\right] C_4 \left(\frac{\alpha}{\pi}\right)^2, \tag{4.30}$$

where C_4 denotes the coefficient of the $(\alpha/\pi)^2$ contribution in the expansion of the free-electron magnetic anomaly a_{e}. The expansion coefficient is taken from Ref. [12]. Uncertainties from higher-order contributions are estimated by using the formula for the $(Z\alpha)^4$ contribution from Ref. [30].

For B-like systems, we have an analytic expression to order $(Z\alpha)^0$. It is given by [105]

$$g_{2p_{1/2},\mathrm{two-loop}} = -\frac{2}{3} C_4 \left(\frac{\alpha}{\pi}\right)^2. \tag{4.31}$$

We estimate the uncertainty due to terms of higher order in $Z\alpha$ following the method of Ref. [30] as

$$g_{\mathrm{h.o.}}^{(2)} = 2 g_{\mathrm{h.o.}}^{(1)} \frac{g^{(2)}[(Z\alpha)^0]}{g^{(1)}[(Z\alpha)^0]}, \tag{4.32}$$

where $g_{\mathrm{h.o.}}^{(n)}$ is the n-loop higher-order QED contribution and $g^{(n)}[(Z\alpha)^0]$ is the n-loop $(Z\alpha)^0$ QED contribution. The contribution $g_{\mathrm{h.o.}}^{(1)}$ as well as the contributions of order $(Z\alpha)^0$ are calculated with the formulas of Ref. [105].

4.4. Results and summary

In Table 4.4 and Table 4.5 we present numerical results for all the contributions discussed in Ref. [1], for Li-like and B-like ions, respectively. Contributions obtained as a part of this work are marked by the symbol *. In Table 4.4, we include previous results for the total g factor of Li-like ions from Refs. [59, 60] for comparison. Our results independently confirm these calculations within the given uncertainties. The results feature a smaller uncertainty for high-Z ions than the results of Ref. [60] from 2004 due to an improved calculation of the screened self-energy contributions. We also include screened vacuum-polarization contributions which become visible in the high-Z regime. Ref. [59] treats many-electron QED effects rigorously by the evaluation of the corresponding photon exchange QED screening diagrams and two-photon exchange diagrams, and thus provides the most precise results for the few atomic numbers considered therein. Our value for the g factor of $^{40}Ca^{17+}$ agrees also with the experimental value

$$g_{\mathrm{exp}}(^{40}\mathrm{Ca}^{17+}) = 1.999\,202\,040\,5\,(11)$$

from Ref. [21] within the given uncertainties.

For low atomic numbers, i.e. lower than those considered here, the nonrelativistic QED approach employing explicitly correlated three-electron wave functions was found to improve the overall theoretical uncertainty [106]. For Li-like $^{28}Si^{11+}$, the most precise experimental and theoretical g factor values can be found in the very recent Ref. [107].

In Table 4.5, we include previous results for the total g factor of B-like ions from Refs. [61–64]. Our results confirm the calculations of Refs. [61, 62] within the uncertainties. The uncertainties have been improved compared to these works due to an improved treatment of the self-energy contributions.

Recently, the g factor of B-like $^{40}Ar^{13+}$ was measured by the ALPHATRAP experiment [22] at the Max Planck Institute for Nuclear Physics [6]. The experiment constitutes the first high-precision measurement of the bound-electron g factor of a B-like ion, greatly improving the previous experimental value of Ref. [23] obtained by optical emission spectroscopy employing an electron beam ion trap. The measured value for $^{40}Ar^{13+}$ is [6]

$$g_{\mathrm{exp}}(^{40}\mathrm{Ar}^{13+}) = 0.663\,648\,455\,32\,(93)\,.$$

Within the given uncertainty, this value agrees with our result listed in Table 4.5. Our calculation in this work agrees also with a combined theoretical value $g(^{40}Ar^{13+}) = 0.663\,648\,12\,(58)$ of Ref. [6].

Currently, the main limitation for the calculation of the g factor of B-like argon stems from the contribution resulting from the higher-order interelectronic interactions. For heavy ions (from Xe^{49+} on), the uncertainties of the screened self-energy

Table 4.4.: Contributions to the bound-electron g factor of lithium-like ions. The uncertainties given in parentheses indicate the uncertainty of the last digit(s). If no uncertainty is given, all digits of the quoted value are significant. Contributions obtained within this thesis are marked by the symbol *.

Contribution	$^{40}Ar^{15+}$	$^{40}Ca^{17+}$	$^{52}Cr^{21+}$	$^{74}Ge^{29+}$
Dirac value*	1.997 108 8	1.996 426 0	1.994 838 1	1.990 752 3
Finite nuclear size*	0.000 000 0	0.000 000 0	0.000 000 0	0.000 000 2
Electron correlation:				
one-photon exchange*, $(1/Z)^1$	0.000 414 5	0.000 461 1	0.000 555 2	0.000 746 5
$(1/Z)^{2+}$, CI-DFS	−0.000 006 7(2)	−0.000 006 7(2)	−0.000 006 7(2)	−0.000 006 7(3)
Nuclear recoil	0.000 000 1	0.000 000 1	0.000 000 1	0.000 000 1
One-loop QED:				
SE, $(1/Z)^0$	0.002 325 1	0.002 325 7	0.002 327 2	0.002 331 7
SE, $(1/Z)^{1+}$	−0.000 000 4(1)	−0.000 000 4(1)	−0.000 000 5(1)	−0.000 000 8(2)
VP*, $(1/Z)^0$	−0.000 000 1	−0.000 000 1	−0.000 000 2	−0.000 000 8
VP*, $(1/Z)^{1+}$	0.000 000 0	0.000 000 0	0.000 000 0	0.000 000 1
Two-loop QED	−0.000 003 5	−0.000 003 5	−0.000 003 5	−0.000 003 6(2)
Total theory	1.999 837 8(2)	1.999 202 2(2)	1.997 709 7(2)	1.993 819 0(4)
Theory, Ref. [60]	1.999 837 75(14)	1.999 202 24(17)	1.997 709 70(26)	1.993 819 14(46)
Theory, Ref. [59]		1.999 202 041(13)		
Contribution	$^{132}Xe^{51+}$	$^{208}Pb^{79+}$	$^{238}U^{89+}$	
Dirac value*	1.972 750 2	1.932 002 9	1.910 723	
Finite nuclear size*	0.000 003 4	0.000 078 7(1)	0.000 242	
Electron correlation:				
one-photon exchange*, $(1/Z)^1$	0.001 306 2	0.002 148 3	0.002 510	
$(1/Z)^{2+}$, CI-DFS	−0.000 006 8(3)	−0.000 007 6(4)	−0.000 008(1)	
Nuclear recoil	0.000 000 2	0.000 000 4	0.000 001	
One-loop QED:				
SE, $(1/Z)^0$	0.002 358 1(1)	0.002 454 7	0.002 527	
SE, $(1/Z)^{1+}$	−0.000 001 6(5)	−0.000 003 6(11)	−0.000 005(1)	
VP*, $(1/Z)^0$	−0.000 006 3(1)	−0.000 043 2(7)	−0.000 081(1)	
VP*, $(1/Z)^{1+}$	0.000 000 3(1)	0.000 001 6(1)	0.000 003(1)	
Two-loop QED	−0.000 003 6(2)	−0.000 003 6(12)	−0.000 004(2)	
Total theory	1.976 400 1(6)	1.936 628 6(18)	1.915 908(3)	
Theory, Ref. [60]	1.976 399 9(14)	1.936 625 3(35)	1.915 900 2(50)	
Theory, Ref. [59]		1.936 627 2(6)	1.915 904 8(11)	

Table 4.5.: Contributions to the bound-electron g factor of boron-like ions. The uncertainties given in parentheses indicate the uncertainty of the last digit(s). If no uncertainty is given, all digits of the quoted value are significant. Contributions obtained within this thesis are marked by the symbol *.

Contribution	$^{40}Ar^{13+}$	$^{40}Ca^{15+}$	$^{52}Cr^{19+}$	$^{74}Ge^{27+}$
Dirac value*	0.663 775 5	0.663 092 7	0.661 504 7	0.657 419 0
Finite nuclear size*	0.000 000 0	0.000 000 0	0.000 000 0	0.000 000 0
Electron correlation:				
one-photon exchange*, $(1/Z)^1$	0.000 657 5	0.000 732 0	0.000 882 4	0.001 190 3
$(1/Z)^{2+}$, CI-DFS	−0.000 007 6(4)	−0.000 007 7(4)	−0.000 008 2(5)	−0.000 011 2(7)
Nuclear recoil	−0.000 009 1(2)	−0.000 009 3(2)	−0.000 007 3	−0.000 005 3
One-loop QED:				
SE, $(1/Z)^0$	−0.000 768 4	−0.000 766 8	−0.000 762 8	−0.000 751 1
SE, $(1/Z)^{1+}$	−0.000 001 0(2)	−0.000 001 1(2)	−0.000 001 5(2)	−0.000 002 5(3)
VP*, $(1/Z)^0$	−0.000 000 0	−0.000 000 0	−0.000 000 0	−0.000 000 0
VP*, $(1/Z)^{1+}$	0.000 000 0	0.000 000 0	0.000 000 0	0.000 000 0
Two-loop QED	0.000 001 2(1)	0.000 001 2(1)	0.000 001 2(1)	0.000 001 2(1)
Total theory	0.663 648 1(5)	0.663 041 0(5)	0.661 608 5(5)	0.657 840 4(8)
Theory, Ref. [61]	0.663 648 8(12)	0.663 041 8(12)		
Theory, Ref. [62]	0.663 647 7(7)			
Theory, Ref. [63]	0.663 899(2)	0.663 325(56)	0.661 955(68)	0.658 314(93)
Theory, Ref. [64]	0.663 728	0.663 130	0.661 714	
Contribution	$^{132}Xe^{49+}$	$^{208}Pb^{77+}$	$^{238}U^{87+}$	
Dirac value*	0.639 416 9	0.598 669 6	0.577 389	
Finite nuclear size*	0.000 000 1	0.000 006 8	0.000 029	
Electron correlation:				
one-photon exchange*, $(1/Z)^1$	0.002 118 2	0.003 654 9	0.004 394	
$(1/Z)^{2+}$, CI-DFS	−0.000 011 0(5)	−0.000 019 9(7)	−0.000 023	
Nuclear recoil	−0.000 003 0	−0.000 001 8	−0.000 001	
One-loop QED:				
SE, $(1/Z)^0$	−0.000 683 3	−0.000 474 8	−0.000 345	
SE, $(1/Z)^{1+}$	−0.000 006 9(6)	−0.000 016 6(15)	−0.000 022(2)	
VP*, $(1/Z)^0$	−0.000 000 2(1)	−0.000 005 5(5)	−0.000 014(1)	
VP*, $(1/Z)^{1+}$	0.000 000 2(1)	0.000 001 7(2)	0.000 003(1)	
Two-loop QED	0.000 001 2(1)	0.000 001 2(3)	0.000 001(1)	
Total theory	0.640 832 2(8)	0.601 815 6(18)	0.581 411(3)	
Theory, Ref. [63]	0.641 61(18)	0.602 86(33)	0.582 48(40)	

contribution dominate over the other uncertainties. Also, vacuum-polarization effects become more visible and need to be taken into account. Accordingly, the results for the g factors of B-like ions can be improved by calculating two-photon exchange contributions (as has been done in Ref. [59] for Li-like ions) and by rigorously calculating the screened self-energy effects (as has been done in Refs. [59, 99] for Li-like ions). Furthermore, for a significant increase of the theoretical precision in case of the heaviest elements such as Pb^{77+} and U^{87+}, which are relevant for an improved determination of the fine-structure constant α, two-loop contributions need to be calculated non-perturbatively in the nuclear-coupling strenght $Z\alpha$. First milestones have been achieved for the $1s$ ground state of hydrogen-like systems in Refs. [5, 49]; these calculations need to be extended to the $2p$ valence electron of B-like ions.

In summary, we performed a systematic calculation of interelectronic and radiative effects on the one-loop level to the ground-state g factor of Li-like and B-like ions. These calculations for B-like ions have been extended, for the first time, to heavy elements. Within this thesis, the interelectronic interaction on the level of one-photon exchange and the leading-order screening effect for VP corrections has been calculated explicitly using perturbation theory. Estimated theoretical uncertainties have been supplemented for each value.

5. The Reduced g Factor of Hydrogenlike Ions

The calculations of the ground-state g factor of Li- and B-like ions in Chapter 4 were partly motivated by ideas to determine the fine-structure constant α using weighted differences of H-like and Li- or B-like ions to suppress nuclear structure effects [51–54]. However, besides an improvement of the theory of single-electron systems, these methods require a significant development of the many-electron theory as well. While important improvements have been achieved (see e.g. [1, 6, 20, 21, 106, 107]), theoretical uncertainties need to be decreased by orders of magnitude, as our results in Section 4.4 for B-like $^{40}Ar^{13+}$ show. Therefore, it is preferable to avoid many-electron effects and find ways of determining α using only observables of H-like systems. In the following, we suggest and investigate such a scheme.

We consider in the following a weighted difference of the g factor and the bound-electron energy in units of the electron mass of a H-like ion, given by

$$\widetilde{g} = g - x\frac{E}{m_e}\,, \tag{5.1}$$

where x denotes the weight. We call this weighted difference the reduced g factor. The idea is then to choose the weight x such that a strong suppression of nuclear structural effects is achieved. We show in this chapter that it follows from basic properties of the electronic wave functions that [108]

$$x = \frac{4}{3}(2\gamma + 1)\,, \tag{5.2}$$

with $\gamma = \sqrt{1-(Z\alpha)^2}$ for this purpose.

The leading Dirac contribution to the ground-state bound-electron g factor in the ground ($1s$) state H-like ions is

$$g_D = -\frac{8}{3}\int_0^\infty dr\, rG(r)F(r)\,, \tag{5.3}$$

where G and F denote the upper and lower radial components of the bound-electron wave function given in Eq. (2.11), with $n = 1$ and $\kappa = -1$. For a point-like nucleus, the integral in Eq. (5.3) can be evaluated analytically, with the result [25]

$$g_{D,pnt} = \frac{2}{3}(1 + 2\gamma)\,. \tag{5.4}$$

Eq. (5.4) together with the leading free-QED correction α/π has an uncertainty $\delta(g_{\mathrm{D,pnt}} + \alpha/\pi)$ which results only from the uncertainty $\delta\alpha$ of the fine-structure constant and is given by

$$\delta\left(g_{\mathrm{D,pnt}} + \frac{\alpha}{\pi}\right) = \left|-\frac{4}{3}\frac{Z\alpha}{\gamma}Z + \frac{1}{\pi}\right|\delta\alpha\,. \tag{5.5}$$

For an extended nucleus, we calculate the integral in Eq. (5.3) numerically, solving the radial Dirac equation using the DKB approach [56] (see also Chapter 2) implemented in quadruple precision. The result is denoted by $g_{\mathrm{D,ext}}$. The leading FNS contribution to the bound-electron g factor is the difference

$$g_{\mathrm{D,fns}} = g_{\mathrm{D,ext}} - g_{\mathrm{D,pnt}}\,. \tag{5.6}$$

We use first the two-parameter Fermi distribution as the nuclear charge distribution and take RMS radii from Ref. [84]. There is an uncertainty $\delta_{\mathrm{RMS}}g_{\mathrm{D,fns}}$ resulting from the uncertainties of the RMS radii. Additionally, in order to estimate the dependence $\delta_{\mathrm{model}}g_{\mathrm{D,fns}}$ of the FNS effect on the nuclear model, we also calculate the radial distribution of protons performing Hartree-Fock-Skyrme nuclear structural calculations [109], and take the difference of the values obtained with the different distributions. In Ref. [110] it was observed that nuclear charge distributions resulting from Skyrme forces are in good agreement with distributions measured in electron scattering experiments. The total uncertainty of the FNS contribution is then given by

$$\delta g_{\mathrm{D,fns}} = \sqrt{(\delta_{\mathrm{RMS}}g_{\mathrm{D,fns}})^2 + (\delta_{\mathrm{model}}g_{\mathrm{D,fns}})^2}\,. \tag{5.7}$$

Fig. 5.1a compares the uncertainty of the g factor due to the current absolute standard uncertainty of the fine-structure constant [111] $\delta\alpha$ given in Eq. (5.5) and the uncertainty caused by the FNS effect given in Eq. (5.7). Already for low values of Z, the uncertainties due to FNS are approximately an order of magnitude larger than the uncertainty due to $\delta\alpha$, and the discrepancy grows for heavier elements.

The leading contribution to the ground-state electron energy assuming a point-like nucleus is given by

$$E_{\mathrm{D,pnt}} = m_{\mathrm{e}}\gamma\,, \tag{5.8}$$

and its uncertainty $\delta E_{\mathrm{D,pnt}}$ due to $\delta\alpha$ is

$$\delta E_{\mathrm{D,pnt}} = \frac{Z\alpha}{\gamma}Z\delta\alpha\,. \tag{5.9}$$

For an extended nucleus, we again obtain the ground-state energy $E_{\mathrm{D,ext}}$ from the solution of the radial Dirac equation and the FNS contribution is given by

$$E_{\mathrm{D,fns}} = E_{\mathrm{D,ext}} - E_{\mathrm{D,pnt}}\,. \tag{5.10}$$

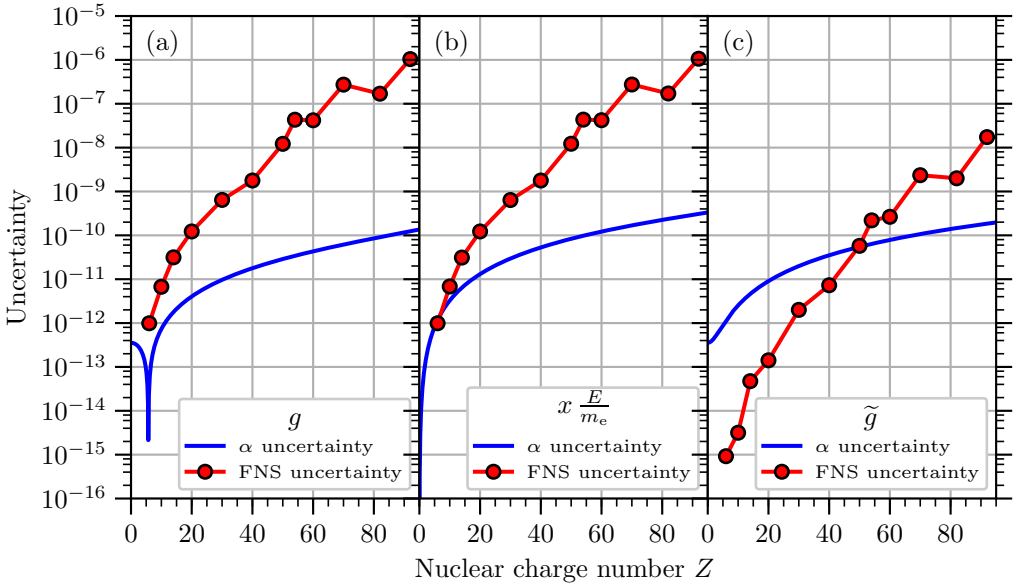

Figure 5.1.: Comparison of the uncertainties due to the uncertainty of the fine-structure constant (blue) to the uncertainty of the finite nuclear size effect (red). The comparisons are done for the ground-state g factor of H-like ions g in (a), for the weighted dimensionless energy $x\,E/m_e$ in (b), and the reduced g factor $\widetilde{g}$ in (c).

The calculation of $E_{D,fns}$ and the determination of its uncertainty $\delta E_{D,fns}$ is performed similarly as explained above for the g factor.

Using the Dirac equation and its radial counterpart, Eq. (5.3) for the relativistic g factor may be rewritten as [108]

$$g_D = \frac{2}{3}\left(1 + 2\frac{\partial E_D}{\partial m_e}\right) . \tag{5.11}$$

To a good approximation, $E_{D,fns} \sim m_e(2Z\alpha m_e R)^{2\gamma}$ [112], where R denotes a effective nuclear radius. Therefore, the FNS effect of the g factor and the energy can be related to each other with the formula [108]

$$g_{D,fns} \approx \frac{4}{3}(2\gamma + 1)\frac{E_{D,fns}}{m_e} . \tag{5.12}$$

This motivates the choice of the weighted difference of the g factor and the energy in units of electron mass in Eq. (5.1), since we expect that the FNS effect in $\widetilde{g}$ cancels to a significant degree. Similarly to the previous figure, in Fig. 5.1b we compare the uncertainties of the weighted energy value divided by m_e (assuming a

fixed weight x) due to $\delta\alpha$ and due to the FNS effect. As expected from Eq. (5.12), the FNS uncertainties are of comparable magnitude as the ones for the g factor. Also, as in the case of the g factor, the FNS effect causes larger uncertainties than $\delta\alpha$ in the (weighted) energy.

The relevant uncertainties of $\widetilde{g}$ are depicted in Fig. 5.1c. The FNS uncertainties are reduced by 2–3 orders of magnitude, and for $Z \lesssim 50$, these uncertainties are smaller than the ones due to $\delta\alpha$, rendering a broad range of elements ideal for an α determination. Furthermore, as compared to the curve of the g factor, the sensitivity due to $\delta\alpha$ is even improved, since

$$\frac{\partial}{\partial\alpha}\left(\widetilde{g}_{\mathrm{D,pnt}} + \frac{\alpha}{\pi}\right)\bigg|_{x=4(2\gamma+1)/3} = -2\gamma\frac{\partial g_{\mathrm{D,pnt}}}{\partial\alpha} + \frac{1}{\pi} \tag{5.13}$$

contains an enhancement factor of the magnitude $2\gamma \approx 2$ for low Z. This favors the reduced g factor scheme to those employing specific differences of g factors in different charge states [51, 52], since in those cases the sensitivity to $\delta\alpha$ is slightly reduced in the difference.

QED corrections to the electronic energy levels as well as the g factor arise from one-loop self-energy and vacuum polarization diagrams. The FNS corrections to these effects have been evaluated e.g. in Ref. [81] for the Lamb shift and in Ref. [95] for the g factor. We use tabulated values from these papers to determine the uncertainty of the QED-FNS effect of the reduced g factor as the square root of the quadratic sum of the Lamb shift and the g factor uncertainties. We find that the uncertainties of the QED-FNS effect only slightly raise the FNS correction to the reduced g factor and the statements of the previous paragraph remain unchanged.

Additionally, the nuclear polarization effect was calculated by N. S. Oreshkina, I. A. Valuev, and V. Debierre. It was found that the nuclear polarization effect significantly cancels in the reduced g factor and that uncertainties due to nuclear polarization are of the same magnitude as the FNS effect, thus posing no problem for the determination of α.

In summary, a weighted difference of the bound-electron g factor and energy in units of the electron mass of H-like ions is put forward. The weight is chosen such that nuclear structural effects are surpressed. The surpression of the FNS uncertainty and its radiative correction is investigated. We also find that this reduced g factor features an enhanced sensitivity to α as compared to the regular g factor. This results in an efficient scheme for the determination of the fine-structure constant from measurement of these quantities.

Summary and Outlook

In this thesis we theoretically investigated QED effects in highly charged ions. In particular, we have developed and applied analytical and numerical methods to precisely calculate atomic properties, i.e. energies and g factors of atomic states, which can be scrutinized with modern high-precision trapped-ion experiments.

In Chapter 1 we present the theoretical framework of atomic systems using the derivations and results of Refs. [65, 67]. The inclusion of the nuclear potential into the QED Lagrangian as a classical external field is justified considering limiting forms of the electron-nucleus scattering amplitude [67]. The formalism of Ref. [65] is used to relate Feynman diagram techniques to the calculation of energy shifts and exemplary calculations are presented.

In Chapter 2 we present numerical methods used within this thesis to calculate QED effects in atomic systems. Finite basis set approaches are by now well established and widely used methods for these kinds of calculations. Besides their efficiency, their main advantage is that there is a direct correspondence between the spectrum generated by the finite basis set approach and perturbative expressions involving spectral sums over the whole Dirac spectrum. This allows for the development of computational methods that can be used in different types of bound-state QED calculations. We have used these methods to calculate the self-energy effect and a variety of contributions to the g factor of Li- and B-like ions. In this context, we developed a code base for perturbative calculations in atomic systems.

In Chapter 3, we present our self-energy calculations. The self-energy contribution is split into three different parts using the derivations of Ref. [58]. These are the zero-potential contribution, where the virtual, intermediate-state electron is a free electron, the one-potential contribution, where the virtual free electron interacts once with the nucleus, and the many-potential contribution, which contains the remaining terms. Each of these terms is discussed and expressions for their evaluation are presented. Numerical calculations of Fourier transforms of the wave functions generated using the finite basis approach are necessary for the evaluation of the zero-, and one-potential contributions and are discussed in detail. These are performed using expansions of the numerical wave functions in terms of piecewise polynomials and an iterative evaluation of spherical Bessel transforms. In evaluating the many-potential term, we use the approach of Ref. [57] based on finite basis sets, however we use the DKB approach of Ref. [56] to generate the basis functions and

use the contour of integration in Ref. [58] in order to avoid subtractions of many pole terms for self-energy calculations of excited hydrogenic states. Calculations of the self-energy effect for valence electrons in many-electron systems are performed using the screening potential approximation, where the core electrons generate a potential that screens the nuclear potential. Our self-energy calculations are motivated by the measurement of the binding energy of the valence electron in $^{131}Xe^{17+}$ and the difference of the energies of the ground and metastable states of $^{187}Re^{29+}$ by the PENTATRAP experiment [2, 4]. We find that the self-energy correction to the binding energy in $^{131}Xe^{17+}$ is approximately 21 meV, and that the difference of the ground and metastable states of $^{187}Re^{29+}$ is approximately -30 meV, both of which are currently not visible within the experimental precision. However, such effects will be clearly observable in higher ionization states, e.g. in planned experiments with Na-like Xe ions. These studies will allow, for the first time, the test of QED effects via mass measurements, highlighting the need for precise theoretical predictions.

In Chapter 4, we present our calculations of the g factor of Li- and B-like ions. We discuss systematically the calculation of various contributions to the bound-electron g factor. Again, we use the finite basis set approach to perform these calculations. Interelectronic interacion corrections are treated perturbatively to the level of one-photon exchange. Results for single-electron and first-order screened vacuum polarization contributions are presented. We calculate both contributions resulting from electric and magnetic loop effects. The electric loop contributions are separated into an Uehling and Wichmann-Kroll part. The Wichmann-Kroll contribution is determined numerically using the approach of Ref. [91] with a homogeneously charged sphere as the nucleus. The propagator of the electron in the nuclear field is calculated numerically using the approach of Refs. [96, 97] to solve the radial Dirac equation. Magnetic loop contributions are included using the formulas of Refs. [42, 43]. We compare our results to existing measurements and theoretical calculations. In the case of Li-like ions, we find that our values agree at the level of precision we can achieve in our calculations. In the case of B-like ions, we improve the uncertainty of the g factor of B-like $^{40}Ar^{13+}$. Further, we perform for the first time the calculation of interelectronic and radiative effects on the one-loop level to the ground-state g factor of B-like ions for a broad range of elements, including B-like $^{208}Pb^{77+}$ and $^{238}U^{87+}$. In particular, the ground-state g factor of B-like $^{40}Ar^{13+}$ has been recently measured by the ALPHATRAP experiment [6] to be

$$g_{\mathrm{exp}}(^{40}\mathrm{Ar}^{13+}) = 0.663\,648\,455\,32\,(93)\,.$$

Our calculations give for the same g factor the value

$$g_{\mathrm{theo}}(^{40}\mathrm{Ar}^{13+}) = 0.663\,648\,1(5)\,,$$

which, while agreeing with the experimental value, is far away from the experimental level of precision, yet it is the most accurate theoretical value for the g factor of a five-electron ion. This study constitutes an important step towards the projected determination of the fine-structure constant from the g factor of highly charged ions.

In Chapter 5, we proposed a weighted difference of the bound-electron g factor and the total energy of the bound electron in units of the electron rest energy of H-like ions, calling it the reduced g factor, as a new approach of determining α. Among the advantages of using H-like systems is the avoidance of many-electron effects. Our investigation shows that for a particular choice of the weight, nuclear structural effects, which constitute the largest obstacle in determining α using solely H-like systems, are suppressed. This is explicitly demonstrated for the FNS effect and radiative corrections to it. Further, we observe that the sensitivity of this reduced g factor to the uncertainty of α is enhanced as compared to the regular g factor. Therefore, we find that existing and projected experimental methods and theoretical developments will allow improving the uncertainty of α by several orders of magnitude in the foreseeable future.

Progress in experimental techniques and the prospect of accurately determining fundamental constants will continue to challenge our understanding of QED effects in highly charged ions while providing further motivation to perform theoretical investigations. Our calculation of the self-energy effect in many-electron ions uses the screening-potential approximation, effectively reducing the problem to the calculation of the single-electron self-energy contribution of the valence electron. This approach works, however, only for monovalent ions. For ions with many valence electrons, a general scheme with reasonable accuracy needs to be developed.

Already as of today, experimental measurements are often ahead of theoretical calculations as the calculation of the g factor of B-like $^{40}Ar^{13+}$ in this thesis shows. Currently, the main limitations result from higher-order interelectron-interaction contributions, the screening of the self-energy contribution, and magnetic-loop contributions to the vacuum-polarization effect. The developments of the theory of the Lamb shift and the bound-electron g factor are to a certain extent intertwined: An improvement in light-by-light scattering calculations will benefit both theories. The high-precision non-perturbative evaluation of two-loop light-by-light scattering diagrams will be required to implement the plan of α determination with H-like ions outlined in Chapter 5. To improve the QED theory of the g factor of Li- and B-like ions, the complete calculation of two-electron light-by-light scattering effects is also necessary.

From a more practical point of view and for an accurate treatment of higher-order electron correlation effects, a fusion of numerical calculations of QED effects and of relativistic atomic many-body methods appears to be necessary. In this context, basis set methods based on B-splines can be extended to configuration

interaction, relativistic many-body perturbation theory, or multiconfiguration Dirac-Fock calculations. B-spline basis functions seem to be particularly well suited for this task due to their flexibility, e.g. by the possibility of including the negative Dirac spectrum, which is typically neglected in atomic structure calculations, yet it was found to be crucial in g factor calculations. Basis set methods are also expected to be a good common ground to unify relativistic atomic structure methods with bound-state QED, potentially leading to a more precise evaluation of QED screening effects.

A. Feynman Rules

In the following, we list the Feynman rules for the calculation of the Fourier-transformed Green's function (see Eq. (1.60))

$$G((E_1', \boldsymbol{x}_1'), \ldots, (E_N', \boldsymbol{x}_N'); (E_1, \boldsymbol{x}_1), \ldots, (E_N, \boldsymbol{x}_N)) \,.$$

The Feynman rules listed here are taken from Ref. [65].

Figure A.1.: An electron in the field of the nucleus.

In Fig. A.1, an electronic line is depicted. We make the fermion flow explicit here, despite leaving it implicit in the main part of the thesis. This component of a Feynman diagram can be an external line, an internal line, or a disconnected line. If it is an external line, we associate the term

$$\frac{i}{2\pi} S(\omega, \boldsymbol{y}, \boldsymbol{x})$$

with it, where S is the propagator of the electron in the field of the nucleus given in Eq. (1.56). If it is an internal line, we additionally integrate over its virtual energy, that is, we associate

$$\int d\omega \, \frac{i}{2\pi} S(\omega, \boldsymbol{y}, \boldsymbol{x}) \,,$$

where the integral over ω is performed in the final expression. If it is a disconnected line, then we associate the term

$$\frac{i}{2\pi} S(\omega, \boldsymbol{y}, \boldsymbol{x}) \delta(\omega' - \omega)$$

with it.

Figure A.2.: The internal photon line.

In Fig. A.2, an internal photon line is depicted. We associate as usual a photon propagator

$$\int d\omega \, \frac{i}{2\pi} D_{\mu\nu}(\omega, \boldsymbol{y} - \boldsymbol{x})$$

with it, where $D_{\mu\nu}$ denotes here the photon propagator in the mixed energy-position representation. The order of $\boldsymbol{x}$ and $\boldsymbol{y}$ does not matter since the photon propagator is symmetric with respect to their exchange. In Feynman gauge, the propagator reads

$$D_{\mu\nu}(\omega, \boldsymbol{x}) = -g_{\mu\nu} \int \frac{d^3q}{(2\pi)^3} \frac{1}{\omega^2 - \boldsymbol{q}^2 + i0^+} e^{i\boldsymbol{q}\cdot\boldsymbol{x}} \,.$$

In Coulomb gauge, we have

$$D_{00}(\omega, \boldsymbol{x}) = \frac{1}{4\pi|\boldsymbol{x}|} \,,$$

$$D_{jk}(\omega, \boldsymbol{x}) = \int \frac{d^3q}{(2\pi)^3} \frac{1}{\omega^2 - \boldsymbol{q}^2 + i0^+} \left(\delta_{jk} - \frac{q_j q_k}{\boldsymbol{q}^2}\right) e^{i\boldsymbol{q}\cdot\boldsymbol{x}} \,,$$

for $j, k = 1, 2, 3$, where δ_{jk} is the usual Kronecker delta, and

$$D_{0j}(\omega, \boldsymbol{x}) = 0 = D_{j0}(\omega, \boldsymbol{x}) \,,$$

for $j = 1, 2, 3$.

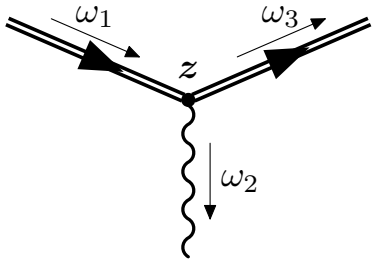

Figure A.3.: The vertex diagram.

In Fig. A.3, the electron-photon vertex is depicted. Associated with it is the term

$$-2\pi i e \gamma^\mu \delta(\omega_1 - \omega_2 - \omega_3) \int d^3z \,.$$

The delta function enforces energy conservation at each vertex. The integral over the vertex position $\boldsymbol{z}$ is understood to be taken in the final expression.

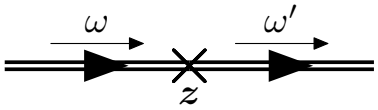

Figure A.4.: The diagram of the mass renormalization counterterm.

In Fig. A.4, the diagram of the mass renormalization counterterm is depicted. We associate with it the term

$$2\pi i \, \delta m_e \, \delta(\omega' - \omega) \int d^3x \,,$$

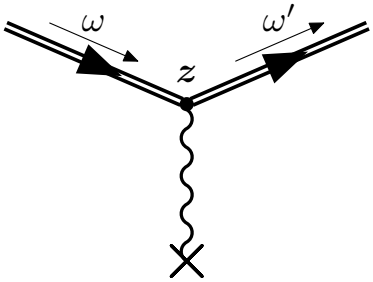

Figure A.5.: The diagram of the potential insertion.

where, again, the integral over $\boldsymbol{x}$ is taken in the final expression.

In Fig. A.5, we depict the diagram of the potential insertion. This diagram arises in calculations, if there is a static external potential term in the Lagrangian. An example for this is the external magnetic field (in which case, we use a triangle instead of a cross in the main text). If the external potential is denoted by V, then the diagram corresponds to the term

$$-2\pi i\gamma^0\delta(\omega'-\omega)\int d^3x\, V(\boldsymbol{x})\,,$$

where the integral over the vertex $\boldsymbol{x}$ is taken in the final expression.

There is a symmetry factor $\operatorname{sign}\sigma$, where σ is the permutation of the final electron coordinates with respect to the initial ones. There is also an additional factor of -1 for every closed electron loop.

B. The Photon Interaction Matrix Elements

We introduced the photon interaction operator in Eq. (1.90). It is essentially the photon propagator contracted with the Dirac α matrices. The matrix elements of this operator appear in calculations of self-energy as well as interelectronic effects. The matrix elements of the operator with respect to electronic wave functions are given by

$$\langle ab|\, I(\omega)\, |cd\rangle = e^2 \int d^3x \int d^3y\, (\psi_a^\dagger(\boldsymbol{x})\alpha^\mu\psi_c(\boldsymbol{x}))(\psi_b^\dagger(\boldsymbol{y})\alpha^\nu\psi_d(\boldsymbol{y}))D_{\mu\nu}(\omega, \boldsymbol{x}-\boldsymbol{y})\,. \tag{B.1}$$

Using the fact that the angular and radial dependences are separated in the electronic wave functions and the partial-wave expansion of the photon propagator, the angular parts of the integrals in Eq. (B.1) can be done explicitly leaving only radial integrals for numerical evaluation. The expression in Eq. (B.1) then takes the form [57, 71, 113]

$$\langle ab|\, I(\omega)\, |cd\rangle = \alpha \sum_{L=0}^{\infty} J_L(abcd) R_L(\omega; abcd)\,. \tag{B.2}$$

The factor $J_L(abcd)$ depends only on the total angular momentum and magnetic quantum numbers and reads [57, 71]

$$J_L(abcd) = \sum_{m_L=-L}^{+L} (-1)^{j_a-m_a+L-m_L+j_b-m_b} \begin{pmatrix} j_a & L & j_c \\ -m_a & m_L & m_c \end{pmatrix} \begin{pmatrix} j_b & L & j_d \\ -m_b & -m_L & m_d \end{pmatrix}, \tag{B.3}$$

where

$$\begin{pmatrix} j_1 & j_2 & j_3 \\ m_1 & m_2 & m_3 \end{pmatrix} \tag{B.4}$$

denotes the Wigner 3j symbol [71]. The explicit expression for the factor $R_L(\omega; abcd)$ depends on the gauge choice. However, it can be expressed using the same set of integrals for both the Coulomb gauge and the Feynman gauge. The function is separated into two pieces as [57, 71]

$$R_L(\omega; abcd) = R_{1,L}(\omega; abcd) + R_{2,L}(\omega; abcd)\,, \tag{B.5}$$

with

$$R_{1,L}(\omega; abcd) = (-1)^L \langle \kappa_a \| C^L \| \kappa_c \rangle \langle \kappa_b \| C^L \| \kappa_d \rangle\, \mathcal{I}_L(\omega; abcd)\,, \tag{B.6}$$

and

$$R_{2,L}(\omega; abcd) = (-1)^{L+1}\langle -\kappa_a \| C^L \| \kappa_c \rangle \langle -\kappa_b \| C^L \| \kappa_d \rangle \frac{(\kappa_a + \kappa_c)(\kappa_b + \kappa_d)}{L(L+1)} \mathcal{J}_L(\omega; abcd)\,. \tag{B.7}$$

In Eqs. (B.6) and (B.7), $\langle \kappa_a \| C^L \| \kappa_b \rangle$ denotes a reduced matrix element. These reduced matrix elements are given by [71]

$$\langle \kappa_a \| C^L \| \kappa_b \rangle = (-1)^{j_a+1/2}\sqrt{(2j_a+1)(2j_b+1)} \begin{pmatrix} j_a & j_b & L \\ -1/2 & 1/2 & 0 \end{pmatrix} \Pi(\ell_a + \ell_b + L)\,, \tag{B.8}$$

where

$$\Pi(\ell) = \begin{cases} 1, & \text{if } \ell \text{ is even,} \\ 0, & \text{otherwise}\,. \end{cases} \tag{B.9}$$

The expressions $\mathcal{I}_L(\omega; abcd)$ and $\mathcal{J}_L(\omega; abcd)$ contain the radial integrals.

In order to give explicit formulas for these two integrals, we introduce the following radial functions

$$U_{ab}(r) = -G_a(r)F_b(r) + F_a(r)G_b(r)\,, \tag{B.10}$$

$$V_{ab}(r) = -G_a(r)F_b(r) - F_a(r)G_b(r)\,, \tag{B.11}$$

$$W_{ab}(r) = G_a(r)G_b(r) + F_a(r)F_b(r)\,, \tag{B.12}$$

and

$$P_{L,ab}(r) = \frac{\kappa_b - \kappa_a}{L} V_{ab}(r) + U_{ab}(r)\,, \tag{B.13}$$

$$Q_{L,ab}(r) = \frac{\kappa_b - \kappa_a}{L+1} V_{ab}(r) - U_{ab}(r)\,. \tag{B.14}$$

The integral $\mathcal{J}_L(\omega; abcd)$ is the same for both the Coulomb and Feynman gauges and reads [57, 71, 113]

$$\mathcal{J}_L(\omega; abcd) = i\omega(2L+1)\int_0^\infty dr_1 \int_0^\infty dr_2\, j_L(\omega r_<) h_L^{(1)}(\omega r_>) V_{ac}(r_1) V_{bd}(r_2)\,, \tag{B.15}$$

where j_L is the spherical Bessel function and $h_L^{(1)}$ is the spherical Hankel function of first kind of order L, and $r_<$ and $r_>$ denote the smaller and the larger one of r_1 and r_2, respectively. The expression for the integral $\mathcal{I}_L(\omega; abcd)$ depends on the choice of gauge. In the Feynman gauge, it reads [57, 113]

$$\mathcal{I}_L(\omega; abcd) = \mathcal{I}_{1,L}(\omega; abcd) + \frac{L+1}{2L+3}\mathcal{I}_{2,L}(\omega; abcd) + \frac{L}{2L-1}\mathcal{I}_{3,L}(\omega; abcd)\,, \tag{B.16}$$

where we have

$$\mathcal{I}_{1,L}(\omega;abcd) = i\omega(2L+1)\int_0^\infty dr_1 \int_0^\infty dr_2\, j_L(\omega r_<)h_L^{(1)}(\omega r_>)W_{ac}(r_1)W_{bd}(r_2)\,, \tag{B.17}$$

$$\mathcal{I}_{2,L}(\omega;abcd) = i\omega(2L+3)\int_0^\infty dr_1 \int_0^\infty dr_2\, j_{L+1}(\omega r_<)h_{L+1}^{(1)}(\omega r_>)Q_{L,ac}(r_1)Q_{L,bd}(r_2)\,, \tag{B.18}$$

$$\mathcal{I}_{3,L}(\omega;abcd) = i\omega(2L-1)\int_0^\infty dr_1 \int_0^\infty dr_2\, j_{L-1}(\omega r_<)h_{L-1}^{(1)}(\omega r_>)P_{L,ac}(r_1)P_{L,bd}(r_2)\,. \tag{B.19}$$

In the Coulomb gauge, we have [71, 113]

$$\begin{aligned}\mathcal{I}_L(\omega;abcd) = \mathcal{I}_{1,L}(0;abcd) + \frac{L(L+1)}{2L+1}\Bigg[&\frac{1}{2L+3}\mathcal{I}_{2,L}(\omega;abcd)\\ &+\frac{1}{2L-1}\mathcal{I}_{3,L}(\omega;abcd) - \mathcal{I}_{4,L}(\omega;abcd) - \mathcal{I}_{4,L}(\omega;badc)\Bigg]\,,\end{aligned} \tag{B.20}$$

where we have the additional integral

$$\begin{aligned}&\mathcal{I}_{4,L}(\omega;abcd)\\ &= \int_0^\infty dr_1 \int_0^{r_1} dr_2 \left[i\omega j_{L-1}(\omega r_2)h_{L+1}^{(1)}(\omega r_1) - \frac{2L+1}{\omega^2}\frac{r_2^{L-1}}{r_1^{L+2}}Q_{L,ac}(r_1)P_{L,bd}(r_2)\right]\\ &\qquad + i\omega\int_0^\infty dr_1 \int_{r_1}^\infty dr_2\, j_{L+1}(\omega r_1)h_{L-1}^{(1)}(\omega r_2)Q_{L,ac}(r_1)P_{L,bd}(r_2)\,.\end{aligned} \tag{B.21}$$

The values or these integral functions for $\omega = 0$ are obtained by using the limiting behaviour of the spherical Bessel and Hankel functions. Namely, we have [76]

$$j_L(x) \sim \frac{x^L}{(2L+1)!!}\,, \tag{B.22}$$

$$h_L^{(1)}(x) \sim \frac{(2L-1)!!}{x^{L+1}}\,, \tag{B.23}$$

as $x \to 0$, where $n!! = n(n-2)\cdots 4\cdot 2$ for even n and $n!! = n(n-2)\cdots 3\cdot 1$ for odd n is the double factorial.

Bibliography

[1] H. Cakir, V. A. Yerokhin, N. S. Oreshkina, B. Sikora, I. I. Tupitsyn, C. H. Keitel, and Z. Harman, Phys. Rev. A, in print (2020), arXiv:2004.06607 [physics.atom-ph] .

[2] R. X. Schüssler, H. Bekker, M. Braß, H. Cakir, J. R. Crespo López-Urrutia, M. Door, P. Filianin, Z. Harman, M. W. Haverkort, W. J. Huang, P. Indelicato, C. H. Keitel, C. M. König, K. Kromer, M. Müller, Y. N. Novikov, A. Rischka, C. Schweiger, S. Sturm, S. Ulmer, S. Eliseev, and K. Blaum, Nature, in print (2020).

[3] N. S. Oreshkina, H. Cakir, B. Sikora, V. A. Yerokhin, V. Debierre, Z. Harman, and C. H. Keitel, Phys. Rev. A **101**, 032511 (2020).

[4] A. Rischka, H. Cakir, M. Door, P. Filianin, Z. Harman, W. J. Huang, P. Indelicato, C. H. Keitel, C. M. König, K. Kromer, M. Müller, Y. N. Novikov, R. X. Schüssler, Ch. Schweiger, S. Eliseev, and K. Blaum, Phys. Rev. Lett. **124**, 113001 (2020).

[5] B. Sikora, V. A. Yerokhin, N. S. Oreshkina, H. Cakir, C. H. Keitel, and Z. Harman, Phys. Rev. Research **2**, 012002(R) (2020).

[6] I. Arapoglou, A. Egl, M. Höcker, T. Sailer, B. Tu, A. Weigel, R. Wolf, H. Cakir, V. A. Yerokhin, N. S. Oreshkina, V. A. Agababaev, A. V. Volotka, D. V. Zinenko, D. A. Glazov, Z. Harman, C. H. Keitel, S. Sturm, and K. Blaum, Phys. Rev. Lett. **122**, 253001 (2019).

[7] B. Sikora, H. Cakir, N. Michel, V. Debierre, N. S. Oreshkina, N. A. Belov, V. A. Yerokhin, C. H. Keitel, and Z. Harman, Phys. Rev. D **97**, 111301(R) (2018).

[8] H. Cakir, N. S. Oreshkina, I. A. Valuev, V. Debierre, V. A. Yerokhin, C. H. Keitel, and Z. Harman, Phys. Rev. Lett., submitted (2020).

[9] Z. Harman, B. Sikora, V. A. Yerokhin, H. Cakir, V. Debierre, N. Michel, N. S. Oreshkina, N. A. Belov, J. Zatorski, and C. H. Keitel, J. Phys. Conf. Ser. **1138**, 012002 (2018).

[10] J. Breidenbach, E. Dizer, H. Cakir, and Z. Harman, in preparation (2020).

[11] T. Beier, I. Lindgren, H. Persson, S. Salomonson, P. Sunnergren, H. Häffner, and N. Hermanspahn, Phys. Rev. A **62**, 032510 (2000).

[12] P. J. Mohr, D. B. Newell, and B. N. Taylor, Rev. Mod. Phys. **88**, 035009 (2016).

[13] R. Bouchendira, P. Cladé, S. Guellati-Khélifa, F. Nez, and F. Biraben, Phys. Rev. Lett. **106**, 080801 (2011).

[14] R. H. Parker, C. Yu, W. Zhong, B. Estey, and H. Müller, Science **360**, 191 (2018).

[15] H. Häffner, T. Beier, N. Hermanspahn, H.-J. Kluge, W. Quint, S. Stahl, J. Verdú, and G. Werth, Phys. Rev. Lett. **85**, 5308 (2000).

[16] S. Sturm, F. Köhler, J. Zatorski, A. Wagner, Z. Harman, G. Werth, W. Quint, C. H. Keitel, and K. Blaum, Nature **506**, 467 (2014).

[17] J. Verdú, S. Djekić, S. Stahl, T. Valenzuela, M. Vogel, G. Werth, T. Beier, H.-J. Kluge, and W. Quint, Phys. Rev. Lett. **92**, 093002 (2004).

[18] S. Sturm, A. Wagner, B. Schabinger, J. Zatorski, Z. Harman, W. Quint, G. Werth, C. H. Keitel, and K. Blaum, Phys. Rev. Lett. **107**, 023002 (2011).

[19] S. Sturm, A. Wagner, M. Kretzschmar, W. Quint, G. Werth, and K. Blaum, Phys. Rev. A **87**, 030501 (2013).

[20] A. Wagner, S. Sturm, F. Köhler, D. A. Glazov, A. V. Volotka, G. Plunien, W. Quint, G. Werth, V. M. Shabaev, and K. Blaum, Phys. Rev. Lett. **110**, 033003 (2013).

[21] F. Köhler, K. Blaum, M. Block, S. Chenmarev, S. Eliseev, D. A. Glazov, M. Goncharov, J. Hou, A. Kracke, D. A. Nesterenko, Y. N. Novikov, W. Quint, E. Minaya Ramirez, V. M. Shabaev, S. Sturm, A. V. Volotka, and G. Werth, Nat. Commun. **7**, 10246 (2016).

[22] S. Sturm, I. Arapoglou, A. Egl, M. Höcker, S. Kraemer, T. Sailer, B. Tu, A. Weigel, R. Wolf, J. R. Crespo López-Urrutia, and K. Blaum, Eur. Phys. J. Spec. Top. **227**, 1425 (2019).

[23] R. Soria Orts, J. R. Crespo López-Urrutia, H. Bruhns, A. J. González Martínez, Z. Harman, U. D. Jentschura, C. H. Keitel, A. Lapierre, H. Tawara, I. I. Tupitsyn, J. Ullrich, and A. V. Volotka, Phys. Rev. A **76**, 052501 (2007).

[24] I. Arapoglou, *First measurement of the ground-state g-factor of boronlike argon* $^{40}Ar^{13+}$ *in ALPHATRAP*, Ph.D. thesis, Heidelberg University (2019).

[25] G. Breit, Nature **122**, 649 (1928).

[26] R. Faustov, Phys. Lett. B **33**, 422 (1970).

[27] H. Grotch, Phys. Rev. Lett. **24**, 39 (1970).

[28] F. E. Close and H. Osborn, Phys. Lett. B **34**, 400 (1971).

[29] K. Pachucki, U. D. Jentschura, and V. A. Yerokhin, Phys. Rev. Lett. **93**, 150401 (2004).

[30] K. Pachucki, A. Czarnecki, U. D. Jentschura, and V. A. Yerokhin, Phys. Rev. A **72**, 022108 (2005).

[31] K. Pachucki and M. Puchalski, Phys. Rev. A **96**, 032503 (2017).

[32] V. A. Yerokhin, P. Indelicato, and V. M. Shabaev, Phys. Rev. Lett. **89**, 143001 (2002).

[33] V. A. Yerokhin, P. Indelicato, and V. M. Shabaev, Phys. Rev. A **69**, 052503 (2004).

[34] V. A. Yerokhin and U. D. Jentschura, Phys. Rev. Lett. **100**, 163001 (2008).

[35] V. A. Yerokhin and U. D. Jentschura, Phys. Rev. A **81**, 012502 (2010).

[36] V. A. Yerokhin and Z. Harman, Phys. Rev. A **95**, 060501 (2017).

[37] T. Beier, Phys. Rep. **339**, 79 (2000).

[38] S. G. Karshenboim, Phys. Lett. A **266**, 380 (2000).

[39] S. G. Karshenboim, V. G. Ivanov, and V. M. Shabaev, Can. J. Phys. **79**, 81 (2001).

[40] S. G. Karshenboim, V. G. Ivanov, and V. M. Shabaev, J. Exp. Theor. Phys. **93**, 477 (2001).

[41] S. G. Karshenboim and A. I. Milstein, Phys. Lett. B **549**, 321 (2002).

[42] R. N. Lee, A. I. Milstein, I. S. Terekhov, and S. G. Karshenboim, Phys. Rev. A **71**, 052501 (2005).

[43] R. N. Lee, A. I. Milstein, I. S. Terekhov, and S. G. Karshenboim, Can. J. Phys. **85**, 541 (2007).

[44] M. I. Eides and H. Grotch, Ann. Phys. **260**, 191 (1997).

[45] A. Czarnecki, K. Melnikov, and A. Yelkhovsky, Phys. Rev. A **63**, 012509 (2000).

[46] U. D. Jentschura, A. Czarnecki, K. Pachucki, and V. A. Yerokhin, Int. J. Mass Spectrom. **251**, 102 (2006).

[47] A. Czarnecki and R. Szafron, Phys. Rev. A **94**, 060501 (2016).

[48] A. Czarnecki, M. Dowling, J. Piclum, and R. Szafron, Phys. Rev. Lett. **120**, 043203 (2018).

[49] V. A. Yerokhin and Z. Harman, Phys. Rev. A **88**, 042502 (2013).

[50] P. J. Mohr, B. N. Taylor, and D. B. Newell, Rev. Mod. Phys. **84**, 1527 (2012).

[51] V. A. Yerokhin, E. Berseneva, Z. Harman, I. I. Tupitsyn, and C. H. Keitel, Phys. Rev. Lett. **116**, 100801 (2016).

[52] V. M. Shabaev, D. A. Glazov, N. S. Oreshkina, A. V. Volotka, G. Plunien, H.-J. Kluge, and W. Quint, Phys. Rev. Lett. **96**, 253002 (2006).

[53] V. M. Shabaev, D. A. Glazov, M. B. Shabaeva, V. A. Yerokhin, G. Plunien, and G. Soff, Phys. Rev. A **65**, 062104 (2002).

[54] V. A. Yerokhin, E. Berseneva, Z. Harman, I. I. Tupitsyn, and C. H. Keitel, Phys. Rev. A **94**, 022502 (2016).

[55] J. Repp, C. Böhm, J. R. Crespo López-Urrutia, A. Dörr, S. Eliseev, S. George, M. Goncharov, Y. N. Novikov, C. Roux, S. Sturm, S. Ulmer, and K. Blaum, Appl. Phys. B **107**, 983 (2012).

[56] V. M. Shabaev, I. I. Tupitsyn, V. A. Yerokhin, G. Plunien, and G. Soff, Phys. Rev. Lett. **93**, 130405 (2004).

[57] S. A. Blundell, Phys. Rev. A **46**, 3762 (1992).

[58] V. A. Yerokhin and V. M. Shabaev, Phys. Rev. A **60**, 800 (1999).

[59] A. V. Volotka, D. A. Glazov, V. M. Shabaev, I. I. Tupitsyn, and G. Plunien, Phys. Rev. Lett. **112**, 253004 (2014).

[60] D. A. Glazov, V. M. Shabaev, I. I. Tupitsyn, A. V. Volotka, V. A. Yerokhin, G. Plunien, and G. Soff, Phys. Rev. A **70**, 062104 (2004).

[61] V. A. Agababaev, D. A. Glazov, A. V. Volotka, D. V. Zinenko, V. M. Shabaev, and G. Plunien, J. Phys. Conf. Ser. **1138**, 012003 (2018).

[62] A. A. Shchepetnov, D. A. Glazov, A. V. Volotka, V. M. Shabaev, I. I. Tupitsyn, and G. Plunien, J. Phys. Conf. Ser. **583**, 012001 (2015).

[63] J. P. Marques, P. Indelicato, F. Parente, J. M. Sampaio, and J. P. Santos, Phys. Rev. A **94**, 042504 (2016).

[64] S. Verdebout, C. Nazé, P. Jönsson, P. Rynkun, M. Godefroid, and G. Gaigalas, At. Data Nucl. Data Tables **100**, 1111 (2014).

[65] V. M. Shabaev, Phys. Rep. **356**, 119 (2002).

[66] W. Greiner, *Relativistic Quantum Mechanics: Wave Equations* (Springer Berlin Heidelberg, 2012).

[67] S. Weinberg, *The Quantum theory of fields. Vol. 1: Foundations* (Cambridge University Press, 2005).

[68] W. H. Furry, Phys. Rev. **81**, 115 (1951).

[69] W. Greiner and J. Reinhardt, *Quantum Electrodynamics* (Springer Berlin Heidelberg, 2009).

[70] M. Srednicki, *Quantum Field Theory* (Cambridge University Press, 2007).

[71] W. R. Johnson, *Atomic Structure Theory* (Springer Berlin Heidelberg, 2007).

[72] J. Sapirstein and W. R. Johnson, J. Phys. B **29**, 5213 (1996).

[73] W. R. Johnson, S. A. Blundell, and J. Sapirstein, Phys. Rev. A **37**, 307 (1988).

[74] H. Bachau, E. Cormier, P. Decleva, J. E. Hansen, and F. Martín, Reports on Progress in Physics **64**, 1815 (2001).

[75] N. J. Snyderman, Ann. Phys. **211**, 43 (1991).

[76] M. Abramowitz and I. A. Stegun, *Handbook of Mathematical Functions, With Formulas, Graphs, and Mathematical Tables,* (Dover Publications, Inc., USA, 1974).

[77] R. Piessens, E. de Doncker-Kapenga, C. W. Überhuber, and D. K. Kahaner, *Quadpack* (Springer-Verlag Berlin Heidelberg, 1983).

[78] P. Sunnergren, *Complete One-Loop QED Calculations for Few-Electron Ions*, Ph.D. thesis, Göteborg University (1998).

[79] P. J. Mohr, Phys. Rev. A **46**, 4421 (1992).

[80] P. J. Mohr and G. Soff, Phys. Rev. Lett. **70**, 158 (1993).

[81] V. A. Yerokhin, Phys. Rev. A **83**, 012507 (2011).

[82] V. A. Yerokhin, K. Pachucki, and V. M. Shabaev, Phys. Rev. A **72**, 042502 (2005).

[83] P. Jönsson, X. He, C. Froese Fischer, and I. Grant, Comput. Phys. Commun. **177**, 597 (2007).

[84] I. Angeli and K. P. Marinova, At. Data Nucl. Data Tables **99**, 69 (2013).

[85] J. Sapirstein and K. T. Cheng, Phys. Rev. A **73**, 012503 (2006).

[86] K. Blaum and S. Eliseev, private communication (2020).

[87] S. A. Zapryagaev, Opt. Spektrosc. **47**, 9 (1979).

[88] D. A. Glazov, A. V. Volotka, A. A. Schepetnov, M. M. Sokolov, V. M. Shabaev, I. I. Tupitsyn, and G. Plunien, Phys. Scr. **T156**, 014014 (2013).

[89] I. I. Tupitsyn, V. M. Shabaev, J. R. Crespo López-Urrutia, I. Draganić, R. Soria Orts, and J. Ullrich, Phys. Rev. A **68**, 022511 (2003).

[90] I. I. Tupitsyn, A. V. Volotka, D. A. Glazov, V. M. Shabaev, G. Plunien, J. R. Crespo López-Urrutia, A. Lapierre, and J. Ullrich, Phys. Rev. A **72**, 062503 (2005).

[91] G. Soff and P. J. Mohr, Phys. Rev. A **38**, 5066 (1988).

[92] L. W. Fullerton and G. A. Rinker, Phys. Rev. A **13**, 1283 (1976).

[93] S. Klarsfeld, Phys. Lett. B **66**, 86 (1977).

[94] E. H. Wichmann and N. M. Kroll, Phys. Rev. **101**, 843 (1956).

[95] V. A. Yerokhin, C. H. Keitel, and Z. Harman, J. Phys. B **46**, 245002 (2013).

[96] F. Salvat and R. Mayol, Comput. Phys. Commun. **62**, 65 (1991).

[97] F. Salvat, J. Fernández-Varea, and W. Williamson, Comput. Phys. Commun. **90**, 151 (1995).

[98] A. G. Fainshtein, N. L. Manakov, and A. A. Nekipelov, J. Phys. B **24**, 559 (1991).

[99] D. A. Glazov, A. V. Volotka, V. M. Shabaev, I. I. Tupitsyn, and G. Plunien, Phys. Rev. A **81**, 062112 (2010).

[100] A. N. Artemyev, T. Beier, G. Plunien, V. M. Shabaev, G. Soff, and V. A. Yerokhin, Phys. Rev. A **60**, 45 (1999).

[101] V. M. Shabaev, D. A. Glazov, A. V. Malyshev, and I. I. Tupitsyn, Phys. Rev. A **98**, 032512 (2018).

[102] D. A. Glazov, A. V. Malyshev, V. M. Shabaev, and I. I. Tupitsyn, Opt. Spectrosc. **124**, 457 (2018).

[103] I. A. Aleksandrov, D. A. Glazov, A. V. Malyshev, V. M. Shabaev, and I. I. Tupitsyn, Phys. Rev. A **98**, 062521 (2018).

[104] D. A. Glazov, A. V. Malyshev, V. M. Shabaev, and I. I. Tupitsyn, Phys. Rev. A **101**, 012515 (2020).

[105] H. Grotch and R. Kashuba, Phys. Rev. A **7**, 78 (1973).

[106] V. A. Yerokhin, K. Pachucki, M. Puchalski, Z. Harman, and C. H. Keitel, Phys. Rev. A **95**, 062511 (2017).

[107] D. A. Glazov, F. Köhler-Langes, A. V. Volotka, K. Blaum, F. Heiße, G. Plunien, W. Quint, S. Rau, V. M. Shabaev, S. Sturm, and G. Werth, Phys. Rev. Lett. **123**, 173001 (2019).

[108] S. G. Karshenboim, R. N. Lee, and A. I. Milstein, Phys. Rev. A **72**, 042101 (2005).

[109] G. Colò, L. Cao, N. V. Giai, and L. Capelli, Comput. Phys. Commun. **184**, 142 (2013).

[110] I. A. Valuev, Z. Harman, C. H. Keitel, and N. S. Oreshkina, submitted (2020), arXiv:2002.02227 [physics.atom-ph] .

[111] E. Tiesinga, P. J. Mohr, D. B. Newell, and B. N. Taylor, "The 2018 CODATA Recommended Values of the Fundamental Physical Constants," `http://physics.nist.gov/constants` (2020), (Web Version 8.1) Database developed by J. Baker, M. Douma, and S. Kotochigova, National Institute of Standards and Technology, Gaithersburg, MD 20899.

[112] V. M. Shabaev, J. Phys. B **26**, 1103 (1993).

[113] K.-N. Huang, Rev. Mod. Phys. **51**, 215 (1979).

Acknowledgments

A PhD is a big undertaking for the student as well as his advisor. Therefore, I thank you PD Dr. Zoltán Harman for your time and your efforts. It was and still is a pleasure to work with you. You are a very kind person and I know that I can count on you whenever I need help or guidance.

Thank you Honorarprof. Dr. Christoph H. Keitel for making this PhD work possible. It is an honor for me to be part of the Theory Division at the Max Planck Institute for Nuclear Physics. Thank you for your support and your guidance.

I thank Prof. Dr. Maurits W. Haverkort for refereeing my thesis and for being an examiner in my PhD exam. I also thank Prof. Dr. Werner Aeschbach and PD Dr. Wolfgang Quint for being part of my examination committee.

I consider myself lucky to be part of a great group. This made many fruitful collaborations possible. In particular, I want to thank PD Dr. Natalia S. Oreshkina, Dr. Vincent Debierre, and Dr. Bastian Sikora.

I thank Prof. Dr. Vladimir A. Yerokhin for the many discussions about QED calculations which helped me greatly to develop an understanding of the theory. Thank you Vladimir for your time and efforts.

I thank Sreya Banerjee, Dr. Vincent Debierre, Eugen Dizer, PD Dr. Zoltán Harman, Dr. Chunhai Lyu, PD Dr. Natalia S. Oreshkina, Dr. Suvam Singh, and Igor A. Valuev for proof-reading my thesis and, thus, greatly improving its quality.

A special place in my heart occupies my office at the Bothe laboratory. I think that I am not exagerating by saying that it is the coolest office of our division and probably of the whole institute. I had the pleasure to meet and be friends with a lot of people in that office. There has been many interesting conversations on physics and beyond and it is always fun there. An office is of course only as cool as its occupants are. My current office mates are: Petar Andrejic, Daniel Bakucz Canário, Sreya Banarjee, Eugen Dizer, and Maitreyi Sangal. Former notable members of the Office 367 are: Dr. Alessandro Angioi, Dr. Sergey Bragin, Dr. Stefano M. Cavaletto, Dr. Ujjwal Sinha, and Dr. Oleg Skoromnik. So, thank all of you guys for the great time. Special thanks to Stefano and Oleg who essentially shaped the atmosphere in the office. Grazie a Stefano ho iniziato a studiare l'italiano.

I thank my mother Nurcan Çakır, my father Hasan Çakır, and my brother Burak Çakır for their love and for their support not only throughout my PhD, but also beyond that. Anne, hatırlarsan sana bir zaman evvel, şakayla da karışık olsa, bir

gün bir başarı elde edersem senin desteğini özellikle anacağımı söylemiştim. Bugün o sözümü yerine getirmenin gururunu ve mutluluğunu hissediyorum. Şunu bilmeni isterim ki bu başarım senin de başarın. Emeğin ve sabrın için sana çok teşekkür ediyorum. İyi ki varsın.